

Elucidating the role of lymphatic vessels within the tumor microenvironment of breast cancer

THÈSE N° 7522 (2017)

PRÉSENTÉE LE 31 MARS 2017

À LA FACULTÉ DES SCIENCES DE LA VIE

PROGRAMME DOCTORAL EN BIOTECHNOLOGIE ET GÉNIE BIOLOGIQUE

ÉCOLE POLYTECHNIQUE FÉDÉRALE DE LAUSANNE

POUR L'OBTENTION DU GRADE DE DOCTEUR ÈS SCIENCES

PAR

Ingrid Maria VAN MIER

acceptée sur proposition du jury:

Prof. M. Dal Peraro, président du jury
Prof. M. Swartz, Prof. M. De Palma, directeurs de thèse
Prof. C. Halin Winter, rapporteuse
Prof. T. Petrova, rapporteuse
Prof. E. Oricchio, rapporteuse



ÉCOLE POLYTECHNIQUE
FÉDÉRALE DE LAUSANNE

Suisse
2017

Acknowledgments

First and foremost, I would like to thank my supervisor Prof. Melody Swartz for giving me the opportunity to do my thesis in her lab, and for all of her support during this time. Without her enthusiasm for science and her continuous encouragement this work would have hardly been possible. I also would like to express my warmest gratitude to my thesis co-supervisor, Prof. Miki De Palma, for his guidance and excellent scientific insights that helped me to become a better scientist over the years. Furthermore, I would also like to use this opportunity to thank the members of my thesis committee, Prof. Matteo Dal Perraro, Prof. Cornelia Halin Winter, Prof. Elisa Oricchio and Prof. Tatiana Petrova for taking the time to be on my jury.

I would like to thank all current and former lab members of the Swartz lab for creating a nice spirit in the lab, and especially Jennifer Munson for helping me to find my way in this big lab when I first started. At this occasion, I would also like to thank Catherine Card, Maria Broggi, Efthymia Vokali and Sachiko Hirose for the many helpful discussions that we had, as well as Witek Kilarski, to whom I am grateful for introducing me to the world of microscopy, and Manuel Fankhauser for being able to always depend on you. Finally, I would also like to acknowledge Patricia Corthésy and Yassin Ben Saida for excellent technical support throughout this time. Your help in the lab has been essential for all practical aspects of my thesis.

My heartfelt gratitude goes to all current and former lab members of the De Palma lab for giving me a second home. You accepted me in your midst without question and made me feel part of the team, both inside and outside the lab. I would like to particularly thank Mario Squadrito, for his assistance with the lentiviral vectors, but also for always making the time to brainstorm or to answer my questions, no matter how silly. Moreover, I would like to show my deep appreciation to Martina Schmittnägel, for your support as a scientist and as a friend. Although stressful at times, it was always fun to do experiments together with you in the lab. I am also indebted to Ioanna Keklikoglou, who helped me greatly by providing the cell line on which a lot of this thesis work is based, but also for the many valuable advices, big or small. Furthermore, I would like to acknowledge Damya Laoui, Caroline Baer, Céline Wyser-Rmili and Danielle Thompson for their valuable support in the lab. Finally, I would also like to thank Ece Kadioglu, for your friendship.

I am particularly grateful to the EPFL core facilities, which never ceased to support me with helpful discussions and excellent technical support. I would like to express my gratitude to the Histology Core Facility (HCF), especially Jessica Sordet-Dessimoz, for her generous support in the world of histology, as well as Agnès Hautier, Gianni Mancini, Natalie Müller and Vanessa Mack, who were always ready to help with a smile. Furthermore, I owe my deepest appreciation to Nadine Stokar, who under the impending deadline for the submission of my thesis made the greatest efforts to provide me with the pathology analysis of the various models employed in this thesis. I am also obliged to Olivier Burri and Romain Guiet of the Bioimaging and Optics Platform

(BIOP), who created the macro for the area measurements, and who were always set to track down the next bug when necessary. Last, but not least, I would also like to acknowledge the Flow Cytometry Core Facility (FCCF), and Miguel Garcia and Loic Tauzin in particular, for excellent assistance in flow cytometry.

From the bottom of my heart, I would like to thank my parents, Jan and Ria van Mier, and my brother Martijn, who have supported me through the good and the bad. You never stopped believing in me, and you never gave up on me. Dad, your long emails were always a highlight that brightened up my day, every single day. Mom, no matter what, you were always there to listen to me when I needed to talk. Without you, I would have never been able to finish this journey. I am forever grateful for your unconditional support, and to you I dedicate this thesis.

Thank you, Sebi Bernet, for your endless encouragement during the past years, and especially just now. For taking care of me, for feeding me, for feeding me some more, and for always having faith in me whenever I lost mine. Thank you so much for all that you have done for me.

I would also like to thank my friends inside and outside of EPFL, who made sure to remind me that there is a life outside of the lab on numerous occasions. I owe my deepest gratitude to Adrienne Mottis, who has been an invaluable friend throughout all. No matter what the circumstances were, you were always there to share a piece of cake with. I would also like to especially thank Sophie Vieweg, for your unconditional support. I really appreciate your loyalty and your friendship. My dear Zuzana Tatarova, I will never forget our many conversations in the hallway were the way to our labs parted. Also, a special thank you to Beatrice Volpe, who always encouraged me to never give up. Furthermore, I would also like to thank my close friends from Zürich, Andrea Stucki and Hau-Kit Man. Finally, I would also like to thank my neighbours, Jean-Michel and Gaby Lehmanns, who have always been there. Last but not least, I would also like to thank Evelyne Kappel, who has helped me so much to get here in the first place. Without all of you, none of this would have been possible.

Ingrid van Mier,
Lausanne, December 2016

Abstract

Breast cancer is the most common cancer in women worldwide, with an estimated 1.7 million newly diagnosed cases in 2012. Despite the many clinical manifestations, metastatic disease is the main cause of death, and is responsible for 90% of all breast cancer-related deaths. Aggressive carcinomas of the breast preferentially spread via the lymphogenous route, and often co-opt and actively remodel the lymphatic vasculature in order to invade and metastasize to their draining lymph nodes (LNs) and, ultimately, to distant organs. Indeed, expression of vascular endothelial growth factor (VEGF)-C, the principal lymphangiogenic growth factor, by the tumor or recruited ancillary cells has been shown to correlate both with LN and distant metastasis, and shorter overall survival (OS), and LN status represents an important prognostic factor for patients diagnosed with breast cancer. Although traditionally considered as passive conduits that solely mediate tumor cell escape, more recent research aimed at discerning the interactions between the developing tumor and its associated lymphatic vessels has revealed that the lymphatic vasculature actively promotes lymphogenous metastasis of invasive tumor cells. Likewise, collaborative interactions between tumor cells and a multitude of other tissue-resident and recruited ancillary cells, which together constitute the tumor microenvironment, not only coercively contribute to tumor growth, progression and metastasis, but also suggest that interactions among primed stromal cells themselves may be important in the process of metastatic dissemination as well. Notably, expansion of tumor-associated lymphatic vessels in the tumor periphery leads to increased lymphatic drainage from the tumor to the tumor-draining LN, and interstitial flow-induced mechanical changes may alter tensional homeostasis within the tumor through stimulation of local fibroblasts that remodel and stiffen the extracellular matrix (ECM). Furthermore, VEGF-C-induced remodeling of the tumor-associated lymphatic vasculature has been shown to directly suppress the anti-tumor immune response, thereby promoting tolerance to the nascent tumor. Thus, to explore whether tumor-associated lymphatic vessels promote tumor metastasis not only via interactions with the incipient tumor, but also through cross-talk with the surrounding stromal cells, the different components of the tumor microenvironment, specifically tensional homeostasis and anti-tumor immunity, were evaluated upon modulation of lymphatic vessel growth in various experimental models of breast cancer. Accordingly, inhibition of VEGFR-3-mediated signaling upon administration of an antagonistic antibody in a genetically engineered preclinical mouse model specifically reduced the number of lymphatic endothelial cells (LECs) in the tumor, whereas conversely, orthotopic inoculation of a stable murine breast cancer cell line with enhanced expression of VEGF-C induced an expansion of the lymphatic endothelium. Although either experimental approach affected either regional or distant metastatic dissemination of the primary tumor to LN or the lungs, respectively, these effects did not seem to be mediated by interactions of the tumor-associated lymphatic vasculature with the tumor microenvironment in these particular experimental models.

Key words: breast cancer, metastasis, tumor microenvironment, lymphatic vessels, VEGF-C, VEGFR-3

Zusammenfassung

Brustkrebs ist weltweit die am häufigsten auftretende Krebsart bei Frauen mit geschätzten 1,7 Millionen neu diagnostizierte Fälle im Jahr 2012. Obwohl es sehr viele klinische Erscheinungsformen dieser Erkrankung gibt, sind Metastasen als Haupttodesursache für 90% aller von Brustkrebs verursachten Todesfälle verantwortlich. Aggressive Karzinome der Brust verbreiten sich bevorzugt über die lymphogene Route, wobei die invasiven Tumorzellen die Gefäße oft kooptieren und das lymphatische Gefäßsystem umgestalten um so in den Lymphknoten (LN) einzudringen und dort zu metastasieren, sowie letztlich auch entfernte Organe anzugreifen. Tatsächlich korreliert die Expression des vaskulären endothelialen Wachstumsfaktors (VEGF)-C, des primären lymphangiogenetischen Wachstumsfaktors, im Tumor oder durch rekrutierte Zusatzzellen mit der Präsenz von LN und weiter entfernten Metastasen, sowie einer generell kürzeren Überlebenszeit (OS), und der LN-Status ist daher ein wichtiger prognostischer Faktor für Patienten bei denen Brustkrebs diagnostiziert wurde. Obwohl die Lymphgefäße traditionell nur als passive Kanäle, die invasiven Tumorzellen bei ihrer Ausbreitung einen Ausweg vom primären Tumor bieten, betrachtet wurden, ist es durch rezente Forschung, welche darauf zielte die Interaktionen zwischen dem Tumor und ihrer assoziierten Gefäße besser zu verstehen klar geworden, dass das lymphatische Gefäßsystem eine aktivere Rolle bei der Förderung des Tumorwachstums und der Metastasierung spielt als bisher angenommen. Allerdings führt ein Zusammenspiel zwischen Tumorzellen und einer Vielzahl an sowohl residente als auch rekrutierte Hilfszellen, welche zusammen das Tumor Mikroumfeld bilden, nicht nur zu einem beträchtlichen Beitrag zum progressiven Wachstums und der Ausbreitung des Tumors, sondern deutet auch darauf hin, dass Interaktionen zwischen den aktivierten Zellen des Stromas auch Bedeutung im Prozess der Metastase haben. So führt eine Erweiterung der Lymphgefäße in der Peripherie des Tumors zu einer erhöhten Lymphdrainage zu den ableitenden LNs, und die daraus folgenden mechanischen Änderungen könnten durch die Stimulation von lokalen Fibroblasten, welche die extrazelluläre Matrix formen und erneuern, einen Einfluss auf das Kraftgleichgewicht im Tumor nehmen. Des Weiteren kann eine VEGF-C-induzierte Umgestaltung des Tumor-assoziierten lymphatischen Gefäßsystems außerdem die Anti-Tumor-Immunantwort direkt unterdrücken, wodurch das Wachstum des sich ausbreitenden Tumors erleichtert wird. Um deshalb herauszufinden, ob die mit dem Tumor assoziierten Lymphgefäße die Metastase des primären Tumors nicht nur durch Interaktionen mit den heranreifenden Tumorzellen, sondern auch durch eine Synergie mit den umliegenden Zellen des Stromas begünstigen, wurden die verschiedenen Komponenten des Tumor Mikroumfelds, insbesondere das Kraftgleichgewicht und die Anti-Tumor Immunantwort, nach Modulation der Lymphgefäße in experimentellen Modellen von Brustkrebs evaluiert. Dementsprechend führte eine Inhibierung des VEGFR-3-induzierten Signalweges durch die Verabreichung eines antagonistischen Antikörpers in einem genetischen präklinischen Brustkrebs-Modell zu einer Reduktion in der Anzahl lymphatischer Endothelzellen (LECs) im Tumor, sowie umgekehrt auch die orthotope Inokulation einer stabilen Brustkrebszelllinie, die eine erhöhte Expression von VEGF-C aufwies, zu einer Expansion des lymphatischen vaskulären Endotheliums.

Obwohl beide experimentelle Ansätze also zu einer Modulation der Tumor-assoziierten lymphatischen Vaskulatur führten, sowie entweder die Ausbreitung zu den lokalen LNs oder zu den Lungen beeinflussten, schienen diese Effekte in diesen bestimmten Tumormodellen eher nicht durch einer Interaktion zwischen den Lymphgefäßen und dem Tumor Mikroumfeld zustande gekommen zu sein.

Schlüsselwörter: Brustkrebs, Metastase, Tumor Microenvironment, Lymphgefäße, VEGF-C, VEGFR-3

Table of Contents

ACKNOWLEDGMENTS	3
ABSTRACT	7
ZUSAMMENFASSUNG	8
TABLE OF CONTENTS	11
ACRONYMS AND ABBREVIATIONS	15
LIST OF FIGURES AND TABLES	19
INTRODUCTION AND STATE-OF-THE-ART	21
1.1 The lymphatic vascular system in breast cancer	22
1.1.1 Structure and function of the lymphatic vascular system	23
1.1.2 Clinical manifestations of breast cancer	24
1.1.3 Lymphatic metastasis in breast cancer	26
1.1.4 Molecular regulation of lymphangiogenesis	28
1.1.5 Interactions between lymphatic vessels and tumor cells	29
1.2 The tumor microenvironment in breast cancer	30
1.2.1 General concept of the tumor microenvironment	30
1.2.2 Cancer-associated fibroblasts and tensional homeostasis	31
1.2.3 Innate and adaptive immune responses in cancer	33
SCOPE	39
2.1 General aims	40
RESULTS	45
3.1 Characterization and modulation of tumor-associated lymphatic vessels in a genetically engineered mouse model of breast cancer	46
3.1.1 Tumor growth and progression in the MMTV-PyMT model of breast cancer is accompanied by tumor-associated lymphangiogenesis and angiogenesis	47
3.1.2 Invasive mammary tumors in MMTV-PyMT ⁺ transgenic mice infrequently induce the formation of metastatic lesions in the local tumor-draining LN	49
3.1.3 Inhibition of VEGFR-3 signaling with an antagonistic antibody does not affect primary tumor growth, but reduces pulmonary metastasis	51
3.2 Development of an orthotopic tumor model to induce lymphatic vessel growth in the context of breast cancer	54
3.2.1 Production and titration of lentiviral vectors for transduction of murine breast cancer tumor cell lines	54
3.2.2 Characterization of stable VEGF-C ⁺ and control breast cell lines <i>in vitro</i>	54

3.2.3 Expression of VEGF-C within the tumor does not affect the growth rate of the primary tumor <i>in vivo</i>	56
3.2.4 Expression of VEGF-C within the tumor reliably induces tumor-associated lymphangiogenesis <i>in vivo</i>	56
3.2.5 Disseminated VEGF-C ⁺ tumor cells induce expansion of the sinusoidal lymphatic endothelium in the draining LN	59
3.3 Deconvolution of the breast cancer microenvironment during tumor growth and progression, and its interactions with tumor-associated lymphatic vessels	61
3.3.1 Tumor-associated lymphatic vessels do not alter the desmoplastic response that accompanies incipient tumors	61
3.3.2 Tumor-associated lymphatic vessels do not alter the innate immune response to the developing tumor	64
3.3.3 Tumor-associated lymphatic vessels do not alter the T-cell-mediated adaptive anti-tumor immune response	71
DISCUSSION AND PERSPECTIVES	81
<hr/>	
4.1 Experimental modulation of lymphatic vessels in the context of breast cancer	82
4.2 Tumor-associated lymphangiogenesis and metastasis	84
4.3 The tumor microenvironment	85
4.4 VEGF-C / VEGFR-3 signaling and angiogenesis	87
4.5 Lymphogenous or hematogenous metastasis?	90
EXPERIMENTAL PROCEDURES	93
<hr/>	
5.1 Modulation of tumor-associated lymphatic vessels in different mouse models of breast cancer	94
5.1.1 Inhibition of tumor-associated lymphangiogenesis during tumor progression in a transgenic mouse model of breast cancer	95
The MMTV-PyMT mouse model of breast cancer	95
Inhibition of tumor-associated lymphangiogenesis	95
5.1.2 Development of an orthotopic tumor model to induce lymphatic vessel growth in the context of breast cancer	96
5.1.2.1 Generation of stable VEGF-C-overexpressing (VEGF-C ⁺) tumor cell lines	96
Plasmid DNA for lentiviral expression vectors	96
Amplification and purification of plasmid DNA	96
Production and titration of lentiviral vectors	97
Transduction of murine breast cancer cell lines	97
Selection of stable VEGF-C ⁺ and control breast cancer cell lines	97
5.1.2.2 Characterization of stable VEGF-C ⁺ and control breast cell lines <i>in vitro</i>	98
Calculation of lentiviral DNA copy number	98
Determination of cell division rate	98
Analysis of VEGF-C expression levels <i>in vitro</i>	99
5.1.2.3 Induction of tumor-associated lymphangiogenesis upon orthotopic injection of VEGF-C ⁺ breast cancer cell lines <i>in vivo</i>	99
Orthotopic inoculation of tumor cells	99

5.2 Deconvolution of the tumor microenvironment during tumor growth and progression in transgenic and orthotopic mouse models of breast cancer	100
5.2.1 Enzyme-Linked ImmunoSorbent Assay	100
5.2.2 Flow cytometry	101
Preparation of single cell suspensions	101
Staining procedure for flow cytometry	101
5.2.3 Histological analysis	102
Preparation of tissue sections	102
Histological evaluation of tumor progression and metastasis	102
Immunofluorescence staining procedure	102
Quantification of blood and lymphatic vessel area	104
Quantification of ECM deposition	104
Statistical analysis	105
APPENDICES	106
Appendix 1: Supplementary Experimental Procedures	106
A1.1: Primer sequences and qPCR conditions	106
A1.2: Flow cytometry: antibodies and reagents	107
A1.3: Flow cytometry: phenotype of cells in the tumor microenvironment	108
A1.4: Histology: antibodies and reagents	109
A1.5: Macro for area measurements	110
BIBLIOGRAPHY	119
CURRICULUM VITAE	131

Acronyms and Abbreviations

A

α -SMA	α -smooth muscle actin
AKT	Akt1, also known as protein kinase B
Ang-1/-2	angiopoietin-1/-2
APC	antigen-presenting cell

B

BEC	blood endothelial cell
BRCA1-2 / <i>BRC A1-2</i>	breast cancer-1/-2 / <i>gene encoding BRCA1/2</i>
BVD	blood vessel density
BVI	blood vessel invasion

C

CAF	cancer-associated fibroblast
CCL-x	chemokine (C-C motif) ligand, with x designating CCL-number
CCR-x	C-C-chemokine receptor, with x designating CCR-number
CDx	cluster of differentiation, with x designating CD-number
CSC	cancer stem cell
CTL	CD8 ⁺ cytotoxic T cell

D

DAB	3',3-diaminobenzidine
DAPI	4',6-diamino-2-phenylindole
DC	dendritic cell
DFS	disease-free survival
DNA	deoxyribonucleic acid

E

EC	endothelial cell
ECM	extracellular matrix
ED-A	extra domain-A of fibronectin
EF-1 α	elongation factor-1 α
EGF	epidermal growth factor
ELISA	enzyme-linked immunosorbent assay
EpCAM	epithelial cell adhesion molecule
ER / <i>ESR1</i>	estrogen receptor- α / <i>gene encoding estrogen receptor-α</i>
ERK1/2	extracellular signal-related kinase 1/2

F

F4/80	mouse macrophage marker
FACS	fluorescence-activated cell sorting
FBS	fetal bovine serum
FOXA1 / <i>FOX A1</i>	forkhead box protein A / <i>gene encoding FOXA1</i>

FoxP3	forkhead box protein 3
FRC	follicular reticular cell
FSP-1	fibroblast-specific protein-1
FvB/N	transgenic mouse strain, Friend virus B-type susceptibility
G	
Gag / <i>gag</i>	group-specific antigen / <i>gene encoding</i> Gag
GATA3 / <i>GATA3</i>	transcription factor / <i>gene encoding</i> GATA3
gp38	glycoprotein38, also known as podoplanin
Gr-1	myeloid cell differentiation antigen
GRB7 / <i>GRB7</i>	growth factor receptor-bound protein-7 / <i>gene encoding</i> GRB7
H	
H&E	hematoxylin and eosin
HEK293T	human embryonic kidney 293T cell line
HER2 / <i>HER2</i>	human epidermal growth factor-2 / <i>gene encoding</i> HER2
HGF	hepatocyte growth factor
HPRE	Hepatitis B virus posttranscriptional regulatory element
HIV-1	human immunodeficiency virus-1
I	
IC	infiltrating immune cell
IFN- γ	interferon- γ
Ig(G)	immunoglobulin (G)
IGF	insulin-like growth factor
IL-x	interleukin, with x designating IL-number
i.p.	intraperitoneal
L	
LEC	lymphatic endothelial cell
LN	lymph node
LOX	lysyl oxidase
LPS	lipopolysaccharide
LVD	lymphatic vessel density
LVI	lymphatic vessel invasion
Ly6C	lymphocyte antigen 6 complex, locus C
Ly6G	lymphocyte antigen 6 complex, locus G
Lyve-1	lymphatic vessel hyaluronan receptor-1
M	
MDSC	myeloid-derived suppressor cell
mF4-31C1	antagonistic antibody to VEGFR-3
MHC-II	major histocompatibility class II
MMP	matrix metalloprotease
MMTV	mouse mammary tumor virus

MOI	multiplicity of infection
MVD	microvessel density
N	
Nrp-1/-2	neuropilin-1/-2
O	
OS	overall survival
P	
p24	p24 protein of the HIV-1 capsid
PBS	phosphate-buffered saline
PD-1	programmed cell death protein-1
pD2109-control	transfer plasmid backbone without mVEGF-C gene sequence
pD2109-mVEGFC	transfer plasmid containing the mVEGF-C gene sequence
PDGF	platelet-derived growth factor
PFA	paraformaldehyde
PI	propidium iodide
PI3K	phosphatidylinositol-4,5-bisphosphate 3-kinase
PGK	phosphoglycerate kinase promoter
PKC	protein kinase C
pMD2	lentiviral envelope plasmid, expressing the VSV-G envelope
pMDLg/pRRE	lentiviral packaging plasmid, expressing Gag and Pol
PR	progesterone receptor
pRSV-Rev	lentiviral packaging plasmid, expressing REV
PyMT	polyoma middle T antigen
Q	
qPCR	quantitative polymerase chain reaction
R	
RB1 / <i>RB1</i>	retinoblastoma protein / <i>gene encoding RB1</i>
RNS	reactive nitrogen species
ROI	region of interest
ROS	reactive oxygen species
RT	reverse transcription
S	
SEM	standard error of mean
T	
TAM	tumor-associated macrophage
TBS	tris-buffered saline
TC	tumor cell
TCR- β	T cell receptor β chain

TEM	Tie-2-expressing macrophage
TIE	tyrosine kinase with Ig and EGF homology domains
TIMP	tissue inhibitor of metalloprotease
TGF- β 1	transforming growth factor- β 1
TLR	toll-like receptor
TNBC	triple-negative breast cancer
TNF- α	tumor-necrosis factor- α
TP53 / <i>TP53</i>	tumor protein p53 / <i>gene encoding</i> TP53
TU	transducing unit

V

VEGF-A/-B/-C/-D	vascular endothelial growth factor-A/-B/-C/-D
VEGFR-1/-2/-3	VEGF receptor-1/-2/-3

W

WT	wildtype
----	----------

X

XBP1 / <i>XBP1</i>	X-box binding protein 1 / <i>gene encoding</i> XBP1
--------------------	---

List of Figures and Tables

Figures

Fig. 1: Tumor growth and progression in the transgenic MMTV-PyMT model of breast cancer coincides with the growth of tumor-associated lymphatic vessels.	48
Fig. 2: Invasive carcinomas in MMTV-PyMT ⁺ tumor-bearing mice only infrequently metastasize to the local tumor-draining LN.	50
Fig. 3: Inhibition of tumor-associated lymphangiogenesis in the MMTV-PyMT model of breast cancer does not affect primary tumor growth but reduces pulmonary metastasis.	52
Fig. 4: Administration of an antagonistic antibody that ablates VEGFR3 signaling does not affect the sinusoidal lymphatic endothelium of the draining LN.	53
Fig. 5: Generation and characterization of newly generated VEGF-C ⁺ and control-transduced breast cancer cell lines <i>in vitro</i> .	55
Fig. 6: Experimental design and characterization of tumor growth after orthotopic injection of VEGF-C ⁺ and control-transduced breast cancer cell lines <i>in vivo</i> .	57
Fig. 7: Orthotopic injection of VEGF-C ⁺ breast cancer cell lines <i>in vivo</i> reproducibly leads to the formation of tumors that are rich in lymphatic vessels.	58
Fig. 8: Orthotopic inoculation of VEGF-C ⁺ tumors promotes regional metastasis of the primary tumor to the tumor-draining LN.	60
Fig. 9: Tumor growth and progression in the transgenic MMTV-PyMT model of breast cancer is accompanied by increased collagen deposition and crosslinking.	62
Fig. 10: Inhibition of VEGFR-3-mediated signaling in transgenic MMTV-PyMT ⁺ tumor-bearing mice did not affect ECM deposition at the invasive edge of the tumor.	63
Fig. 11: Early hyperplastic lesions in the MMTV-PyMT model of breast cancer are accompanied by a potent inflammatory reaction to the developing tumor.	65
Fig. 12: Inhibition of tumor-associated lymphangiogenesis in the MMTV-PyMT model of breast cancer does not alter tumor-related inflammation in the primary tumor.	67
Fig. 13: Enhanced VEGF-C expression in the primary tumor does not affect the innate immune cells of the myeloid lineage.	69
Fig. 14: Enhanced VEGF-C expression in the primary tumor does not affect TAM infiltration or phenotype.	70
Fig. 15: Tumor growth and progression in the MMTV-PyMT model of breast cancer is characterized by early CD8 ⁺ T cell activation that becomes eventually dampened.	72
Fig. 16: Inhibition of VEGFR-3-mediated signaling does not affect the induction of an acquired T-cell-mediated immune response against the tumor.	74
Fig. 17: Enhanced expression of VEGF-C does not alter overall T cell infiltration, but affects the activation status CD8 ⁺ cytotoxic T cells in the tumor.	76
Fig. 18: VEGF-C-mediated activation of the lymphatic vasculature in the tumor-draining LN changes the activation of CD8 ⁺ T cells in the LN.	78

Tables

Table 1: Primer and probe sequences for TaqMan qPCR	106
Table 2: Primer and probe sequences for SYBR Green qPCR	106
Table 3: Antibodies used for flow cytometry	107
Table 4: Antibodies used for histology	109
Table 5: Antibodies used for histology	109

1

Introduction and State-of-the-art

1.1 The lymphatic vascular system in breast cancer

1.1.1 Structure and function of the lymphatic vascular system

The circulatory system consists of the blood and lymphatic vascular system, which, although functionally related yet distinct, act in concert to maintain tissue homeostasis. The blood circulation, a closed system featuring the heart as a central pump, serves to provide sustenance through transportation of nutrients, hormones and cells to tissues, as well as removal of carbon dioxide and waste products. Although often considered the second vascular system, the lymphatic vascular system fulfills vital functions in tissue fluid homeostasis and absorption of dietary fats and fat-soluble vitamins in the intestine that complement the actions of the blood vascular system (Tammela and Alitalo, 2010). Furthermore, as a significant component of the immune system, lymphatic vessels mediate immune surveillance by providing a conduit system for the transport of antigens and antigen-presenting cells (APCs) from the periphery to the draining lymph node (LN), where subsequent adaptive immune responses are mounted (Tammela and Alitalo, 2010). Moreover, more recent research has also demonstrated an important role of lymphatic vessels in the maintenance of peripheral tolerance (Swartz, 2014). Correspondingly, dysfunctional lymphatic vessels can give rise to pathological conditions with significant morbidity, such as chronic edema, obesity and impaired immune responses.

Lymphatic vessels are commonly found in most vascularized tissues, with the exception of the bone marrow and certain avascular tissues such as the epidermis, hair and nails, although the density of the lymphatic plexus can vary greatly between the different organs (Swartz and Skobe, 2001). In general, tissues with frequent exposure to foreign antigens, such as the skin, lungs and gastrointestinal tract, are particularly rich in lymphatic vessels (Tammela and Alitalo, 2010). Interestingly, despite the fact that the central nervous system was previously believed to be devoid of lymphatic vasculature, the presence of functional lymphatic vessels was recently discovered in the brain (Louveau et al., 2015).

Excess protein-rich interstitial fluid and cells of the immune system enter the lymphatic vascular system through blind-ended initial lymphatic capillaries, which constitute the absorptive part of the lymphatic vascular network in the periphery, and are collectively designated as lymph once inside (Alitalo et al., 2005). Initial lymphatic vessels converge into larger pre-collecting, and subsequently collecting lymphatic vessels, which are interspersed by one or more LNs that perform a sieving function, ultimately connecting to the thoracic duct, from which the fluid is returned to the blood circulation via the subclavian vein (Alitalo et al., 2005). In contrast to the blood vascular system, the lymphatic vascular system thus represents an open system, in which transport of protein-rich fluid and cells occurs solely unidirectional.

The structure of the lymphatic vascular system is optimally adapted to its physiological functions. Initial lymphatic vessels are thin-walled vessels of 30-80 μm in diameter, and consist of a single layer of lymphatic endothelial cells (LECs), which are surrounded by a thin layer of fenestrated basement membrane, but not covered by pericytes or smooth muscle cells, thus rendering these vessels highly permeable for the uptake of interstitial

fluid and cells (Alitalo et al., 2005). LECs lining the initial lymphatic vessels display a characteristic oak-leaf shape, and partially overlapping flaps of neighboring LECs are interconnected by discontinuous ‘button-like’ junctions, which create primary valve structures in the endothelium that are indispensable for the formation of lymph and facilitate the entry of cells into lymphatic vessels (Baluk et al., 2007). Finally, thin anchoring filaments consisting of fibrillin and emilin-1 connect the LECs of initial capillaries to the extracellular matrix (ECM), where they also regulate the entry of lymph (Tammela and Alitalo, 2010). In contrast to initial lymphatic capillaries, however, pre-collector and collector vessels are surrounded by a basement membrane and show an increased coverage by smooth muscle cells. LECs of collecting lymphatic vessels are connected by zipper-like junctions, which prevent leakage of its contents into the extracellular space (Baluk et al., 2007). Finally, collecting vessels typically contain valves, which prevent retrograde flow of lymph to the periphery. The vessel segment between two valves is commonly referred to as the lymphangion, and represents the primary pumping unit of the lymphatic vascular system (Padera et al., 2016).

The development of the lymphatic vascular system occurs principally during gestation, and once formed, lymphatic vessels are largely quiescent in the adult (Coso et al., 2014). With the notable exception of postnatal mammary gland remodeling, lymphangiogenesis, or the growth of new lymphatic vessels from pre-existing ones, is thus a phenomenon that is mostly associated with pathological conditions in the adult, such as inflammation (both acute and chronic), wound healing and tumor metastasis (Betterman et al., 2012; Tammela and Alitalo, 2010).

1.1.2 Clinical manifestations of breast cancer

Breast cancer is the most common cancer in women worldwide, with an estimated 1.7 million newly diagnosed cases in 2012, corresponding to 25% of all new cases of cancer in women (WHO GLOBOCAN 2012, Global Cancer Facts and Figures, 3rd edition). Notwithstanding the notion that cancer is generally viewed as a disease of the western world, more than 50% of new breast cancer cases occur in developing countries. Nevertheless, as the developing world includes the majority of the world population, breast cancer incidence varies greatly worldwide as a result, being lowest in economically developing and highest in developed countries, respectively. Even so, despite its low incidence in developing countries, breast cancer is associated with high mortality in these geographical locations. Indeed, with an estimated 522'000 deaths in 2012, breast cancer is also the leading cause of mortality in women worldwide, accounting for nearly 15% of cancer-related deaths in women (WHO GLOBOCAN 2012, Global Cancer Facts and Figures, 3rd edition). Up to present date, the exact causes of breast cancer are not known, but important risk factors for development of the disease include family history, i.e. germ line mutations in *BRCA1* or *BRCA2*, reproductive history, particularly increased exposure to estrogen due to early menarche or late onset of menopause, or advanced-age pregnancy, and lifestyle factors, such as diet, alcohol intake and lack of exercise.

Although typically considered as one disease, breast cancer is in fact a complex and heterogeneous disease, which can manifest itself in many different forms and result in at

least as many different outcomes. In the clinic, breast cancers are primarily distinguished based on the anatomical location where the disease first emerges. Amongst these histological subtypes, invasive ductal carcinoma, which arises in the epithelial cells lining the milk ducts, is by far the most common and constitutes approximately 80% of all breast cancers, followed by invasive lobular carcinoma, which originates in the milk-producing lobules and constitutes another 10-15% of all breast cancers (Cancer Facts and Figures, 2015; Reed et al., 2015). The remaining 5-10% of diagnosed breast cancers comprises relatively rare types of breast cancer, including sarcomas of the connective tissue.

In addition to a distinction based on the histological features of the tumor, extensive gene expression profiling recently classified ductal carcinomas of the breast into four molecular subtypes that were observed to correlate with clinical outcome, further adding to the heterogeneity of the disease (Perou et al., 2000; Sørlie et al., 2001; Koboldt et al., 2012). These so-called 'intrinsic subtypes' of breast cancer include estrogen receptor (ER)⁺ and/or progesterone receptor (PR)⁺ luminal tumors, which can be further divided into luminal A and luminal B subtypes, respectively, as well as HER2-enriched and basal-like tumors as discernible disease entities. Accordingly, the improved taxonomy of ductal carcinomas not only confirms previous observations that hormone receptor-positive and HER2-amplified tumors represent distinct cancers that display different behavior in the clinic, but also provides an improved organization of the remaining tumors that neither express hormone receptors nor HER2, often referred to as triple-negative breast cancers (TNBCs), as these were observed to constitute a separate group. Interestingly, similar gene expression profiling studies were recently performed for lobular carcinomas of the breast, which, among other findings, confirmed loss of E-Cadherin expression as one of the main features of these tumors (Ciriello et al., 2015).

Among ductal carcinomas of the breast, ER⁺ luminal tumors are distinguished based on expression of a luminal signature, which includes expression of cytokeratins 8 and 18, which are specifically expressed by the luminal epithelium, as well as ER, PR, and ER-regulated genes, including *ESR1*, *GATA3*, *FOXA1* and *XBP1* (Koboldt et al., 2012). Although the luminal subtype comprises two distinct groups, luminal A and luminal B, which amount to 40% and 20% of all ductal carcinomas, respectively, these tumors can be difficult to distinguish in the clinic, as many features that define this subtype are shared among both groups of tumors. In general, luminal tumors have a relatively favorable prognosis, with luminal A cancers being associated with the highest overall and disease-free survival (OS and DFS, respectively) (Sørlie et al., 2001). As such, luminal A tumors are often low-grade, show low levels of proliferation, and mostly retain the activity of tumor suppressors TP53 and RB1, whereas luminal B tumors, on the other hand, show higher levels of proliferation, and more frequent mutations in TP53, correlating with their overall better and worse disease outcome, respectively.

Tumors of the HER2-enriched subtype comprise 15-20% of all ductal carcinomas, and are most clearly distinguished based on expression of the HER2-cluster, which includes amplification of the *HER2* gene, and genes that are located in close proximity to *HER2* in the genome, such as *GRB7* (Koboldt et al., 2012). In contrast to luminal tumors, tumors of the HER2-enriched subtype are typically associated with a worse prognosis, and as such are often high-grade and highly proliferative (Sørlie et al., 2001).

Interestingly, only approximately 50% of HER2⁺ tumors are allocated to the HER2-enriched subtype when based on gene expression data alone, with the remaining tumors typically being observed among the luminal B tumors, suggesting that the clinical behavior of these tumors cannot be predicted solely upon histological examination of HER2 expression.

Finally, the fourth group portrays basal-like tumors, which constitute approximately 15% of all ductal carcinomas. Basal-like tumors are mainly distinguished based on expression of the basal cluster, which includes cytokeratins 5, 6, 14 and 17 that are specific for myoepithelial cells of the milk duct (Koboldt et al., 2012). As these tumors are mostly negative for ER, PR and HER2, basal-like tumors are often referred to as triple-negative; however, only 75% percent of triple-negative tumors are contained within this group. Tumors of the basal-like subtype generally are associated with the worst prognosis, as these tumors show high expression of the proliferation cluster, as well as the highest frequency of *TP53* mutations and loss of *RB1* (Sørlie et al., 2001). An intriguing finding among tumors of this subtype is the notion that germ line mutations in *BRCA1* were almost exclusively found to lead to the formation of basal-like ductal carcinoma of the breast.

1.1.3 Lymphatic metastasis in breast cancer

Although the different clinical manifestations described in paragraph 1.1.2 are associated with different clinical outcomes, metastatic disease is the leading cause of death in patients diagnosed with breast cancer (Fidler, 2003). The circulatory system represents the primary route of metastatic dissemination of malignant tumor cells to distant organs, and the relative contributions of hematogenous and lymphogenous spread, respectively, depend largely on the origin of the primary tumor. Epithelial tumors, most notably breast and skin cancers, are known to preferentially disseminate through the lymphatic vascular system (Ran et al., 2010). Indeed, clinical data has demonstrated that, although blood vessel and lymphatic vessel invasion (in the following abbreviated as BVI and LVI, respectively) both occur in surgical specimens of breast cancer, tumor cells preferentially invade lymphatic vessels (van den Eynden et al., 2006). Moreover, LVI has also been found to correlate with metastatic dissemination of the primary tumor to the tumor-draining LN, as well as worse disease outcome (van den Eynden et al., 2006; Schoppmann et al., 2004). Interestingly, the tumor-draining LN has since long been observed to be the initial site of metastasis in patients diagnosed with breast cancer, and the presence of tumor cells in sentinel or distant nodes is a major prognostic factor for survival, independent of size or histological grade of the primary tumor, thus illustrating the importance of lymphatic vessels for metastatic dissemination of breast cancer (Tuttle, 2004).

Invasive tumors may enter the lymphatic vasculature either by engaging pre-existing vessels, or by actively driving lymphangiogenesis in their microenvironment. Although lymphangiogenesis is thought to expedite metastatic dissemination of the primary tumor, whether or not tumors induce the formation of new lymphatic vessels has been a matter of intense dispute, mainly due to limited detection of actively proliferating lymphatic

endothelium within the tumor (Williams et al., 2003). Furthermore, intratumoral lymphatic vessels are often observed to be collapsed and non-functional (Padera, 2002). Consequently, the role of tumor-associated lymphatic vessels in metastatic dissemination of the incipient tumor has largely been considered passive by solely providing an escape route for invasive tumor cells to the tumor-draining LN. However, more recent research shows that tumors actively induce remodeling of the lymphatic vasculature, both at the level of the primary tumor and beyond (Stacker et al., 2014). Indeed, despite the initially presumed absence of lymphangiogenesis within the tumor, more detailed analysis demonstrated frequent lymphatic hyperplasia in the tumor periphery in clinical specimens of breast cancer, which was found to positively correlate with LN metastasis and decreased OS (Bono et al., 2004; Mohammed et al., 2009).

In line with these observations, expression of vascular endothelial growth factor (VEGF)-C, the principal growth factor known to induce proliferation and expansion of the lymphatic vasculature through activation of VEGF receptor (VEGFR)-3 (a process that is outlined in more detail in section 1.1.4), in human ductal carcinomas of the breast has been shown to associate with increased LN metastasis, as well as reduced DFS and OS (Mohammed et al., 2007; Nakamura et al., 2005, 2003). Moreover, modulation of the VEGF-C/VEGF-D - VEGFR-3 signaling axis in various experimental models of breast cancer has provided additional evidence for a causal link between induction of lymphangiogenesis and tumor metastasis, as enhanced expression of VEGF-C or VEGF-D resulted in lymphatic hyperplasia in and around the tumor, as well as an increased incidence of regional and distant metastasis (Skobe et al., 2001a; Karpanen et al., 2001; Mattila et al., 2002; Stacker et al., 2001). Conversely, inhibition of VEGFR-3-mediated activation of the lymphatic endothelium led to a reduction in lymphatic density in the tumor, and also reduced metastatic dissemination of the primary tumor to the LN and lungs (Roberts, 2006).

Expression of VEGF-C, however, may also promote metastasis by inducing lymphatic remodeling well beyond the initial lymphatic vessels associated with the primary tumor, as enhanced expression of VEGF-C in different experimental models also induced expansion of both afferent and efferent collecting lymphatic vessels, which transport lymph towards and away from the tumor-draining LN, respectively (He et al., 2005; Gogineni et al., 2013). Furthermore, VEGF-C-induced expansion of the lymphatic endothelium, as well as other changes in the tumor-draining LN that are inferred by the tumor prior to the arrival of disseminated tumor cells, may yield a more hospitable environment for metastatic lesions, often referred to as the lymphovascular niche (Hirakawa, 2009; Hirakawa et al., 2006; Qian et al., 2006). Notably, lymphangiogenesis in the sentinel LN was found to associate with metastasis to the axillary LN in patients diagnosed with breast cancer, suggesting that expansion of the lymphatic vascular network in the tumor-draining LN may indeed promote further spread of disseminated tumor cells (van den Eynden et al., 2007). Collectively, these observations thus underline the importance of the lymphatic vascular system in metastatic dissemination of invasive carcinomas of the breast, and suggest that therapeutic targeting of tumor-associated lymphatic vessels may prevent the spread of the primary tumor to the tumor-draining LN and possibly beyond.

1.1.4 Molecular regulation of lymphangiogenesis

The delicate balance between the formation and maintenance of the blood and lymphatic vasculature requires precise control and is in large part mediated through complex signaling pathways that are induced by vascular endothelial growth factors (VEGFs) (Simons et al., 2016). The most important and widely studied modulators of lymphangiogenesis to date are VEGF-C and VEGF-D, respectively, which upon binding to their cognate receptor VEGFR-3, promote survival, proliferation and migration of LECs (Joukov et al., 1996; Achen et al., 1998; Mäkinen et al., 2001). Moreover, VEGF-C and the structurally related VEGF-D potently increase lymphatic vessel density and diameter in both experimental models and cancer (Jeltsch, 1997; Skobe et al., 2001a; Stacker et al., 2001). However, in contrast to VEGF-C, VEGF-D seems to function mainly postnatally, as VEGF-D expression is dispensable for development of the lymphatic system (Karkkainen et al., 2004; Baldwin et al., 2005).

Structurally, VEGFR-3 consists of an extracellular domain comprising seven immunoglobulin (Ig)-like domains, a transmembrane domain and an intracellular tyrosine kinase domain, which becomes autophosphorylated upon binding of VEGF-C or VEGF-D (Joukov et al., 1996; Achen et al., 1998). Activation of the receptor tyrosine kinase VEGFR-3 by its ligands induces various downstream signaling pathways, including protein kinase C (PKC)-mediated stimulation of ERK1/ERK2, or induction of AKT via phosphatidylinositide 3-kinase (PI3K) through the recruitment of adapter proteins, which mandate the subsequent biological response of the lymphatic vascular endothelium (Mäkinen et al., 2001; Deng et al., 2015). Furthermore, proteolytic processing of both VEGF-C and VEGF-D also generates shorter isoforms with an increased affinity for VEGFR-2, which, in contrast to VEGFR-3, is predominantly expressed on blood endothelial cells (BECs) and is known to be a potent mediator of angiogenesis (Joukov et al., 1997; Stacker et al., 1999). However, activation of VEGFR-2 by its ligand VEGF-A, and to a lesser extent through VEGF-C, constitutes the principal axis for the induction of blood vessel growth (Simons et al., 2016). Nonetheless, the common development and the close resemblance of the blood and lymphatic vascular systems imply that some redundancy in the molecular regulation of angiogenesis and lymphangiogenesis must exist. Indeed, more recently, VEGF-A was also discovered to possess lymphangiogenesis-inducing activity, both in the context of chronic inflammation, as well as in cancer (Nagy et al., 2002; Halin et al., 2007; Hirakawa et al., 2005). However, rather than induction of sprouting, VEGF-A was observed to rather increase lymphatic vessel diameter, suggesting that the various growth factors of the VEGF family may exert different effects on the blood and lymphatic vascular endothelium, respectively (Wirzenius et al., 2007).

Moreover, induction of angiogenesis and lymphangiogenesis may be additionally regulated upon the recruitment of different co-receptors, such as neuropilins, further adding to the complexity in the molecular regulation of the sustenance of vascular endothelium (Tammela and Alitalo, 2010). Neuropilin (Nrp)-2, for example, is expressed on the lymphatic endothelium, and can act as a co-receptor for VEGFR-3 ensuing VEGF-C-induced activation of the lymphatic vasculature. Notably, inhibition of Nrp-2 with an antagonistic antibody inhibited tumor-associated lymphangiogenesis and reduced

regional and distant metastasis, demonstrating its importance in VEGFR-3-mediated activation of the lymphatic vascular endothelium (Caunt et al., 2008).

Following the discovery of VEGF-VEGFR signaling, the TIE receptors and their angiopoietin (Ang) ligands have been identified as the second vascular tissue-specific receptor tyrosine kinase system that regulates vascular morphogenesis and homeostasis (Augustin et al., 2009). In contrast to the VEGF-VEGFR axis, Ang-TIE signaling is implicated in the control of vessel quiescence. However, as most research concerning the Ang-TIE axis has focused on delineating the role of the TIE receptors and their ligands in the regulation of developmental and tumor-associated angiogenesis, its role in the regulation of the lymphatic vascular system remains elusive. Nevertheless, Ang-1 has been shown to promote the formation and sprouting of lymphatic vessels, while Ang-2 is required for postnatal lymphatic patterning (Tammela, 2005; Gale et al., 2002). However, much work remains to be done to elucidate the role of Ang-TIE signaling in lymphatic vessel formation and maturation.

In addition to VEGF and angiopoietin signaling, other growth factors, such as platelet-derived growth factor (PDGF; (Cao et al., 2004) and Ephrin-B2 (Mäkinen et al., 2005), as well as pro-inflammatory cytokines (Ristimäki, 1998), have also been shown to induce lymphangiogenesis, but these effects may be secondary to the induction of VEGF-C and VEGF-D expression in different stromal cells, such as inflammatory cells (Schoppmann et al., 2002). Finally, among its many previously described roles, transforming growth factor (TGF)- β 1 has also been described as a negative regulator of lymphangiogenesis (Oka et al., 2008).

1.1.5 Interactions between lymphatic vessels and tumor cells

Although the architecture of lymphatic vessels, dictated by their function in fluid absorption and immune cell trafficking, accordingly renders these vessels highly suitable as a highway for metastatic dissemination of tumor cells, not much is known about how tumor-induced remodeling of the lymphatic vasculature may promote the spread of the primary tumor. In line with the notion that lymphatic vessels were initially considered as passive structures that merely provide a conduit for tumor cells, VEGF-C-mediated expansion of the lymphatic vasculature also enhances lymphatic drainage, which in turn increases the transport of invasive tumor cells from the primary tumor to the tumor-draining LN (Pathak, 2006; Hoshida, 2006; Ruddell et al., 2008). Nevertheless, expression of VEGF-C in carcinomas of the breast may induce other changes in the lymphatic vascular endothelium as well, and thus actively favoring lymphogenous metastasis of the primary tumor (Swartz and Lund, 2012).

First and foremost, VEGF-C expression by breast cancer cells enhances tumor cell chemoinvasion towards lymphatic vessels via both autocrine and paracrine signaling. Notably, VEGF-C-mediated activation of the lymphatic endothelium enhances the expression of CCL-21, which in turn attracts CCR-7⁺ tumor cells, reminiscent of dendritic cell (DC) trafficking to the draining LN in inflammation (Issa et al., 2009). Moreover, increased interstitial flow that is due to an expansion of the tumor-associated lymphatic vasculature may also enhance CCR-7⁺ tumor cell invasion towards lymphatic

vessels via autologous chemotaxis by generating small, localized gradients of chemotactic factors, such as CCL-21, that direct their migration in the direction of the flow (Shields et al., 2007). Importantly, increased interstitial flow in the tumor margin may directly contribute to lymphangiogenesis in the tumor microenvironment, as interstitial flow was shown to act as a morphoregulator of lymphatic vessel formation, thus reinforcing the effects of VEGF-C-induced lymphangiogenesis (Boardman, 2003; Helm et al., 2005). However, active remodeling of lymphatic vessels in the tumor-draining LN by metastatic tumor cells may also contribute to further spread. For instance, LN lymphatic sinuses were recently discovered to control the entry of CCR-8⁺ tumor cells via secretion of CCL-1 (Das et al., 2013). Nevertheless, besides the interplay between the lymphatic vasculature and tumor cells, interactions between lymphatic vessels and the surrounding cells of the tumor microenvironment may additionally promote transition to malignancy and metastatic dissemination in breast cancer.

1.2 The tumor microenvironment in breast cancer

1.2.1 General concept of the tumor microenvironment

Cancer is a disease with complexity beyond measure. For decades, cancer research has focused on the cancer cell itself, trying to understand the transformations leading to uncontrolled cell division and subsequent growth of tumor masses through identification of hitherto unknown dominant oncogenes or tumor suppressor genes. In 2000, Hanahan and Weinberg defined six intrinsic hallmarks of cancer that constitute an organizing principle for rationalizing the complexities of human cancers (Hanahan and Weinberg, 2000). However, this list is not exhausted as new emerging hallmarks and enabling capabilities continue to be discovered. Only recently, reprogramming energy metabolism and evading immune destruction were added to the list of core biological capabilities as emerging hallmarks that are integral to the development of cancer (Hanahan and Weinberg, 2011). Moreover, in recent years the notion that not only changes in tumor cells themselves, but also the surrounding stromal cells actively contribute to manifesting the disease has become more apparent, and the importance of the tumor microenvironment is now widely accepted (Hanahan and Coussens, 2012). Stromal cells promote cancer growth and metastasis via an intricate cross-talk between the two compartments, and these interactions have also been suggested to lead to the co-evolution of tumor cells and their microenvironment as the disease progresses (Polyak et al., 2009). Notably, the tumor stroma can make up as much as 90% of the tumor mass, and the most important cellular constituents include cancer stem cells (CSCs), endothelial cells (ECs) that form the blood and lymphatic vasculature, respectively, pericytes, cancer-associated fibroblasts (CAFs) and infiltrating immune cells (ICs) (Hanahan and Weinberg, 2011). However, components of the biophysical microenvironment, such as increased interstitial flow and mechanical stress-induced changes, may play an equally important role in tumor growth and progression (Swartz and Lund, 2012).

1.2.2 Cancer-associated fibroblasts and tensional homeostasis

Fibroblasts are the non-vascular, non-epithelial and non-inflammatory cells of the connective tissue and constitute its prevailing cellular component (Kalluri and Zeisberg, 2006). Among the many functions of these connective tissue cells, their main function is to provide structural integrity and support to the tissue through deposition of the various components of the extracellular matrix (ECM), which include constituents of the fibrillar ECM, such as type I, III or V collagen and fibronectin, as well as type IV collagen and laminin, which are indispensable for the formation of the basement membrane (Kalluri and Zeisberg, 2006). As such, fibroblasts are instrumental in maintaining tissue homeostasis, but also play a prominent role in the regulation of wound healing and inflammation (Tomasek et al., 2002; Schäfer and Werner, 2008).

The term fibroblast, however, represents an expansive designation for various cells of the connective tissue that exhibit considerable heterogeneity, as fibroblasts from different anatomical locations display distinct functional behavior (Chang et al., 2002). Moreover, a lack of general fibroblast-specific markers further complicates investigation of the disparate biological roles of these stromal cells, and at present, fibroblast-specific protein 1 (FSP-1) seems to be the most specific marker for the detection of fibroblasts in different tissues (Strutz et al., 1995).

Fibroblasts in the tumor stroma, collectively termed cancer-associated fibroblasts (CAFs), acquire an activated phenotype that is similar to the phenotype of myofibroblasts that is observed during wound healing and that is identified by the expression of α -smooth muscle actin (α -SMA) (Skalli et al., 1986; Chang et al., 2004). In fact, already as early as 1986, Dvorak described similarities between the composition of the tumor stroma and the granulation tissue of healing wounds, postulating that 'tumors are wounds that do not heal' (Dvorak, 1986). Notably, early developing tumors of the breast, i.e. carcinomas *in situ*, are typically associated with a similar stroma, which is frequently referred to as reactive stroma, and characterized by enhanced fibroblast proliferation, as well as increased deposition of type I collagen and fibrin, whereas continued activation of fibroblasts during cancer progression induces further deposition, as well as changes in the composition of the ECM, which is then designated as desmoplastic stroma (Rønnov-Jessen et al., 1996).

TGF- β 1 is an important activator of fibroblast activation during the wound healing response, but it can also induce the phenotypic features of CAFs (Desmoulière et al., 1993; Vaughan et al., 2000). Breast cancers in particular express high levels of TGF- β 1, preferably at the invasive edge of the tumor (Gorsch et al., 1992). However, altered mechanical properties of the developing tumor, such as an aberrant fluid balance as a result of the expansion of tumor-associated blood and lymphatic vessels, may also directly influence the differentiation of fibroblasts in the tumor, as increased levels of interstitial flow can also induce fibroblast-to-myofibroblast differentiation via autocrine production of TGF- β 1 by fibroblasts, resulting in matrix alignment and contraction (Ng et al., 2005). Activated myofibroblasts, in turn, also produce TGF- β 1, thus further enforcing the previously initiated contraction of the matrix. Furthermore, in addition to inducing myofibroblast differentiation, flow can also directly activate latent stores of TGF- β 1 that are stored in the ECM (Wipff et al., 2007). Interestingly, mechanical

tension maintains the myofibroblast phenotype, thus suggesting that upon initial activation of fibroblasts, which induces the formation of a reactive stroma, CAFs may continue to contribute to cancer progression and metastasis by promoting a positive feedback loop between sustained fibroblast activation and ensuing deregulated tensional homeostasis.

CAFs may endorse tumor initiation, growth, invasion and metastasis via a variety of mechanisms. Indeed, besides providing a structural scaffold, fibroblasts may also contribute to tissue homeostasis via secretion of growth factors and epithelial-mesenchymal interactions. Notably, these interactions with the adjacent epithelium are fundamental in the development and differentiation of the mammary gland (Wiseman, 2002; Kuperwasser et al., 2004). However, once fibroblasts become activated in the vicinity of developing neoplastic lesions, these stromal cells may directly promote tumor growth upon release of various growth factors, such as epidermal growth factor (EGF), hepatocyte growth factor (HGF), insulin-like growth factor (IGF), platelet-derived growth factor (PDGF) and TGF- β 1 that act in a paracrine manner to support the transformed epithelium (Bhowmick et al., 2004).

Moreover, altered tensional homeostasis as a result of enhanced ECM deposition by activated CAFs may also contribute substantially to tumor growth and progression. Although the reactive stroma is primarily characterized by increased amounts of fibrillar collagens, of which type I collagen is the most abundant, as well as fibronectins containing the extra domain (ED)-A splice variant, proteoglycans and glycosaminoglycans, formation of the desmoplastic stroma also induces *de novo* expression of various ECM constituents, such as tenascin-C, which is absent in the mammary gland under physiological conditions (Rønnov-Jessen et al., 1996). Furthermore, in addition to increased ECM deposition, augmented expression of lysyl oxidase (LOX), an enzyme that covalently and irreversibly cross-links collagen, promotes desmoplastic tissue formation and is correlated with stromal stiffening and tumor progression (Levental et al., 2009). Accordingly, in breast cancer, increased mammographic density is an important prognostic factor that is routinely used in the clinic (Butcher et al., 2009). Interestingly, increased ECM rigidity was demonstrated to directly promote malignant transformation of epithelial cells (Paszek et al., 2005).

Finally, altered ECM turnover also encompasses altered expression of matrix metalloproteases (MMPs) and tissue inhibitors of metalloproteases (TIMPs). One mechanism how increased MMP secretion by fibroblasts increases tumor invasion is by creating channels in the matrix, facilitating tumor cell invasion and metastatic dissemination (Shieh et al., 2011). Alternatively, MMPs may also liberate matrix-bound growth factors, such as VEGF-A, that subsequently stimulate tumor growth through induction of angiogenesis (Bergers et al., 2000). VEGF-A also induces vascular permeability, leading to the extravasation of plasma and plasma proteins into the tumor, which may additionally induce the infiltration of macrophages that may further contribute to the formation of desmoplastic stroma as well as alter host anti-tumor immunity. However, consistent with their role in inflammation, CAFs may also directly coordinate tumor-induced inflammation through secretion of pro-inflammatory cytokines (Erez et al., 2010).

1.2.3 Innate and adaptive immune responses in cancer

Although the link between cancer and inflammation was established more than a century ago, the seemingly paradoxical role of the immune system in enabling or eradicating the growing tumor mass, however, remains a matter of controversial debate. Most evidence for the link between cancer and inflammation comes from epidemiological studies, which have shown that chronic inflammation, whether caused by infection or autoimmune disease, or idiopathic, predisposes for a variety of cancers (de Visser et al., 2006; Mantovani et al., 2008). Moreover, even tumors where no causal relationship between inflammation and cancer development has been established, such as breast cancer, are characterized by 'smoldering' inflammation (Balkwill et al., 2005). In fact, the microenvironment of most tumors, if not all, contains an inflammatory component of varying size, composition and distribution that contributes to tumor growth, both directly via growth factors and indirectly by inducing angiogenesis, and metastasis.

The immune system consists of two compartments that are distinguished based on antigen specificity and the kinetics of activation: innate and adaptive immunity, respectively. Inflammation is a mechanism of innate immunity and represents the first line of defense that is activated to restore the balance when tissue homeostasis is perturbed (de Visser et al., 2006). Normal inflammation is self-limiting and characterized by a plasticity that is due to pro- and anti-inflammatory cytokines that are sequentially induced, whereas chronic inflammation seems to result from the persistence of inflammation-inducing factors, or the failure of mechanisms that normally resolve inflammation (Coussens and Werb, 2002). Cancer-related inflammation is promoted, in part, by cytokines that are secreted either directly by the tumor cells, or by the tumor-infiltrating immune cells, and a pro-inflammatory signature of TNF- α , IL-1 β and IL-6 in particular seems to be associated with a tumor immune microenvironment that favors tumor growth (Germano et al., 2008). Alternatively, the innate cells of the immune infiltrate in developing tumors can also contribute to cancer-related inflammation by the production of cytotoxic mediators and matrix remodeling proteases.

Nevertheless, the concept of immune surveillance also implicates a role for adaptive immune responses in tumor development. High mutation rates drive the expression of immunogenic tumor-specific antigens, and, consequently, adaptive immune responses against the growing tumor can be mounted (Dunn et al., 2004). Nevertheless, nascent tumors can efficiently escape immune destruction through immunoediting and immune subversion via direct cell-cell contacts or production of cytokines that suppress immunity, such as TGF- β 1, resulting in immunological tolerance (Zitvogel et al., 2006). Furthermore, developing tumors have also been observed to promote an immunosuppressive environment in the tumor-draining LN. Interestingly VEGF-C-induced remodeling of the tumor-associated lymphatic vasculature in the draining LN can also directly suppress the anti-tumor response, thereby further promoting tolerance to the tumor (Lund et al., 2012). Evading immune destruction therefore, is an integral component of tumors and has hence been proposed as an emerging seventh hallmark of cancer (Hanahan and Weinberg, 2011; Dunn et al., 2004).

1.2.4 Tumor-associated macrophages

Macrophages are marked by their high capacity to phagocytose cellular debris, dead cells and antigens, which is integral in their function in maintaining tissue homeostasis, wound healing and inflammation (Murray and Wynn, 2011). As such, macrophages are the primary danger sensors of the host and form an essential part of the first line of defense against invading pathogens. However, macrophages also fulfill trophic roles in organ development, tissue homeostasis and wound healing via their secretion of growth factors, cytokines, and proteolytic enzymes, as well as their expression of scavenger receptors (Murray and Wynn, 2011). The ability of macrophages to respond to profoundly distinct environmental stimuli is reflected in their inherent plasticity that enables them to adopt different functional states. The M1/M2 paradigm is the result of an attempt to classify the variety of functional states that macrophages can assume, and is based on the T_H1 - T_H2 nomenclature for polarized T cell responses (Sica and Mantovani, 2012). M1, or 'classically' activated, macrophages are induced by interferon- γ (IFN- γ) priming and subsequent exposure to toll-like receptor (TLR) ligands, such as lipopolysaccharide (LPS) and are characterized by increased phagocytic capacity, expression of activation molecules CD80, CD86 and major histocompatibility (MHC) class II, and a pro-inflammatory cytokine signature. Furthermore, M1 macrophages produce large amounts of reactive oxygen and nitrogen species (ROS and RNS, respectively), increasing their ability to kill pathogens and cells (Biswas and Mantovani, 2010). Conversely, M2 or 'alternatively' activated macrophages differentiate in response to IL-4 and IL-13 and play important trophic roles in tissue homeostasis and wound healing (Gordon and Martinez, 2010). M2 macrophages up-regulate expression of the mannose receptor (CD206), induce arginase-1 expression and are associated with an anti-inflammatory cytokine signature (Stein et al., 1992). However, alternative activation was soon to include all other macrophages than M1 and therefore the M1/M2 classification represents an oversimplification of the large variety of macrophages polarization states observed *in vivo*. Instead, the M1 and M2 phenotype are more likely to represent two extremes of a continuum where the prevalence of intermediate phenotypes is skewed by microenvironmental cues (Sica and Mantovani, 2012).

Tumor-associated macrophages (TAMs) make up a significant amount of the infiltrating immune cells in the tumor. Generally, a high density of TAMs has been found to correlate with poor prognosis in more than 80% of the studies published (Bingle et al., 2002). In breast cancer, macrophage infiltration is associated with transition to malignancy and metastasis (Lin et al., 2001). Indeed, as macrophage polarization is highly context-dependent, this is a feature that can be readily exploited by tumors. Generally, TAMs are described to possess an 'M2-like' phenotype, but different TAM populations may co-exist in the same tumor depending on their localized microenvironment and on the tumor stage (Ruffell et al., 2012). The inflammatory response of macrophages is highly implicated in tumor initiation through the production of mutagenic ROS and RNS that can cause damage to the DNA of cells (Biswas and Mantovani, 2010). However, during tumor progression, tumors create a microenvironment that causes macrophages to suppress immune functions and adopt trophic roles found during development and repair instead (Condeelis and Pollard, 2006). As such, macrophages

have been shown to support tumor progression and metastasis by promoting angiogenesis, enhancing tumor cell invasion, intravasation into blood vessels and extravasation at the metastatic site (Qian and Pollard, 2010). Finally, TAMs may also promote tumor progression and metastasis by suppressing anti-tumor immune responses (Qian and Pollard, 2010). Accordingly, TAMs may contribute to an immune microenvironment that is supportive of tumor growth by altering the local cytokine milieu. Notably, TAMs constitute a prominent source of TGF- β 1 in the tumor microenvironment, thereby exerting a suppressive effect on the various immune cells that are present in the tumor. However, excess amounts of TGF- β 1 may also aid in the gradual progression from an 'M1-like' to an 'M2-like' phenotype of the TAMs within the tumor. Moreover, the transition from 'M1-like' to 'M2-like' is associated with decreased expression of pro-inflammatory cytokines, such as TNF- α and IL-12, and increased expression of IL-10 that may further aid in the induction of an overall immunosuppressive microenvironment (Noy and Pollard, 2014). Nevertheless, although macrophages may aid in actively subverting anti-tumor adaptive immune responses, polarized adaptive immune responses, in turn, may help to maintain a pro-tumor 'M2-like' phenotype of TAMs, as was recently shown to be the case for IL-4-secreting CD4⁺ T_H2 cells (DeNardo et al., 2009).

1.2.5 Interactions between lymphatic vessels and stromal cells

In addition to the different lymphangiogenic signals provided by the nascent tumor mass, various stromal cells may also promote the expansion of the lymphatic network in the tumor microenvironment. Among these, macrophages have been shown to induce lymphangiogenesis in a large variety of different cancers, including breast cancer (Schoppmann et al., 2006). Nevertheless, although the link between tumor-associated macrophages (TAMs) and tumor-associated lymphangiogenesis has previously been established, the exact nature of the contribution remains elusive. Even so, macrophages may contribute to lymphatic vessel growth via a multitude of mechanisms, such as production and secretion of vascular growth factors and cytokines, or physical contact which may distinctly regulate lymphangiogenesis both spatially and temporally depending on the context (Harvey and Gordon, 2012). Indeed, TAMs have been shown to be relevant, if not the main sources of the lymphangiogenic growth factors VEGF-C and -D in the tumor microenvironment (Schoppmann et al., 2002). Moreover, VEGF-C expressed by the tumor recruits VEGFR-3⁺ monocytes to the tumor where they differentiate into macrophages and switch on *de novo* synthesis of VEGF-C and -D, thus reinforcing the process of lymphangiogenesis initially induced by the developing tumor (Skobe et al., 2001b; Schoppmann et al., 2002). Additionally, VEGF-A may also directly recruit VEGF-C and -D-expressing macrophages into the tumor, thus providing another possibility for these cells to support tumor-associated lymphangiogenesis (Cursiefen et al., 2004). Importantly, the tumor immune microenvironment may also indirectly contribute to expansion of the lymphatic vasculature as pro-inflammatory cytokines, such as IL-1 β and TNF- α , may also induce VEGF-C and -D expression in TAMs (Watari et al., 2008).

Alternatively, a subpopulation of macrophages that express the lymphatic marker *lyve-1*, which is often observed in close association with the lymphatic vasculature, has also been reported to contribute to lymphangiogenesis via transdifferentiation into lymphatic progenitor cells (Maruyama et al., 2005; Schledzewski et al., 2006; Zumsteg et al., 2009). However, lineage-tracing experiments have provided strong evidence for the exclusion of cells of the myeloid lineage as a source of such lymphatic progenitor cells (Gordon et al., 2010). Instead, *lyve-1*⁺ macrophages that selectively interact with lymphatic vessels during developmental and tumor-associated lymphangiogenesis were shown to have a gene signature that closely resembles that of *Tie2*-expressing macrophages (TEMs), a distinct subpopulation of macrophages with enhanced pro-angiogenic activity (De Palma et al., 2005; Gordon et al., 2010). Interestingly, TEMs express higher levels of *lyve-1* than their *Tie-2* negative counterparts, and it is thus tempting to speculate that a similar subset of macrophages may be involved in the regulation of tumor-associated lymphangiogenesis (Pucci et al., 2009). Indeed, such a subset of TEMs found in patients diagnosed with breast cancer was recently observed to possess pro-lymphangiogenic activity (Bron et al., 2016). Nevertheless, the exact roles of macrophages in modulating expansion of the lymphatic network are currently poorly understood and many questions still remain to be answered.

2

Scope

2.1 General aims

Although the relevance of the lymphatic vascular system for metastatic dissemination of the primary tumor in patients diagnosed with breast cancer has been well established, less is known about how tumor-associated lymphatic vessels promote the spread of malignant tumor cells to regional LNs or distant organs. Whereas lymphatic vessels have traditionally been considered as passive conduits that solely mediate the transport of metastatic tumor cells, more recent research aimed at discerning the interactions between the developing tumor and its associated lymphatic vessels has revealed that the lymphatic vasculature actively promotes lymphogenous metastasis of invasive tumor cells. Of late, it has indeed become apparent that interactions between thwarted neoplastic cells and both tissue-resident, as well as recruited ancillary cells, which together constitute the tumor microenvironment, substantially contribute to tumor growth, progression and subsequent metastasis (Hanahan and Weinberg, 2000). However, collaborative interactions among the different stromal cells of the tumor microenvironment themselves may also synergize to promote metastatic dissemination of the primary tumor as well, and thus in the thesis work presented herein, I therefore aim to establish a link between previously unrelated components of the tumor stroma, specifically tumor-associated lymphatic vessels, tensional homeostasis and anti-tumor immunity, to elucidate their concerted role in transition to malignancy and metastatic dissemination of breast cancer (Swartz and Lund, 2012).

To this end, the first part of the current thesis will elaborate on the experimental modulation of lymphatic vessels in the context of breast cancer. As activation of the receptor tyrosine kinase VEGFR-3 by its ligands VEGF-C or VEGF-D constitutes the main axis known to induce lymphangiogenesis during development, but also in various pathological conditions in the adult, including cancer, the growth of lymphatic vessels is attuned upon manipulation of different components of the VEGF-C/VEGF-D - VEGFR-3 signaling axis in different experimental breast cancer models. The first approach, which is described in section 3.1, aims to restrict the growth of lymphatic vessels upon administration of an antagonistic antibody that specifically binds to and ablates VEGFR-3-mediated signaling in a relevant preclinical transgenic mouse model of breast cancer (Pytowski et al., 2005). Conversely, the second approach, which is described in section 3.2, aims to induce the growth of lymphatic vessels upon orthotopic implantation of a murine breast cancer cell line that was transduced to stably over-express VEGF-C in the fat tissue surrounding the inguinal mammary gland.

Subsequently, the second part of the current thesis will focus on dissecting the interactions between lymphatic vessels and the disparate stromal cells of the tumor microenvironment in the different experimental models of breast cancer that were employed in this thesis. Notably, as expansion of the lymphatic vasculature in developing tumors also enhances lymphatic drainage to the regional LN, increased interstitial flow at the tumor margin may alter tensional homeostasis within the tumor through local activation of TGF- β 1, which in turns stimulates tissue-resident fibroblasts to induce the formation of a desmoplastic stroma. Furthermore, in light of the recently

described immunomodulatory roles of the lymphatic endothelium in cancer, direct interactions between lymphatic vessels and infiltrating immune cells may additionally induce an immunosuppressive environment that fosters tumor growth and progression (Swartz, 2014). Indeed, inflammation and lymphangiogenesis are two processes that are intimately linked, and, as important mediators of the innate immune response, macrophages have been implicated to contribute to lymphangiogenesis by secreting VEGF-C and VEGF-D in inflammatory settings. Interactions between lymphatic vessels and macrophages, however, may be reciprocal, and conversely, activated lymphatic vessels in the primary tumor may also shift the phenotype of infiltrating TAMs to support progression to malignancy and metastatic dissemination of invasive tumor cells. Finally, VEGF-C-induced remodeling of the tumor-associated lymphatic vasculature has also been shown to directly suppress the adaptive anti-tumor immune response, thereby promoting tolerance to the nascent tumor (Lund et al., 2012). Thus, taking these previous observations into consideration, section 3.3 will therefore focus on the presumed interactions between tumor-associated lymphatic vessels and the different components of the tumor microenvironment, i.e. tensional homeostasis, as well as the innate and adaptive immune responses to the developing tumor.

3

Results

3.1 Characterization and modulation of tumor-associated lymphatic vessels in a genetically engineered mouse model of breast cancer

3.1.1 Tumor growth and progression in the MMTV-PyMT model of breast cancer is accompanied by tumor-associated lymphangiogenesis and angiogenesis

The mouse mammary tumor virus (MMTV)-polyoma middle T antigen (PyMT) model, in the following abbreviated as MMTV-PyMT, currently represents one of the most widely used preclinical transgenic mouse models of breast cancer, as tumor growth and progression in MMTV-PyMT⁺ transgenic animals is known to recapitulate human disease (Guy et al., 1992; Lin et al., 2003). The left panel in Fig. 1A shows a normal mammary gland in the inguinal fat pad in a wildtype (WT) littermate. In female MMTV-PyMT⁺ transgenic mice, expression of the PyMT oncogene, which is under the control of the MMTV promoter and thus directed to the mammary epithelium, results in its transformation throughout the ductal tree, leading to the development of hyperplastic lesions at 6-7 weeks of age that resemble ductal carcinoma *in situ* in humans (Fig. 1A, middle). Hyperplastic lesions then gradually progress and give rise to an invasive carcinoma at 11-12 weeks of age (Fig. 1A, right) that eventually disseminates to form pulmonary metastases, with micrometastatic lesions present in 30% of the animals at this point in time (data not shown). Tumor growth and progression in our transgenic animals therefore follows the kinetics of this model as heretofore described (Lin et al., 2003). Although the onset of hyperplasia and subsequent development of invasive carcinoma has been outlined in detail, it is not known whether this process simultaneously coincides with the induction of tumor-associated lymphangiogenesis in this particular model. To assess its feasibility as a preclinical model in order to examine the importance of tumor-associated lymphangiogenesis for tumor progression and metastatic dissemination in the context of breast cancer, I set out to characterize the growth of tumor-associated lymphatic vessels in MMTV-PyMT⁺ transgenic animals. Analysis of expression levels of VEGF-C and VEGF-D, the principal growth factors known to induce proliferation and expansion of the lymphatic endothelium, demonstrated somewhat elevated levels of VEGF-C, but not of VEGF-D in developing tumors in the MMTV-PyMT mouse model of breast cancer, as compared to corresponding wildtype (WT) littermates, which further increase during progression towards invasive lesions, suggesting that these tumors actively induce remodeling of the lymphatic vasculature (Figs. 1B and C, respectively). Concurrently, the level of VEGF-A within the tumor was also found to be elevated in transgenic MMTV-PyMT⁺ animals, suggesting that these tumors also induce extensive angiogenesis (Fig. 1D). Expression of VEGF-C within the tumor correlates with an induction of tumor-associated lymphangiogenesis, as the number of CD31⁺gp38⁺ lymphatic endothelial cells (LECs) was observed to increase at the time of tumor onset, and continued to increase further during tumor progression as compared to WT tumor-free mice (Fig. 1E). Expansion of tumor-associated lymphatic vessels occurred at least partially at the level of initial lymphatics, as among the LEC population the number of lyve-1⁺ LECs was also increased (Fig. 1F). Finally, tumor growth and progression was also associated with induction of angiogenesis, as the number of CD31⁺gp38⁻ blood endothelial cells (BECs) was increased in both

hyperplastic as well as invasive lesions (Fig. 1G). Taken together, these results indicate that development of hyperplastic lesions and their continuous progression towards an invasive carcinoma is accompanied by induction of both tumor-associated lymphangiogenesis, as well as angiogenesis.

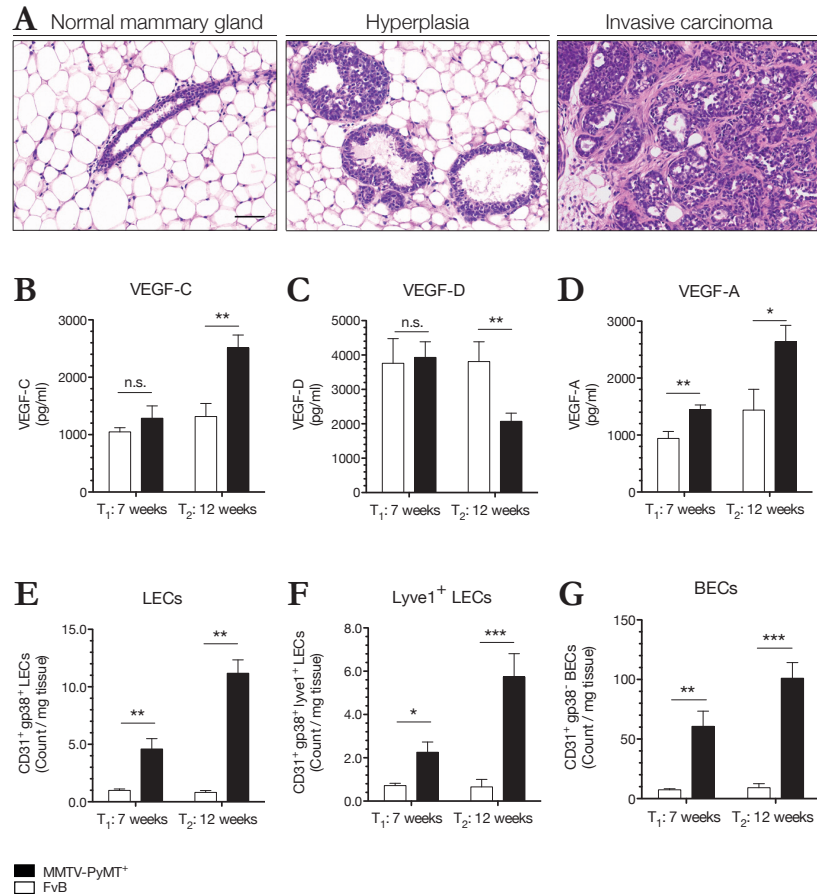


Fig. 1: Tumor growth and progression in the transgenic MMTV-PyMT model of breast cancer coincides with the growth of tumor-associated lymphatic vessels.

A Depiction of a normal mammary gland in an age-matched WT littermate (left), a hyperplastic lesion at 6-7 weeks of age (middle) and an invasive carcinoma at 11-12 weeks of age (right). H&E, magnification 20x, scale bar 50 μ m. **B** Immunoassay for growth factors of the VEGF family on whole tumor lysates shows an increase in VEGF-C, **C** but not VEGF-D expression, which was even strongly decreased in invasive tumors as compared to WT tumor-free mice. **D** VEGF-A expression levels, however, are elevated during tumor growth in transgenic MMTV-PyMT⁺ tumor-bearing mice as compared to WT littermate controls. **E** Increased expression of VEGF-C in hyperplastic lesions and invasive carcinoma correlates with the induction of tumor-associated lymphangiogenesis as the number of CD31⁺gp38⁺ LECs, as well as **F** the number of lyve-1⁺ LECs in within the total LEC population increase. **G** Concurrently with tumor-associated lymphangiogenesis, developing tumors also induce angiogenesis in their microenvironment for sustenance during tumor onset and progression. Plotted values represent mean \pm SEM, statistical analysis by two-tailed unpaired Student's *t*-test. Experiments were performed twice (analysis of expression levels of angiogenic and lymphangiogenic growth factors by ELISA), and once (analysis of the number of LECs and BECs by flow cytometry) with *n* = 10 transgenic MMTV-PyMT⁺ animals and *n* = 6 FvB WT littermate controls per group, respectively.

3.1.2 Invasive mammary tumors in MMTV-PyMT⁺ transgenic mice infrequently induce the formation of metastatic lesions in the local tumor-draining LN

Given the importance of tumor-associated lymphatic vessels for regional metastatic dissemination of the primary tumor to the tumor-draining lymph node (LN) in breast cancer, I next asked whether invasive lesions in MMTV-PyMT⁺ transgenic animals induced the formation of LN metastases (Ran et al., 2010; Skobe et al., 2001a). Routine pathology analysis of H&E-stained sections of the inguinal LN could not detect the presence of disseminated tumor cells, except in one case in which it was unclear whether the tumor cells had entered the tumor-draining LN upon spread via the tumor-associated vasculature, or merely invaded the LN due to an expansion of the transformed epithelium in the adjacent inguinal fat pad (Fig. 2A, incidence 1/10 or 10%). Furthermore, the tumor-draining LNs of MMTV-PyMT⁺ tumor-bearing mice were not enlarged compared to the LNs draining the inguinal mammary fat pad in age-matched WT littermate controls, suggesting that these LNs were indeed not involved (Fig. 2B). Subsequent immunofluorescence with an antibody that specifically recognizes the PyMT antigen also failed to detect the presence of disseminated tumor cells in the inguinal LNs downstream of invasive carcinomas, but confirmed the single invasive lesion previously observed upon histological analysis (Fig. 2C, right, enlarged in inset). Despite the previously observed low incidence of metastatic LNs, however, tumor-induced changes in the draining LN, such as an expansion of the lymphatic plexus, have previously been suggested to precede and promote distant metastasis of malignant tumor cells, and thus I also asked whether developing tumors induce LN lymphangiogenesis in this model (Hirakawa et al., 2006). Quantification of the lyve-1⁺ lymphatic vessel area in the inguinal LN, however, showed no significant change in the percentage of area covered by the lymphatic endothelium (Fig. 2D). Flow cytometry analysis of the tumor-draining LN confirmed these findings, as no change in the total number of CD31⁺gp38⁺ LECs, nor in the subpopulation of lyve-1⁺ LECs, could be observed in the inguinal LN at either time point between tumor-bearing animals and WT littermate controls (Figs. 2E and F, respectively). Moreover, the same appeared to be true for the total number of CD31⁺gp38⁺ BECs in the draining LN, which showed no difference in the total number in the tumor-draining LN as compared to the LN draining the inguinal mammary gland (Fig. 2G). These findings were also reflected in the ratio of LECs to BECs in the inguinal LN, which remained the same in MMTV-PyMT⁺ tumor-bearing mice as compared to WT littermate controls at 7 and 12 weeks of age, respectively (Fig. 2H). Collectively, these data demonstrate that tumor growth and progression in MMTV-PyMT⁺ transgenic animals does not induce expansion of the lymphatic endothelium in the inguinal tumor-draining LN, suggesting that the lymphatic vasculature in the LN may not be involved in metastatic dissemination in this model. Consistent with these findings, and despite the observation of micrometastatic lesions do occur in the lungs of MMTV-PyMT⁺ tumor-bearing mice of 12 weeks of age, metastatic dissemination of invasive carcinomas to the inguinal tumor-draining LN is infrequent in the MMTV-PyMT model of breast cancer, suggesting that lymphatic metastasis may not precede distant metastasis, and hematogenous spread may be the preferred route of metastatic dissemination of the primary tumor instead in this model.

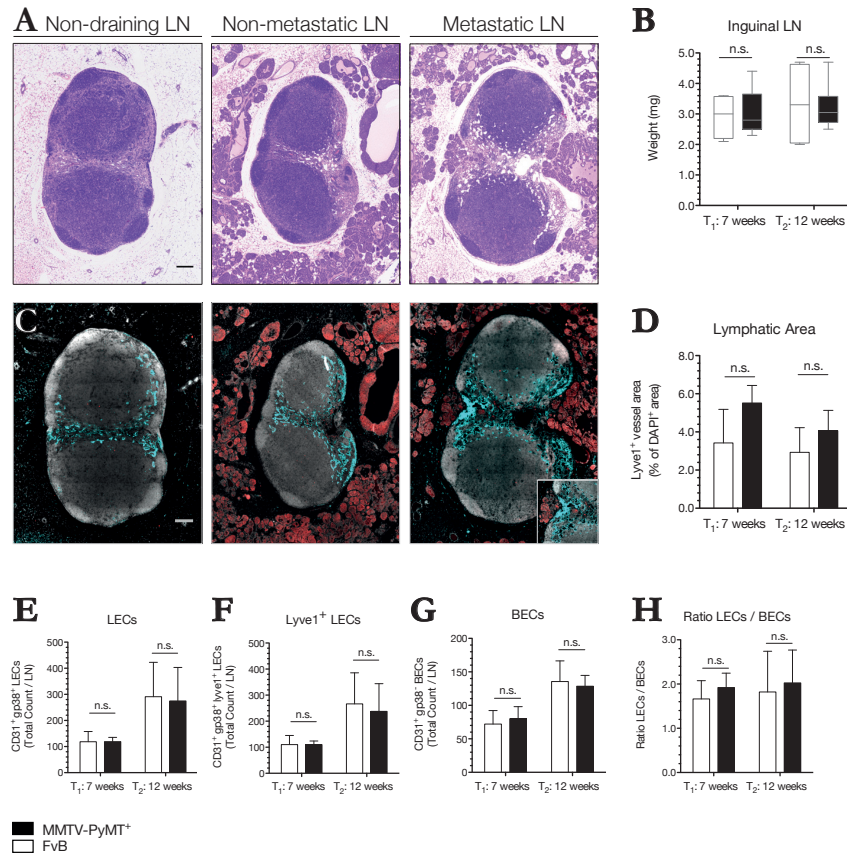


Fig. 2: Invasive carcinomas in MMTV-PyMT⁺ tumor-bearing mice only infrequently metastasize to the local tumor-draining LN.

A Representative H&E images of the inguinal LN draining the fat pad containing the mammary gland in FvB/N WT tumor-free mice at 12 weeks of age (left), or MMTV-PyMT⁺ animals with invasive carcinomas (middle), respectively. The formation of a metastatic lesion in the tumor-draining LN upon pathological analysis was only observed in 1 out of 10 MMTV-PyMT⁺ transgenic animals (right, incidence 10%). Magnification 20x, scale bar 200 μ m. **B** The inguinal LN of MMTV-PyMT⁺ tumor-bearing animals was not enlarged compared to age-matched WT FvB/N littermate controls, suggesting that these LNs indeed are not involved. **C** Immunofluorescence for the PyMT antigen (red) also failed to detect metastatic tumor cells in the tumor-draining LN of MMTV-PyMT⁺ transgenic animals at 12 weeks of age (middle), but confirms the metastatic lesion observed upon analysis of H&E-stained sections by a pathologist (right, enlarged in inset). Lyve-1 staining (teal) of the lymphatic endothelium of the inguinal LN shows that invasive carcinomas of the mammary gland do not induce LN lymphangiogenesis in the MMTV-PyMT model of breast cancer, which is also shown **D** upon quantification of the lymphatic vessel density in the inguinal LN. Magnification 20x, scale bar 200 μ m. Values represent the percentage of lyve-1⁺ area relative to the DAPI⁺ area in one imaging plane. **E** Analysis of the total number of LECs in the tumor-draining LN by flow cytometry confirmed lack of LN lymphangiogenesis in the MMTV-PyMT model of breast cancer, both in of the overall number of CD31⁺gp38⁺ LECs, as well as **F** in the number of CD31⁺gp38⁺lyve1⁺ LECs. **G** Furthermore, the number of CD31⁺gp38⁻ BECs did also not change in the inguinal LN of MMTV-PyMT⁺ transgenic animals, which is also reflected in **H** the ratio of LECs to BECs in the tumor, which also remained the same. Plotted values represent mean \pm SEM, statistical analysis by two-tailed unpaired Student's *t*-test. Experiment was performed once with *n* = 10 transgenic MMTV-PyMT⁺ animals and *n* = 6 FvB WT littermate controls per group, respectively.

3.1.3 Inhibition of VEGFR-3 signaling with an antagonistic antibody does not affect primary tumor growth, but reduces pulmonary metastasis

Although the relevance of lymphatic vessels for breast cancer metastasis has been well established, less is known about how tumor-induced lymphangiogenesis may aid in the metastatic dissemination of malignant tumor cells. To investigate the interplay between tumor-associated lymphatic vessels and the tumor microenvironment, I sought to inhibit lymphangiogenesis in the MMTV-PyMT model of breast cancer upon administration of mF4-31C1, a function-blocking antibody to VEGFR-3 (i.e. α -VEGFR-3), which is predominantly restricted to the lymphatic endothelium in adults (Pytowski et al., 2005). To this end, treatment with α -VEGFR-3, or its corresponding control IgG, respectively, was initiated upon onset of hyperplasia, and continued until lesions progressed to invasive tumors. As shown in Figs. 3A and 3B, respectively, inhibition of VEGFR-3-signaling in MMTV-PyMT⁺ transgenic mice did not affect the growth of the primary tumor. Administration of mF4-31C1, however, did result in reduced pulmonary metastasis, as micrometastases could be observed in the lungs of 2 out of 7 IgG-treated MMTV-PyMT⁺ tumor-bearing mice (i.e. 28.6%), whereas none were found in the lungs of α -VEGFR3-treated animals (Figs. 3C and D). Upon examination of the tumor-associated vasculature, treatment with mF4-31C1 specifically targeted the lymphatic endothelium, as administration of the function-blocking antibody reduced the number of CD31⁺gp38⁺ LECs in the primary tumor, as compared to IgG-treated tumor-bearing mice, whereas the number of CD31⁺gp38⁺ BECs in the tumor was not affected (Figs. 3E-G, respectively).

Next, I assessed the tumor-draining LN. Administration of mF4-31C1 to MMTV-PyMT⁺ tumor-bearing mice did not affect the size or weight of the tumor-draining LN (Figs. 4A and B). In contrast to the observed effects of inhibition of VEGFR-3-mediated signaling on the lymphatic vasculature in developing tumors, but consistent with a lack of lymphangiogenesis in the inguinal LN draining invasive carcinomas, however, treatment with mF4-31C1 appeared to have no effect on the lymphatic endothelium in the tumor-draining LN, as histological examination showed no difference in the lymphatic vessel area in the LNs draining either invasive lesions of α -VEGFR-3- or IgG-treated tumor-bearing mice (Figs. 4C and D, respectively). Flow cytometry analysis confirmed these findings, as the number of CD31⁺gp38⁺ LECs within the tumor-draining LN of α -VEGFR3- and IgG-treated MMTV-PyMT⁺ mice remained the same (Figs. 4E and G). Finally, treatment with mF4-31C1 also did not alter the number of CD31⁺gp38⁺ BECs in the tumor-draining LN (Fig. 4F).

In conclusion, these results demonstrate that, although inhibition of VEGFR-3-mediated signaling within the primary tumor in the MMTV-PyMT model of breast cancer did not affect tumor growth, the treatment did result in reduced pulmonary metastasis. While administration of mF4-31C1 specifically reduced the number of CD31⁺gp38⁺ LECs, but not of CD31⁺gp38⁺ BECs in the primary tumor, no such reduction could be observed for the number of CD31⁺gp38⁺ LECs or CD31⁺gp38⁺ BECs in the tumor-draining LN, suggesting that administration solely targets the tumor-associated lymphatic endothelium in MMTV-PyMT⁺ transgenic mice.

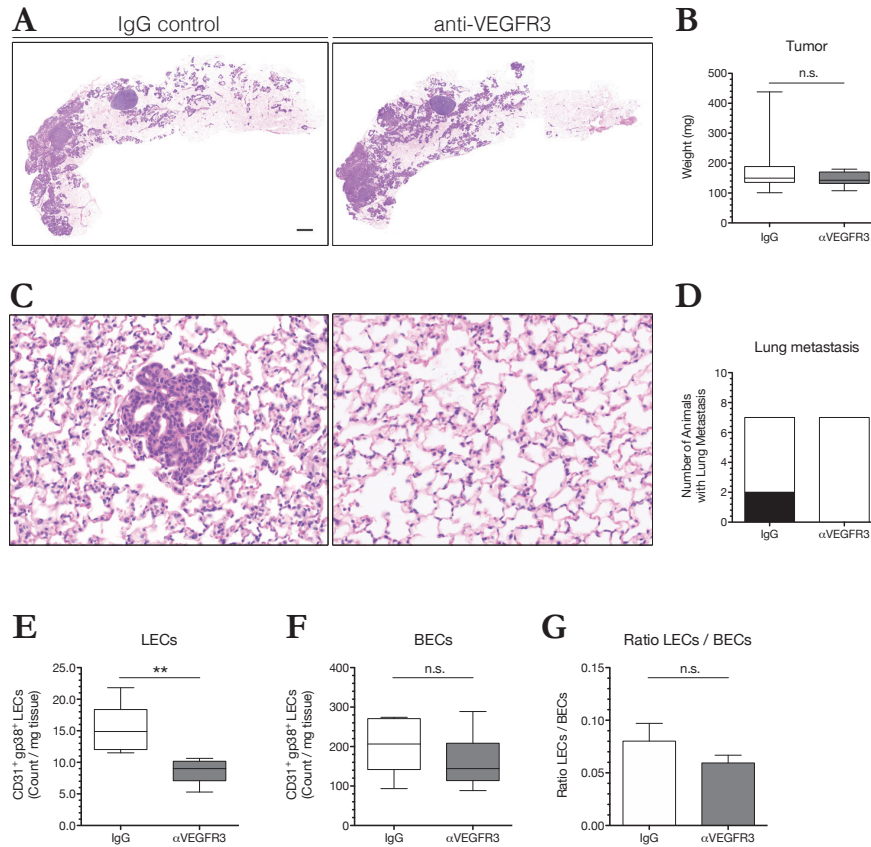


Fig. 3: Inhibition of tumor-associated lymphangiogenesis in the MMTV-PyMT model of breast cancer does not affect primary tumor growth but reduces pulmonary metastasis.

A Administration of mF4-31C1 does not affect the growth of the primary tumor, as shown by H&E staining of the inguinal mammary fat pad containing the transformed mammary epithelium (magnification 20x, scale bar 1 mm), **B** or the tumor weight upon termination of the treatment. **C** Inhibition of tumor-associated lymphangiogenesis in tumor-bearing MMTV-PyMT⁺ mice did, however, result in reduced formation of micrometastases in the lungs of α -VEGFR-3-treated as compared to IgG-treated animals. H&E, magnification 40x. **D** Examination of the lungs by a pathologist revealed the presence of multiple micrometastases in the lungs of IgG-treated animals (filled bars), whereas none of the lungs of α -VEGFR-3-treated animals contained disseminated tumor cells. **E** Analysis of the lymphatic and blood vasculature associated with the nascent tumors by flow cytometry showed that the treatment with mF4-31C1 specifically reduced the numbers of CD31⁺gp38⁺ LECs in the tumor, **F** while not affecting the number of CD31⁺gp38⁻ BECs, suggesting that abrogated VEGFR-3 signaling specifically reduces lymphangiogenesis. **G** The specificity of the treatment is also reflected in the ratio of LECs to BECs in the tumor, which is reduced, albeit not significantly, upon inhibition of VEGFR-3-mediated signaling in MMTV-PyMT⁺ transgenic animals. Flow cytometry for vascular endothelial cells performed by Maria Broggi. Plotted values represent mean \pm SEM, statistical analysis by two-tailed unpaired Student's *t*-test. Experiment was performed once with *n* = 7 MMTV-PyMT⁺ transgenic animals per treatment group.

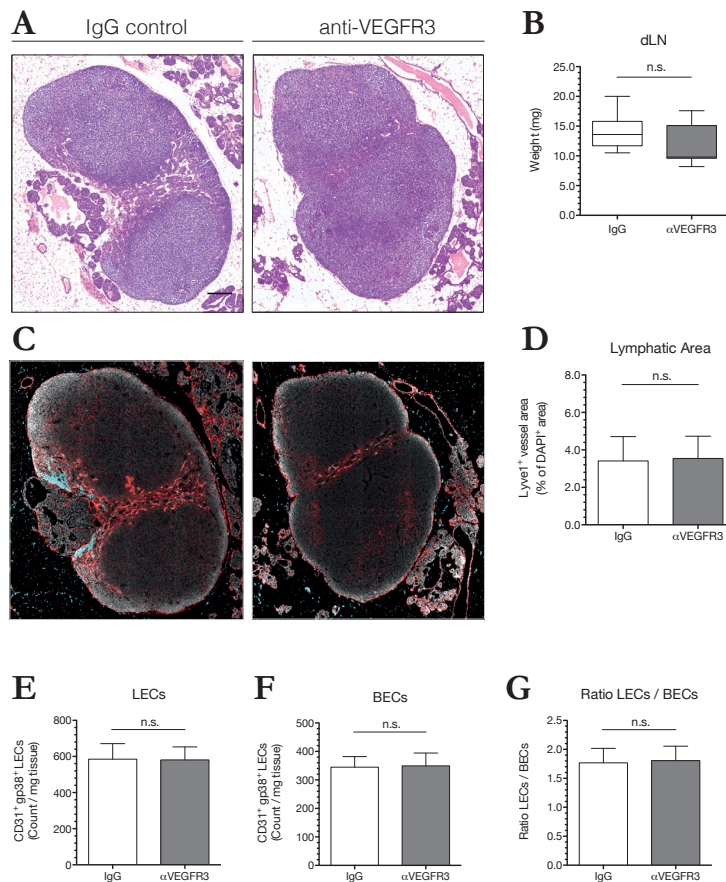


Fig. 4: Administration of an antagonistic antibody that ablates VEGFR3 signaling does not affect the sinusoidal lymphatic endothelium of the draining LN.

A Representative H&E image of the inguinal tumor-draining LN. Magnification 20x, scale bar 200 μ m. **B** Administration of mF4-31C1 does not affect the size of the draining LN, as shown by the LN weight upon termination of the treatment. Plotted values represent the weight of 3 pooled LNs, i.e. the brachial, axillary and inguinal LN. **C** Histological examination and **D** quantification of the lymphatic vessel area in the inguinal LN shows that mF4-31C1 does not affect the lymphatic endothelium in the draining LN. **E** Flow cytometry analysis confirmed these findings, as there was no change in the number of CD31⁺gp38⁺ LECs. **F** Analogous to the observations for the primary tumor, mF4-31C1 did also not affect the number of CD31⁺gp38⁺ BECs in the draining LN, also shown by **G** the ratio of LECs to BECs. Flow cytometry for vascular endothelial cells performed by Maria Broggi. Plotted values represent mean \pm SEM, statistical analysis by two-tailed unpaired Student's *t*-test. Experiment was performed once with *n* = 7 MMTV-PyMT⁺ transgenic animals per treatment group.

To validate the results obtained upon inhibition of VEGFR-3-signaling in MMTV-PyMT⁺ transgenic animals, I also aimed to perform similar experiments upon induction of lymphangiogenesis in the primary tumor. However, as previously described orthotopic models based on enhanced expression of VEGF-C all depend on the use of immune deficient animals due to the human origin of the cell lines that were utilized to inoculate the tumors, and as such limits the investigation of the interaction between lymphatic vessels and the tumor microenvironment, I set out to develop a novel model, which is described in section 3.2.

3.2 Development of an orthotopic tumor model to induce lymphatic vessel growth in the context of breast cancer

3.2.1 Production and titration of lentiviral vectors for transduction of murine breast cancer tumor cell lines

Lentiviral vector stocks for the generation of stable VEGF-C-overexpressing (i.e. VEGF-C⁺) or control murine breast cancer cell lines were generated by co-transfecting human embryonic kidney (HEK)293T cells with the pD2109-mVEGF-C or pD2109-control transfer plasmid, as well as packaging plasmids pMDLg/pRRE and pRSV-Rev, and envelope plasmid pMD2 to yield third-generation chimeric pseudo-lentiviral particles. Calculation of the physical titer from the total concentration of HIV-1-specific p24 antigen as determined by immunoassay yielded $4.69 \cdot 10^9$ and $1.86 \cdot 10^{10}$ pseudo-lentiviral particles of pD2109-mVEGF-C and pD2109-control per ml of unconcentrated vector supernatant, respectively. The biological titer, i.e. the number of infectious particles contained in each vector stock, was determined by TaqMan qPCR assay for HIV-1-specific *gag*, and yielded $1.62 \cdot 10^8$ and $2.31 \cdot 10^8$ transducing units (TU) per ml of unconcentrated vector for pD2109-mVEGF-C and pD2109-control lentiviral vector stocks, respectively. Calculation of the ratio of infectious particles to physical particles demonstrated an adequate packaging efficiency of 0.034 and 0.012 for the newly generated pD2109-mVEGF-C and pD2109-control vector stocks.

3.2.2 Characterization of stable VEGF-C⁺ and control breast cell lines *in vitro*

An invasive primary tumor cell line isolated from the spontaneous MMTV-PyMT mouse model of breast cancer, in the following abbreviated as PyMT tumor cells, were transduced with either pD2109-mVEGF-C or pD2109-control lentiviral vector stock (Fig. 5A) to yield stable VEGF-C⁺ or control-transduced cell lines, respectively. Upon incubation with a 1:1, 1:5 and 1:20 dilution of each vector stock, corresponding to a multiplicity of infection (MOI) of $8.10 \cdot 10^2$ and $1.16 \cdot 10^3$ for pD2109-mVEGF-C and pD2109-control in the highest dose, none of the cells demonstrated visible signs of lentiviral-mediated toxicity. To select only those tumor cells that stably integrated the proviral DNA into their genome, the tumor cells were incubated in the presence of 2 μ g/ml puromycin (Fig. 5B). The resulting polyclonal batch cultures were then analyzed for residual p24 antigen to ensure that no replication-competent recombinant pseudo-lentiviral particles had emerged (data not shown). Prior to functional experiments *in vivo*, each cell line was characterized extensively *in vitro* to ensure proper expression and secretion of the VEGF-C transgene, and that none of the VEGF-C⁺ or control PyMT tumor cell lines were compromised by artifacts induced by exposure to the lentiviral vectors used to generate each cell line. Determination of the number of proviral DNA copies that integrated into the genome of each VEGF-C- and control-transduced PyMT tumor cell line shows a higher genomic copy number of HIV-1-specific *gag* for each control-transduced cell line as compared to their VEGF-C-overexpressing counterpart,

reflecting the higher titer of the pD2109-control vector stock (Fig. 5C). However, the increased lentiviral copy number in control-transduced PyMT tumor cells did not affect cell proliferation rates as demonstrated upon determination of the generation time (Fig. 5D). Notably, solely the tumor cells transduced with the lowest MOI of pD2109-control vector stock showed a significant reduction in generation time. This observation, however, might rather represent an artifact in cell culture, as it is likely due to the fewer cells resulting after the initial selection of antibiotic-resistant cells. Finally, analysis of VEGF-C expression levels *in vitro* showed increased production and secretion of VEGF-C in PyMT tumor cells transduced with pD2109-mVEGF-C as compared to control-transduced PyMT tumor cells (Figs. 5E and 5F, respectively), demonstrating functional expression of the transgene. Therefore, the VEGF-C⁺ and control-transduced PyMT cell lines generated with the highest dose of lentiviral vector stock (i.e. dilution 1:1) were selected for all *in vivo* experiments described in the following sections.

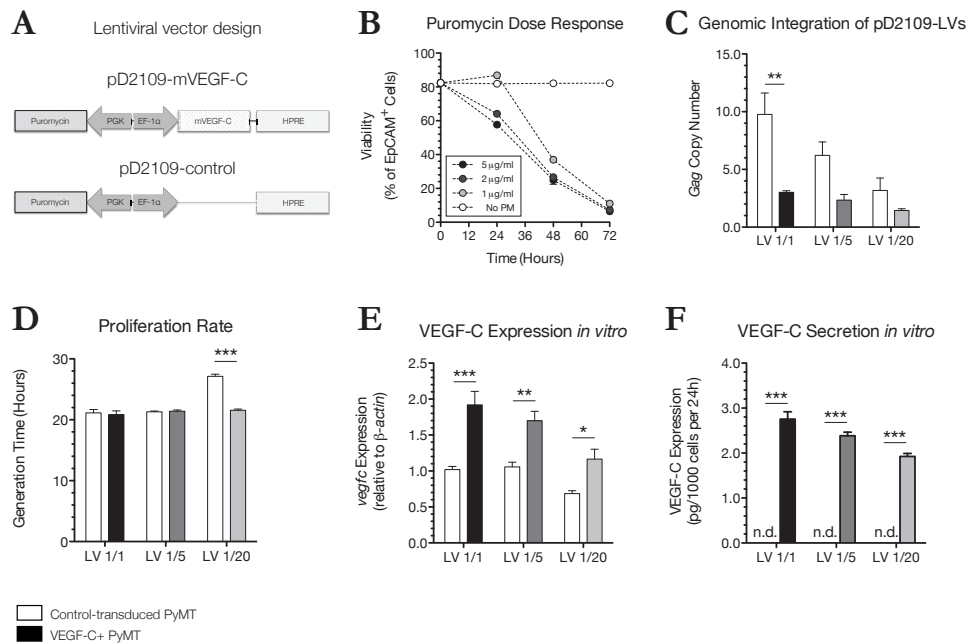


Fig. 5: Generation and characterization of newly generated VEGF-C⁺ and control-transduced breast cancer cell lines *in vitro*.

A Schematic representation of the lentiviral vectors used to generate both the VEGF-C⁺ PyMT tumor cell lines and their corresponding control-transduced counterparts. **B** Determination of the sensitivity of the parental PyMT tumor cell line to puromycin yielded an optimal dose of 2 μg/ml for selection of successfully transduced cell lines. **C** Analysis of the copy number of lentivirus that integrated into the genome upon incubation of the parental PyMT tumor cell line with each vector stock shows that cell lines transduced with pD2109-control vector stock had increased copy numbers, which was due to the higher titer of the lentiviral vector stock. **D** However, this did not affect cell behavior *in vitro* as based on determination of the proliferation rate. **E** Analysis of VEGF-C expression *in vitro* showed that the cell lines transduced with pD2109-mVEGF-C expressed increased VEGF-C at both the mRNA and **F** protein level. Statistical analysis by 2-way ANOVA. Two independent experiments were performed, one of two representative experiments shown.

3.2.3 Expression of VEGF-C within the tumor does not affect the growth rate of the primary tumor *in vivo*

Orthotopic inoculation of either $2.5 \cdot 10^5$ VEGF-C⁺ or control PyMT tumor cells into the fat tissue surrounding the inguinal mammary gland reproducibly led to the formation of tumors in the fat pad. The injection procedure and timeline for each experiment are illustrated in Fig. 6A, whereas a representative image of a tumor implanted in the fat pad, and its draining LN below the timeline. Enhanced expression of VEGF-C by the tumor cells did not accelerate the establishment of the primary tumor, nor did it affect its growth rate, though VEGF-C⁺ tumors were consistently slightly larger than control tumors (Fig. 6B). Pathology analysis of the lungs showed that the formation of pulmonary micrometastases occurred in the lungs of both VEGF-C⁻ and control-tumor-bearing animals 35 days post-tumor inoculation, though there was no difference in the incidence at this time point (1/10 or 10% in each group, Fig. 6C). Therefore, although the primary tumor can be observed to form distant metastases, these data suggest that it is likely too early to detect a difference in the rate of metastasis between VEGF-C⁺ and control tumor cells.

3.2.4 Expression of VEGF-C within the tumor reliably induces tumor-associated lymphangiogenesis *in vivo*

Although increased expression of VEGF-C did not affect tumor growth or the rate of pulmonary metastasis, VEGF-C⁺ tumors were observed to drive substantial peritumoral lymphangiogenesis and promote metastasis to the tumor-draining LN (see Fig. 8). Corresponding to enhanced expression of the transgene *in vitro*, VEGF-C⁺ PyMT tumor cells were found to secrete increased levels of VEGF-C *in vivo* as compared to their control-transduced counterparts, translating into a 44-fold increase in VEGF-C expression within the primary tumor (Fig. 6D). No significant difference could be observed in expression levels of either VEGF-D or VEGF-A within the tumor (Figs. 6E and F, respectively), indicating that any expansion of tumor-associated vessels is due to increased expression and secretion of VEGF-C. Overexpression of VEGF-C specifically induced lymphangiogenesis in and around the primary tumor, as the number of CD31⁺gp38⁺ LECs within VEGF-C⁺ tumors significantly increased as compared to control tumors, whereas the number of CD31⁺gp38⁻ BECs did not change (Figs. 7A-C). Interestingly, in addition to CD31 and gp38, more than 90% of the LECs isolated from VEGF-C⁺ tumors were observed to also express lyve-1, a marker that is mainly found on lymphatic capillaries, suggesting that increased VEGF-C expression first and foremost induced expansion of initial lymphatic vessels surrounding the tumor (see Fig. 7D). Histological analysis of the primary tumor confirmed these findings, as newly formed lymphatic vessels were almost exclusively found peritumorally (Fig. 7D an E, respectively). In addition, these lymphatic capillaries were also observed to express VEGFR-3 (Fig. 7D). However, histological analysis and quantification of the CD31⁺lyve-1⁻ blood vessel area also showed an increase upon increased expression of VEGF-C, suggesting that VEGF-C may not solely affect tumor-associated lymphatic

vessels (Fig. 7F). In conclusion, these results thus provide proof-of-concept that inoculation of VEGF-C⁺ tumor cells within the fat surrounding the inguinal mammary gland reliably induces the formation of lymphangiogenic tumors *in vivo*, thereby demonstrating that the chosen method is a feasible strategy for the development of an orthotopic tumor model that allows modulation of tumor-associated lymphatic vessels *in vivo* in the context of breast cancer.

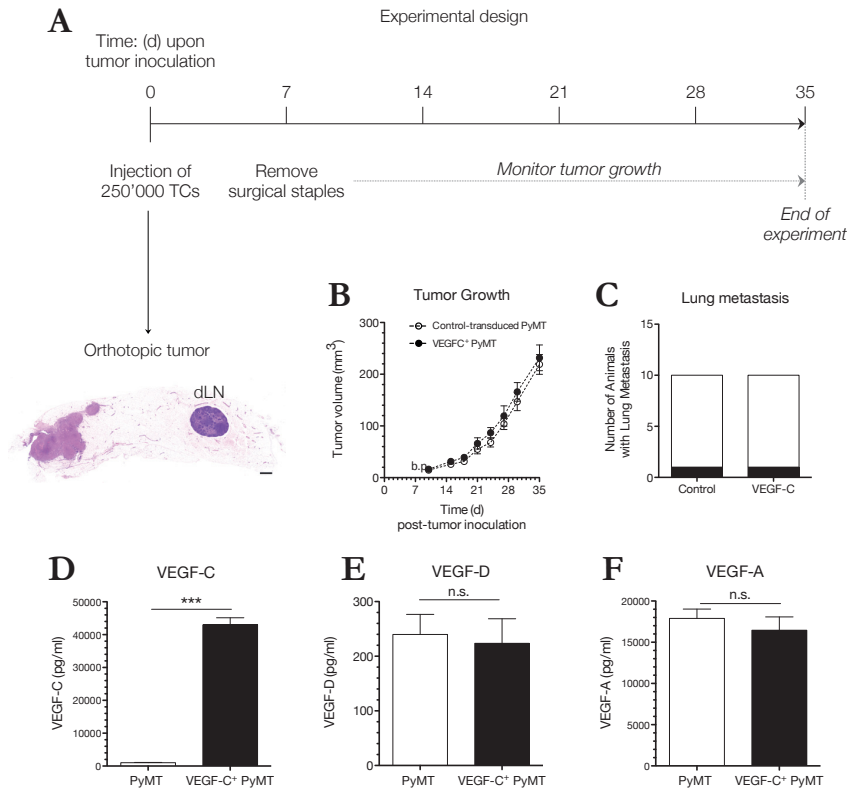


Fig. 6: Experimental design and characterization of tumor growth after orthotopic injection of VEGF-C⁺ and control-transduced breast cancer cell lines *in vivo*.

A Experimental design for orthotopic injection of VEGF-C⁺ PyMT tumor cells into the inguinal mammary fat tissue of 8-10 week old female FvB/N WT mice. All experiments described in the following were terminated at 4.5-5 weeks post-tumor inoculation, at which point in time the blood and lymphatic vasculature, as well as the composition of the tumor microenvironment were analyzed, respectively. The image shown below the timeline depicts a representative H&E-stained longitudinal section of a tumor inoculated into the fat tissue surrounding the inguinal mammary gland and its draining LN. Magnification 20x, scale bar 1 mm. **B** Tumors inoculated upon injection of VEGF-C⁺ or control-transduced PyMT tumor cells did not show a difference in growth rate, nor in **C** the rate of pulmonary metastasis formation (filled part of each bar). **D** Consistent with the analysis of the newly generated cell lines *in vitro*, orthotopic inoculation of sVEGF-C⁺ PyMT tumor cells yields tumors with enhanced VEGF-C expression as compared to injection of control-transduced tumor cells, translating into a 44-fold difference in expression levels. **E** While VEGF-C expression is enhanced, expression levels of VEGF-D and **F** VEGF-A are not affected. Plotted values represent mean \pm SEM, statistical analysis by two-tailed unpaired Student's *t*-test. Tumor growth was measured in 4 out of 5 experiments, evaluation of pulmonary metastasis in one experiment. Figs. 6D-F show one out of two representative experiments for analysis of expression levels of VEGF family members. All experiments were performed with *n* = 10 animals per group.

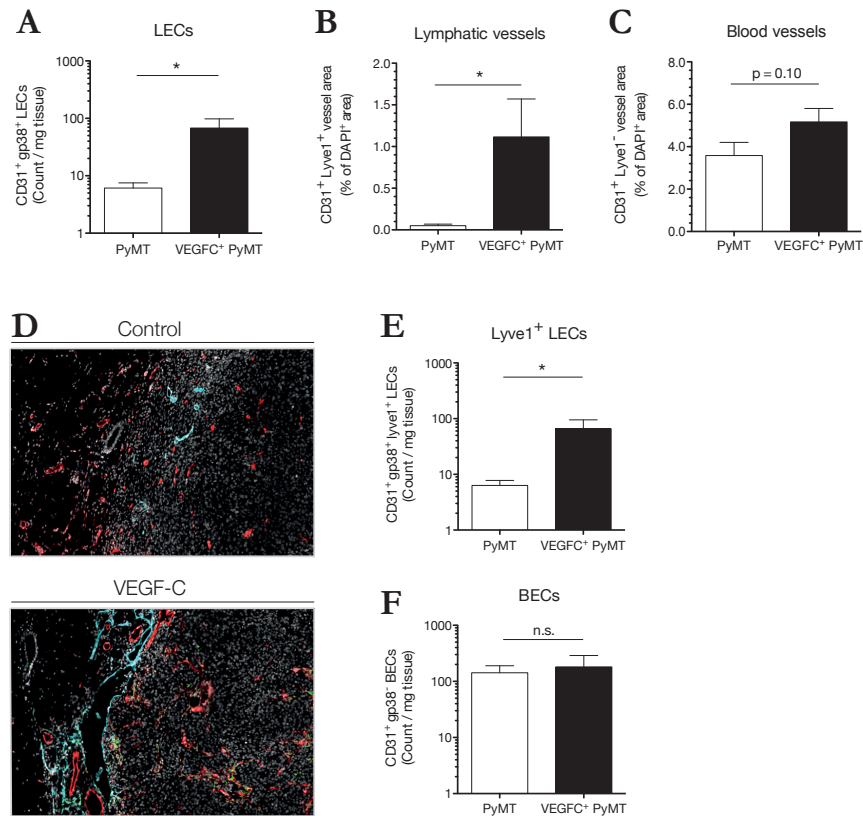


Fig. 7: Orthotopic injection of VEGF-C⁺ breast cancer cell lines *in vivo* reproducibly leads to the formation of tumors that are rich in lymphatic vessels.

A VEGF-C overexpression reproducibly resulted in the formation of lymphangiogenic tumors *in vivo*, as the number of CD31⁺gp38⁺ LECs was increased in these tumors as compared to control tumors. **B** More than 90% of the LECs found in VEGF-C⁺ tumors also expressed lyve1, suggesting an expansion of initial lymphatic vessels. **C** In contrast, orthotopic inoculation of VEGF-C⁺ PyMT tumor cells did not affect the number of CD31⁺gp38⁺ BECs found in the tumor, as compared to control tumors. **D** Histological analysis demonstrated that increased VEGF-C expression led to the formation of peritumoral lymphatic vessels. Immunofluorescence for CD31 (red), lyve-1 (teal) and VEGFR-3 (green) shows that, whereas blood vessels were found scattered throughout the tumor, the formation of new lymphatic vessels was largely induced at the tumor periphery. Immunofluorescence for VEGFR-3 (green) showed its expression on most of lyve-1⁺ lymphatic vessels surrounding the tumor, though it could also be detected on some lyve-1⁻ vessels. Magnification 20x. **E** Quantification of the percentage of positive CD31⁺lyve-1⁺ lymphatic vessel area showed a significant increase in the area covered by newly induced lymphatic vessels, whereas **F** quantification of the percentage of positive CD31⁺lyve-1⁻ blood vessel area revealed also an increase the area covered by blood vessels in VEGF-C⁺ as compared to control tumors, albeit not significant. Plotted values represent the average of 3 imaging planes. All experiments were performed twice, one of two representative experiments shown. Plotted values show mean \pm SEM, statistical analysis performed with two-tailed unpaired Student's *t*-test. All experiments were performed with $n = 10$ animals per group.

3.2.5 Disseminated VEGF-C⁺ tumor cells induce expansion of the sinusoidal lymphatic endothelium in the draining LN

Given the clinical relevance of tumor-associated lymphangiogenesis for regional and distant metastasis in breast cancer, I next examined the inguinal tumor-draining LN for the presence of disseminated tumor cells upon reaching the legal size limit of the primary tumor 35 days post-tumor inoculation. Although enhanced expression of VEGF-C did not affect the growth of the primary tumor, VEGF-C⁺ PyMT tumor cells more readily metastasized to the inguinal tumor-draining LN than control-transduced tumor cells. In line with previous observations, the draining LNs of VEGF-C⁺ tumors were found to be greatly enlarged compared to the draining LNs downstream of control tumors, which is reflected in a three-fold increase in LN weight (Figs. 8A and B, respectively, (Skobe et al., 2001a)). Concurrently, a notable expansion of the lymphatic vascular network within the inguinal draining LN downstream of VEGF-C⁺ tumors was observed, as the total number of CD31⁺gp38⁺ LECs was found to be significantly increased in VEGF-C⁺ tumor-draining LNs as compared to control tumor-draining LNs (Fig. 8C). Tumor cell-derived VEGF-C, however, did not affect the number of CD31⁺gp38⁺ BECs within the draining LN, thus increasing the ratio of LECs to BECs within the VEGF-C⁺ tumor-draining LN (Figs. 8D and E, respectively). Histological examination of VEGF-C⁺ and control tumor-draining LNs confirmed the expansion of the lymphatic sinusoidal endothelium within the VEGF-C⁺ tumor-draining LNs (Fig. 8F). Moreover, in addition to expression of lyve-1, these enlarged lymphatic structures were also found to be positive for VEGFR-3 (Fig. 8F). Finally, immunostaining for the PyMT antigen revealed an increased presence of tumor cells in the tumor-draining LNs downstream of VEGF-C⁺ tumors as compared to those downstream of control tumors (Figs. 8F and H, respectively). Interestingly, all disseminated tumor cells were found in close proximity to the lymphatic vessels of the LN. In conclusion, these results demonstrate that VEGF-C-induced peritumoral lymphangiogenesis around the primary tumor promotes regional dissemination of the tumor cells to the tumor-draining LN, while subsequent remodeling of the lymphatic endothelium in the draining LN may yield a favorable environment for metastasis progression.

Taken together, these data show that experimental modulation of tumor-associated lymphatic vessels can be achieved upon both inhibition, as well as induction of the VEGF-C /VEGFR-3 signaling axis in different experimental models of breast cancer. Section 3.3 will subsequently address the interaction of the lymphatic vasculature with the various components, i.e. the desmoplastic stroma, the innate inflammatory response, and T-cell mediated adaptive immunity, of the tumor microenvironment.

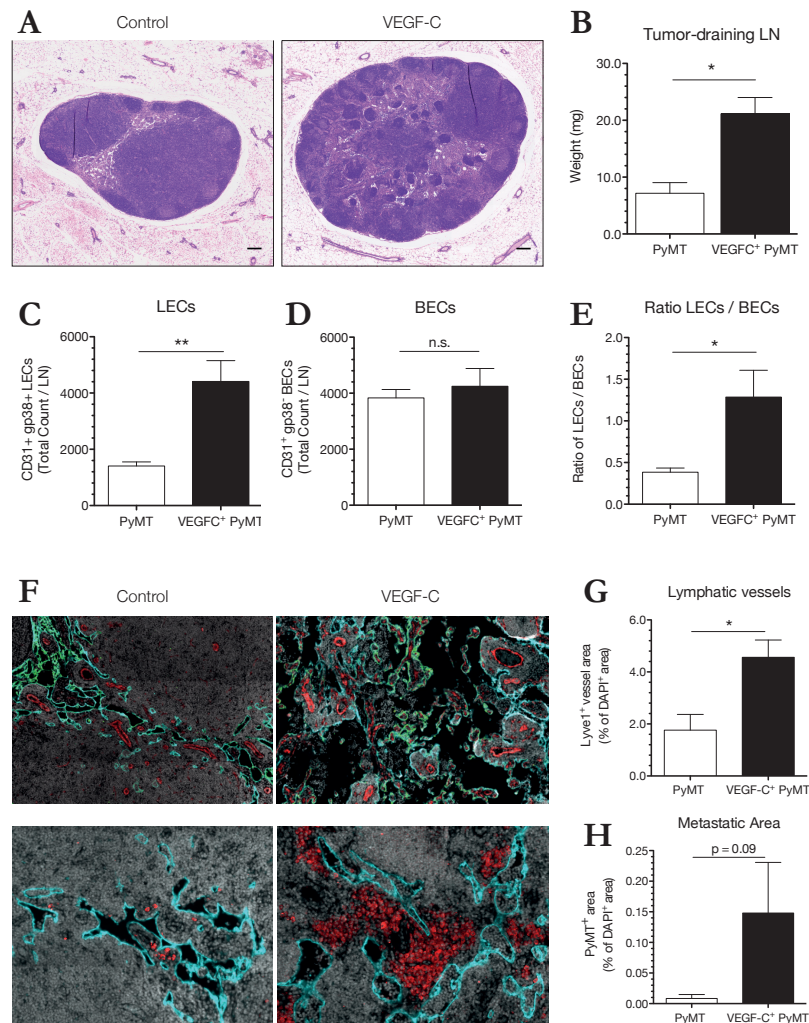


Fig. 8: Orthotopic inoculation of VEGF-C⁺ tumors promotes regional metastasis of the primary tumor to the tumor-draining LN.

A Tumor-draining inguinal LNs downstream of VEGF-C⁺ tumors are greatly enlarged as compared to those downstream of control tumors. H&E, magnification 20x, scale bar 200 μ m. **B** This enlargement is also reflected by a three-fold increase in the weight of the VEGF-C⁺ tumor-draining LN. **C** Concurrently, an expansion of the lymphatic sinusoidal endothelium was observed in the tumor-draining LN, as the number of CD31⁺gp38⁺ LECs was significantly increased in LNs draining VEGF-C⁺ tumors. **D** Similarly to the effects of VEGF-C on the vasculature described for the primary tumor, the number of CD31⁺gp38⁻ BECs in the draining LN was not affected. **E** The specific expansion of LN LECs is also reflected in the ratio of LECs to BECs in the draining LN. **F** Histological analysis of the tumor-draining LN showed a distorted architecture of the lymphatic network in the LN, with enlarged lumens. Magnification 20x. **G** Quantification of the percentage of area covered by lyve-1⁺ lymphatic vessels confirmed the induction of LN lymphangiogenesis in the VEGF-C⁺ tumor-draining LN. Values represent the average of 3 imaging planes. **H** Staining for the PyMT antigen (red) revealed the presence of tumor cells in the draining LN, in particular in close proximity to the lymphatic vessels. Magnification 20x. **I** Quantification of the relative area of the tumor cells in the tumor-draining LN showed an increase in the size of the metastatic lesions in the LN, as, in contrast to the single cells in control tumor-draining LNs, large clusters of tumor cells could be detected in VEGF-C⁺ tumor-draining LNs, suggesting that VEGF-C expression in the primary tumor promotes regional metastasis of the primary tumor. Plotted values represent mean \pm SEM of n = 10 animals per group, statistical analysis with two-tailed unpaired Student's *t*-test.

3.3 Deconvolution of the breast cancer microenvironment during tumor growth and progression, and its interactions with tumor-associated lymphatic vessels

3.3.1 Tumor-associated lymphatic vessels do not alter the desmoplastic response that accompanies incipient tumors

The notion that not only changes in aberrant neoplastic cells (i.e. tumor-intrinsic factors), but also the surrounding tumor stroma, consisting of both tissue-resident and recruited ancillary cells (i.e. tumor-extrinsic factors), substantially contribute to tumor initiation, progression and metastasis gave rise to the concept of the tumor microenvironment (Hanahan and Weinberg, 2000). The MMTV-PyMT model of breast cancer currently represents the gold standard to investigate the interactions between the tumor and its associated stroma, as well as possible ramifications for tumor growth, progression and metastasis. Similar to human breast cancer, developing tumors in MMTV-PyMT⁺ transgenic mice are associated with the induction of a substantial reactive stroma that results in altered tensional homeostasis upon co-evolution of the transformed epithelium and the fibroblasts of the connective tissue. To investigate how tumor-associated lymphatic vessels may alter the desmoplastic response in breast cancer, I first characterized the expanse and composition of the ECM in transgenic MMTV-PyMT⁺ tumor-bearing mice during tumor growth and progression. Histological analysis of the total collagen content in invasive carcinomas by picrosirius red staining showed that, similar to human breast cancer, incipient tumors in MMTV-PyMT⁺ transgenic mice are associated with the induction of a considerable reactive stroma (Fig. 9A). Furthermore, expression of lysyl oxidase (LOX), the principal enzyme that mediates crosslinking of collagen fibers, coincided with the presence of newly deposited collagen within the tumor stroma (Fig. 9A, right). Quantification of the total collagen content in the tumor confirmed these observations (Fig. 9C). Corresponding to the enhanced production of ECM, increased expression of TGF- β 1 was detected in developing tumors in MMTV-PyMT⁺ transgenic mice as compared to age-matched WT littermate controls (Fig. 9B). Interestingly, TGF- β 1 expression levels appeared more elevated in early hyperplastic lesions than invasive carcinomas, suggesting that TGF- β 1-mediated CAF activation generates the reactive stroma that surrounds the transformed epithelium.

Nevertheless, inhibition of VEGFR-3-mediated signaling upon administration of mF4-31C1 in transgenic MMTV-PyMT⁺ tumor-bearing mice did not reduce the deposition of fibrillar collagens at the tumor margin compared to IgG-treated control animals, as demonstrated by picrosirius red staining and subsequent quantification of collagen density (Figs. 9D and E, respectively). Furthermore, upon closer examination of other constituents of the desmoplastic stroma, administration of mF4-31C1 did also not notably alter the density of either collagen-III, fibronectin, or tenascin-C at the tumor margin, respectively (Figs. 10A-F). Collectively, these results demonstrate that tumor-associated lymphatic vessels do not alter the induction or expanse of the desmoplastic response in the transgenic MMTV-PyMT model of breast cancer.

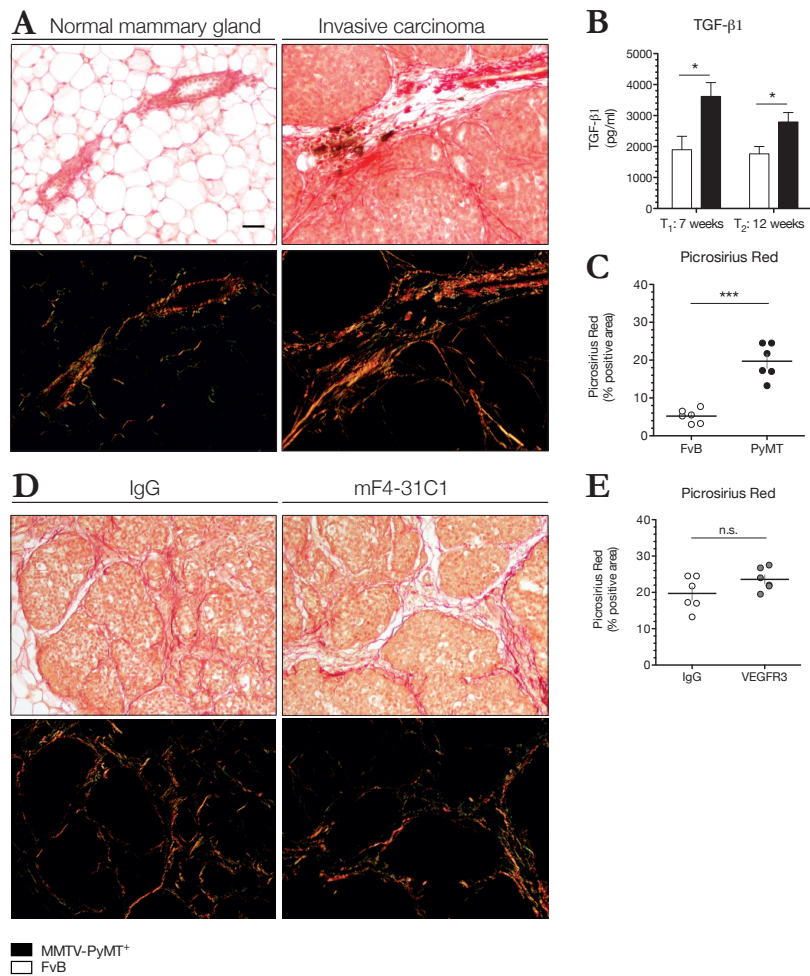


Fig. 9: Tumor growth and progression in the transgenic MMTV-PyMT model of breast cancer is accompanied by increased collagen deposition and crosslinking.

A Invasive lesions in transgenic MMTV-PyMT⁺ tumor-bearing animals show increased deposition of collagen in the stroma as compared to age-matched WT littermate controls. Visualization of these invasive lesions under polarized light shows the collagen fibrils, which are thicker and more cross-linked in the tumor. Immunohistochemistry for LOX (brown) shows that the principal enzyme that mediates cross-linking of the newly deposited collagen spatially coincides with thick bundles of collagen fibrils during tumor progression. Magnification 20x, scale bar 50 μ m. **B** Immunoassay for TGF- β 1 shows elevated levels in MMTV-PyMT⁺ tumor-bearing animals as compared the levels in the inguinal mammary gland in WT FvB/N mice, particularly in hyperplastic lesions. **C** Quantification of the density of total collagen shows an increase in collagen deposition in the tumor as compared to WT tumor-free mice. **D** Evaluation of the desmoplastic response upon administration of mF4-31C1 in MMTV-PyMT⁺ transgenic mice does not notably alter the deposition of collagen in the desmoplastic stroma compared to IgG-treated control animals, which is **E** confirmed by quantification of the relative fraction of collagen at the invasive margin of the tumor. Plotted values represent mean \pm SEM, statistical analysis with two-tailed unpaired Student's *t*-test. Experiment was performed once with *n* = 7 MMTV-PyMT⁺ transgenic animals per treatment group.

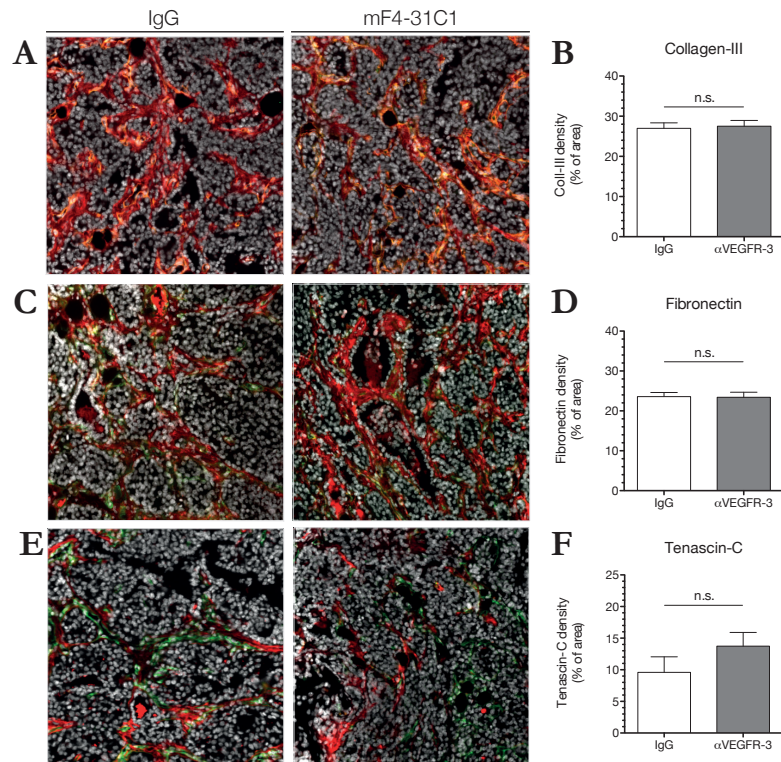


Fig. 10: Inhibition of VEGFR-3-mediated signaling in transgenic MMTV-PyMT⁺ tumor-bearing mice did not affect ECM deposition at the invasive edge of the tumor.

A Inhibition of VEGFR-3-mediated signaling with an antagonistic antibody in MMTV-PyMT⁺ tumor-bearing animals did not notably alter the total deposition or the composition of the fibrillar ECM in the desmoplastic stroma surrounding invasive carcinomas, as compared to IgG-treated control animals. Specifically, immunofluorescence for different components of the fibrillar ECM, i.e. collagen-III, **C** fibronectin, and **E** tenascin-C (all shown in red) showed no difference in the density of these ECM components in invasive lesions upon termination of the treatment with mF4-31C1 in MMTV-PyMT⁺ tumor-bearing mice as compared to IgG-treated control animals. The basement membrane is visualized upon immunofluorescence for collagen-IV (which is shown in green), and used to define the invasive edge of the tumor, as it is disrupted once the tumor invades the surrounding stroma. Quantification of the density of each of these ECM components, i.e. collagen-III, fibronectin and tenascin-C, is shown in **B**, **D**, and **F**, respectively. Plotted values represent mean \pm SEM, statistical analysis with two-tailed unpaired Student's *t*-test. Experiment was performed once with $n = 7$ MMTV-PyMT⁺ transgenic animals per treatment group.

3.3.2 Tumor-associated lymphatic vessels do not alter the innate immune response to the developing tumor

Long since the initial description of the link between inflammation and cancer, innate immune cell infiltrates have now been recognized as a major component of the tumor immune microenvironment, and have been observed to potentiate cancer development (de Visser et al., 2006). As lymphangiogenesis is a process that is closely associated with inflammation, I next asked whether the modulation of components of the VEGF-C / VEGFR-3 signaling axis in different experimental models of breast cancer could affect the innate immune response to the tumor.

First, in order to determine whether inhibition of VEGFR-3-mediated signaling upon treatment with mF4-31C1 might affect the innate inflammatory cells within the incipient tumor, I characterized the infiltration of the different myeloid cell populations during tumor growth and progression in the MMTV-PyMT model of breast cancer by flow cytometry. Overall, although the percentage of CD11b⁺ cells of the myeloid lineage remained the same at either tumor stage in MMTV-PyMT⁺ tumor-bearing animals as compared to age-matched WT littermate controls, the number of CD11b⁺ myeloid cells increased in both hyperplastic and invasive lesions (Figs. 11A and D, respectively). Furthermore, while among the CD11b⁺ myeloid cells that were present in hyperplastic lesions the infiltration of Ly6C⁺F4/80⁻ monocytes did not change, a significant increase in the fraction of F4/80⁺ tumor-associated macrophages (TAMs) could be observed as compared to WT tumor-free mice, that also continued to further increase as the developing tumors progressed (Figs. 11B and C, respectively). Nevertheless, though analysis of the number of infiltrating F4/80⁺ TAMs confirmed the increase seen in the relative fraction of these cells, analysis of the number of infiltrating Ly6C⁺F4/80⁻ monocytes showed an increase in inflammatory monocytes, particularly in invasive carcinomas, thus demonstrating an increase in cells of the myeloid lineage in late-stage tumors in MMTV-PyMT⁺ tumor-bearing mice as compared to the untransformed inguinal mammary gland in WT tumor-free mice (Figs. 11E and F). Interestingly, the majority of the infiltrating TAMs were strongly polarized towards an inflammatory CD11c⁺ M1-like phenotype in both hyperplastic and invasive lesions, whereas an increase in pro-tumor CD206⁺ M2-like TAMs could only be observed in late-stage tumors (Figs. 11G, H, J and K, respectively). Considering the overall ratio of CD11c⁺ M1-like to CD206⁺ M2-like TAMs in these tumors, the phenotype of infiltrating TAMs shows a strong bias towards an M1-like phenotype, implying that tumor development in the MMTV-PyMT model is accompanied by a potent inflammatory response that is mediated by TAMs, especially during tumor onset in early lesions (Fig. 11I).

Fig. 11: Early hyperplastic lesions in the MMTV-PyMT model of breast cancer are accompanied by a potent inflammatory reaction to the developing tumor. ►

A Flow cytometry analysis of developing hyperplastic lesions and invasive carcinomas revealed that although the relative CD11b⁺ myeloid cell infiltration does not change at either time point, significant differences in subsets of CD11b⁺ myeloid cells do occur. **B** While the infiltration of inflammatory monocytes did not change over time, **C** a significant infiltration of TAMs could be observed in hyperplastic lesions, which continues as the tumor progresses towards an invasive lesion. **D** Analysis of

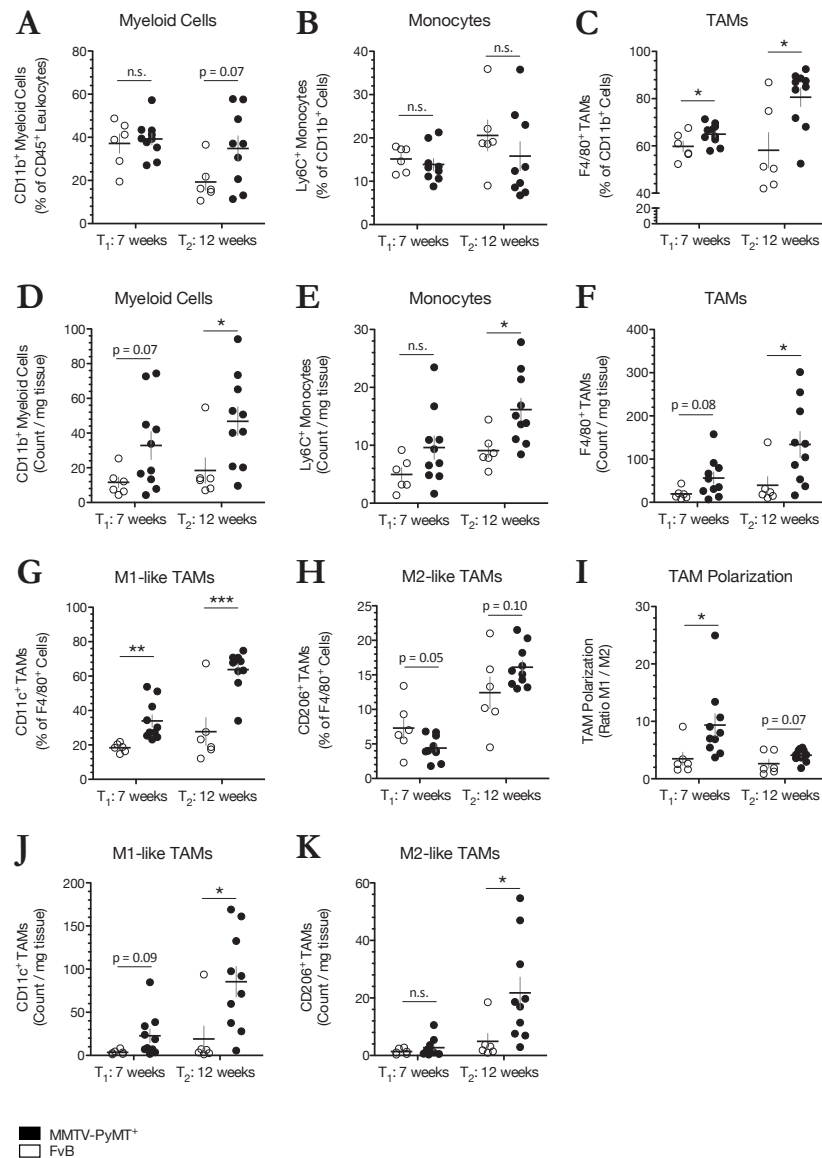


Fig. 11: Early hyperplastic lesions in the MMTV-PyMT model of breast cancer are accompanied by a potent inflammatory reaction to the developing tumor, continued from p. 64.

the number of infiltrating cells of the myeloid lineage, however, shows that total CD11b⁺ myeloid cells, as well as **E** Ly6C⁺F4/80⁻ monocytes and **F** Ly6C⁺F4/80⁺ TAMs are increased in invasive carcinomas of MMTV-PyMT⁺ tumor-bearing mice as compared to the inguinal mammary gland in WT tumor-free mice. **G** TAMs showed a strong polarization towards a CD11c⁺ M1-like phenotype both at both tumor stages, whereas **H** the fraction of CD206⁺ M2-like TAMs did not change until the tumors progressed to late-stage carcinomas, **I** resulting in a bias towards increased M1-polarization, especially at tumor onset. **J** Analysis of the number of CD11c⁺ M1-like and **K** CD206⁺ M2-like TAMs also showed the relative prevalence of the M1-like phenotype in the transformed mammary gland in MMTV-PyMT⁺ transgenic mice at both time points. Plotted values represent mean \pm SEM, statistical analysis by two-tailed unpaired Student's *t*-test. Experiment was performed once with *n* = 10 transgenic MMTV-PyMT⁺ animals and *n* = 6 FvB WT littermate controls per group, respectively.

Nevertheless, administration of mF4-31C1 in transgenic MMTV-PyMT⁺ tumor-bearing mice did not notably alter the innate immune response to the tumor. First of all, the overall infiltration of CD11b⁺ myeloid cells, neither the relative fraction nor the number, did not change in α -VEGFR-3-treated MMTV-PyMT⁺ tumor-bearing mice, as compared to IgG-treated animals (Figs. 12A and D, respectively). Furthermore, among these infiltrating CD11b⁺ myeloid cells, mF4-31C1-mediated inhibition of VEGFR-3 signaling did not result in any difference in the relative fractions or the number of Gr1⁺F4/80⁻ myeloid-derived suppressor cells (MDSCs) or Gr1⁺F4/80⁺ TAMs (Figs. 12B, C, E and F, respectively). A closer examination of the phenotype of the infiltrating TAMs also showed no difference in TAM phenotype, as the fractions of CD11c⁺ M1-like and CD206⁺ M2-like TAMs within the tumor remained the same, which is also reflected in the ratio of CD11c⁺ M1-like to CD206⁺ M2-like TAMs that did not change upon termination of the treatment (Figs. 12G, H, and I, respectively). Analysis of the number of CD11c⁺ M1-like, as well as the number of CD206⁺ M2-like TAMs confirmed these findings, as also no difference in the number of TAMs with either phenotype could be observed upon termination of the treatment with mF4-31C1 in MMTV-PyMT⁺ tumor-bearing animals, as compared to IgG-treated animals (Figs 12J and K, respectively). In conclusion, these data thus demonstrate that, although tumor onset in the MMTV-PyMT model is associated with a strong inflammatory response mediated by TAMs within the developing tumors, inhibition of VEGFR-3-mediated signaling does not affect the innate immune response, and TAMs in particular, to the tumor in this particular model.

Fig. 12: Inhibition of tumor-associated lymphangiogenesis in the MMTV-PyMT model of breast cancer does not alter tumor-related inflammation in the primary tumor. ►

A Flow cytometry analysis showed that administration of mF4-31C1 in transgenic MMTV-PyMT⁺ tumor-bearing mice does not alter the fraction of CD11b⁺ myeloid cells of the innate immune system in the primary tumor, as compared to IgG-treated control animals. **B** Furthermore, among the infiltrating CD11b⁺ myeloid cells in the tumor, neither the fraction of Gr1⁺ MDSCs nor **C** the fraction of Gr1⁺F4/80⁺ TAMs changed in α -VEGFR-3-treated MMTV-PyMT⁺ tumor-bearing mice as compared to IgG-

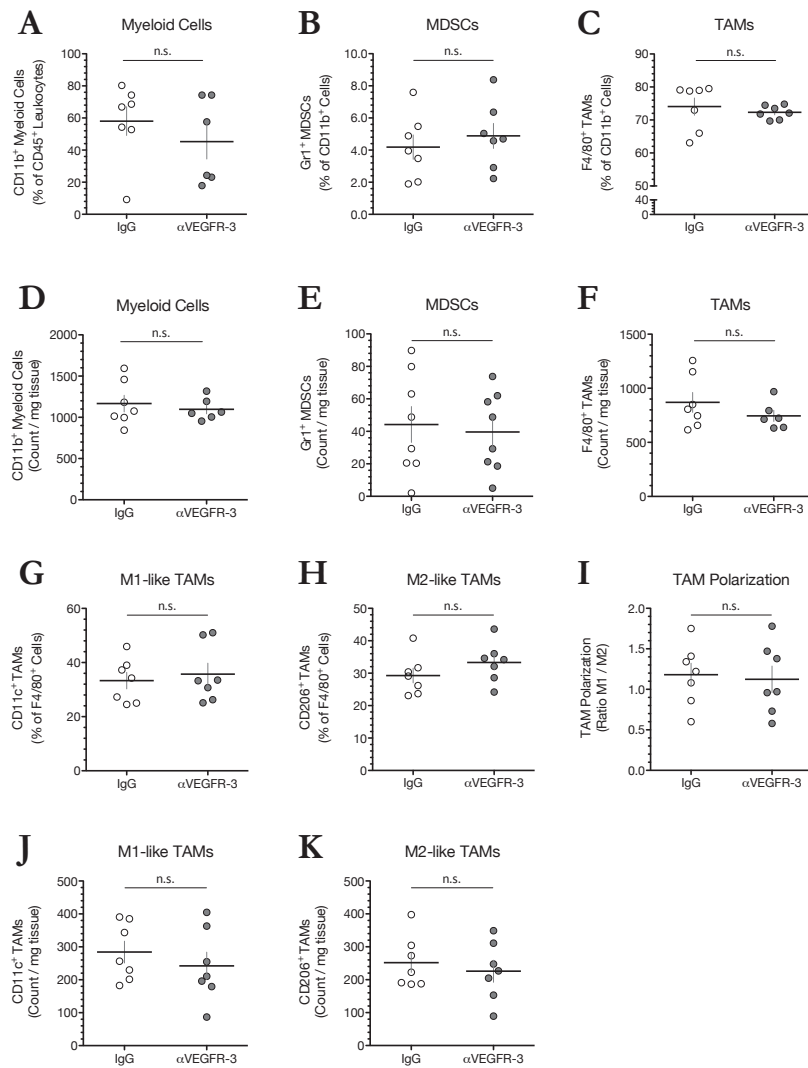


Fig. 12: Inhibition of tumor-associated lymphangiogenesis in the MMTV-PyMT model of breast cancer does not alter tumor-related inflammation in the primary tumor, continued from p. 66.

treated control animals. **D** Analysis of the number of infiltrating CD11b⁺ myeloid cells confirmed these findings, as also the number of these cells did not change upon termination of the treatment. **E** Similarly, the number of Gr1⁺ MDSCs or **F** Gr1⁺F4/80⁺ TAMs remained the same, confirming that abrogated VEGFR-3 signaling upon administration of mF4-31C1 did not affect myeloid cell infiltration into the tumor. **G** Finally, administration of mF4-31C1 did also not affect the phenotype of infiltrating TAMs, as the fractions of CD11c⁺ M1-like or **H** CD206⁺ M2-like TAMs, and consequently **I** the ratio of M1- to M2-like TAMs in the tumor did not change. **J** Analysis of the number of TAMs with either phenotype also showed that inhibition of VEGFR-3-mediated signaling did not affect the prevalence of CD11c⁺ M1-like or **K** CD206⁺ M2-like TAMs in the tumor. Plotted values represent mean ± SEM, statistical analysis by two-tailed unpaired Student's *t*-test. Experiment was performed once with *n* = 7 MMTV-PyMT⁺ transgenic animals per treatment group.

Conversely, enhanced expression of VEGF-C in the primary tumor upon orthotopic inoculation of VEGF-C⁺ PyMT tumor cells into the inguinal fat pad of immune competent FvB/N mice was also not observed to exert a noticeable effect on the immune response to the developing tumor. As shown in Fig. 13A, increased expression levels of VEGF-C did not influence the overall infiltration of CD45⁺ leukocytes into the tumor. Furthermore, there was no difference in the relative engagement of either the innate or the adaptive arm of immunity, as defined by the influx of CD11b⁺ innate cells of the myeloid lineage, NK1.1⁺ innate NK cells of the lymphocyte lineage, and TCRβ⁺ lymphocytes of the acquired immune response (Fig. 13B).

To determine whether VEGF-C-induced lymphangiogenesis affects the innate immune response to the incipient tumor, again I first characterized the CD11b⁺ cells of the myeloid lineage in more detail, analogous to the description of innate immunity in transgenic MMTV-PyMT⁺ animals above. NK cells, as cells of the innate immune system, but of the lymphocyte lineage will be discussed together with the T lymphocytes of the adaptive immune system in section 3.3.3. Analysis of the CD11b⁺ myeloid cells within the tumor demonstrated that expression of VEGF-C in the primary tumor does not affect their overall recruitment, as no difference could be observed in the percentage or number of CD11b⁺ myeloid cells that was present in VEGF-C⁺ or control tumors, respectively (Figs. 13C and F). Moreover, upon further exploration of the various cells of the myeloid lineage in the tumor, there was also no difference in the proportion or the number of Ly6G⁺Ly6C⁻F4/80⁻ neutrophils, or Ly6G⁻Ly6C⁺F4/80⁻ inflammatory monocytes in the tumor (Figs. 13D and E, as well as G and H, respectively). Likewise, increased expression levels of VEGF-C did not affect the overall infiltration of Ly6G⁻Ly6C⁺F4/80⁺ TAMs (Figs. 14A and B). RNA sequencing of F4/80⁺ TAMs isolated from invasive carcinomas of MMTV-PyMT⁺ transgenic mice showed that TAMs do not express VEGFR-3, thus demonstrating that modulation of the VEGF-C / VEGFR-3 signaling axis could not affect the recruitment of TAMs in this particular model (Fig. 14C). Interestingly, while tumors that formed upon orthotopic inoculation of PyMT tumor cells in the fat tissue surrounding the mammary gland contained a similar fraction of TAMs as invasive carcinomas in MMTV-PyMT⁺ transgenic mice of 12 weeks of age, contrary to the genetically engineered model, the phenotype of the TAMs present in these tumors showed a strong polarization towards an M2-like phenotype, as shown by the ratio of CD11c⁺ M1-like to CD206⁺ M2-like TAMs (Fig. 14F, compare with Fig. 11I). However, though both models show an inherent difference in the predominant TAM phenotype, increased expression of VEGF-C did not alter the polarization of the TAMs present, as the relative distribution of CD11c⁺ M1-like or CD206⁺ M2-like TAMs did not change in VEGF-C⁺ or control tumors, respectively (Figs. 14G and H).

Overall, the results obtained upon inhibition of VEGFR-3-mediated signaling within the tumor, as well as by induction of tumor-associated lymphangiogenesis upon enhanced expression of VEGF-C in the tumor are consistent between both models, and demonstrate that modulation of lymphatic vessels through the VEGF-C / VEGFR-3 signaling axis does not alter the innate inflammatory response mediated by cells of the myeloid lineage, and TAMs in particular, to the tumor.

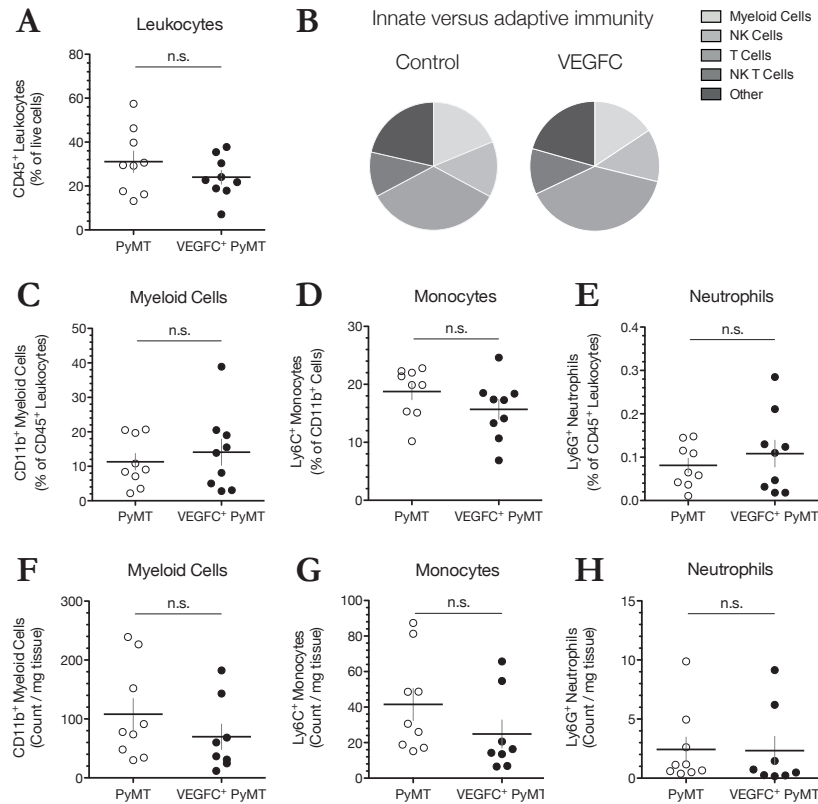


Fig. 13: Enhanced VEGF-C expression in the primary tumor does not affect the innate immune cells of the myeloid lineage.

A Increased expression levels of VEGF-C in the primary tumor did not alter overall CD45⁺ leukocyte infiltration, as determined by flow cytometry. **B** Furthermore, among the infiltrating leukocytes, there was no difference in the relative engagement of the innate or adaptive arm of the immune response in VEGF-C⁺ tumors as compared to control tumors. **C** Total CD11b⁺ myeloid cell infiltration did not change upon increased VEGF-C expression in the primary tumor. **D** Among the CD11b⁺ cells within the tumor, the relative fractions of Ly6G⁺Ly6C⁺F4/80⁻ inflammatory monocytes or **E** of Ly6G⁺ neutrophils did also not change with increased VEGF-C levels. **F** Consistent with the observation that the fraction of CD11b⁺ myeloid cells did not change in VEGF-C⁺ tumors, the number of infiltrating CD11b⁺ myeloid cells also remained the same upon orthotopic inoculation of VEGF-C⁺ tumor cells, as compared to control tumor cells. **G** Likewise, the number of Ly6G⁺Ly6C⁺F4/80⁻ inflammatory monocytes or **H** Ly6G⁺ neutrophils also remained the same in VEGF-C⁺ tumors. Plotted values show mean \pm SEM, each dot represents one animal. Statistical analysis performed with two-tailed Student's *t*-test. Experiment was performed once with *n* = 10 animals per group.

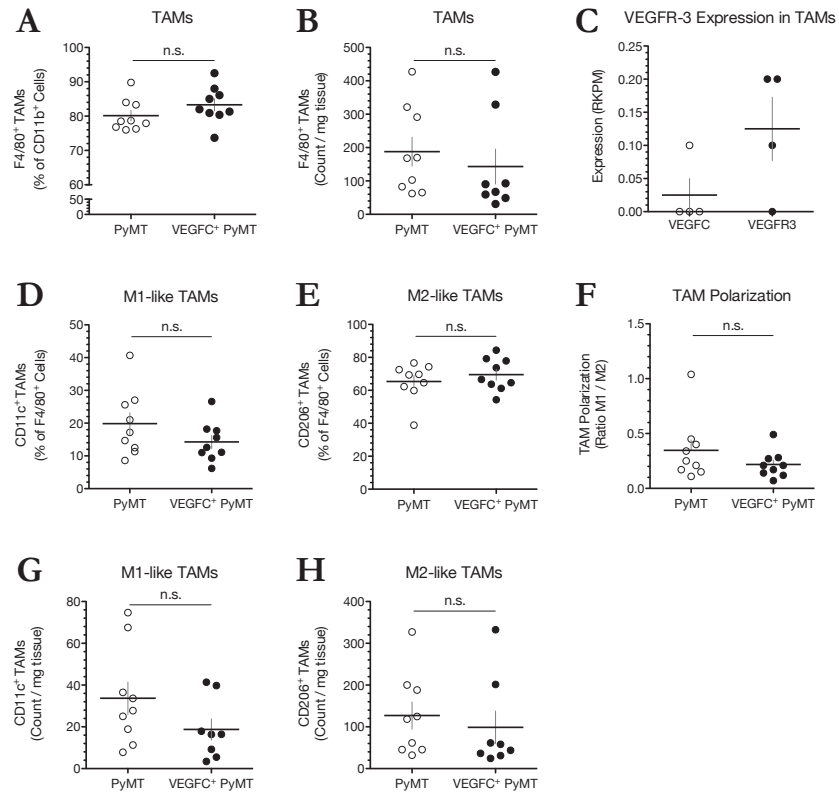


Fig. 14: Enhanced VEGF-C expression in the primary tumor does not affect TAM infiltration or phenotype.

A Consistent with the observations that inhibition of VEGFR-3-mediated signaling did not affect TAM infiltration or phenotype in the tumor, both the relative fraction as well as **B** the number of Ly6G⁺Ly6C⁺F4/80⁺ TAMs did not change in VEGF-C⁺ tumors as compared to control tumors. **C** RNA sequencing of F4/80⁺ TAMs isolated from invasive carcinomas of MMTV-PyMT⁺ transgenic mice demonstrates that TAMs do not express VEGFR-3 in this particular model, thus providing an explanation as to why VEGF-C expression did not affect TAM infiltration. **D** Furthermore, enhanced expression of VEGF-C in the primary tumor did also not affect the relative prevalence of CD11c⁺ M1-like or **E** CD206⁺ M2-like TAMs. **H** Indeed, though TAMs generally assumed an M2-like phenotype in this model, the ratio of M1-like to M2-like TAMs did not change in lymphangiogenic tumors as compared to control tumors. **G** Analysis of the number of CD11c⁺ M1-like or **H** CD206⁺ M2-like TAMs confirmed this, as also here no change was observed. Mario Squadrito kindly provided the RNA sequencing data. Plotted values show mean \pm SEM, each dot represents one animal. Statistical analysis performed with two-tailed Student's *t*-test. Experiment was performed once with $n = 10$ animals per group.

3.3.3 Tumor-associated lymphatic vessels do not alter the T-cell-mediated adaptive anti-tumor immune response

The presence of tumor-related inflammation sets the stage for induction of the more sophisticated adaptive immune response, and therefore I next asked whether and how modulation of tumor-associated lymphangiogenesis upon administration of mF4-31C1 in the MMTV-PyMT model, or orthotopic inoculation of VEGF-C⁺ PyMT tumor cells might affect the extent or the quality of the T-cell-mediated anti-tumor response. Analogous to the description of innate immunity in section 3.3.2, I first characterized the induction of the acquired immune response, and specifically T-cell-mediated acquired immunity, in MMTV-PyMT⁺ tumor-bearing mice upon tumor onset and in invasive lesions. Although total infiltration of TCRβ⁺NK1.1⁻ T cells, or TCRβ⁺NK1.1⁺ NK cells innate cells of the lymphoid lineage did not change in either tumor stage as compared to WT littermate controls (Figs. 15A and B, respectively), the fraction of TCRβ⁺NK1.1⁺ NK T cells was significantly increased in hyperplastic, but not in invasive lesions in MMTV-PyMT⁺ transgenic animals (Fig. 15C). Determination of the number of TCRβ⁺NK1.1⁻ T cells corroborated the observation that overall T cell infiltration did not change at either time point (Fig. 15D). However, although the relative fractions of TCRβ⁺NK1.1⁺ NK cells and TCRβ⁺NK1.1⁺ NK T cells did not seem different in invasive carcinomas, analysis of the number of these cells showed an increase of both TCRβ⁺NK1.1⁺ NK cells as well as TCRβ⁺NK1.1⁺ NK T cells in transgenic MMTV-PyMT⁺ tumor-bearing mice as compared to the untransformed inguinal mammary gland in WT tumor-free mice (Figs. 15E and F). Among the infiltrating T cells in the tumor, an increase in CD8⁺ cytotoxic T cells was observed in early hyperplastic lesions, that continued as these lesions progressed to invasive carcinomas, whereas the fraction of CD4⁺ T cells did not change at either point in time (Figs. 15G and H, respectively). Nevertheless, whereas analysis of the number of infiltrating T cells also showed an increase in CD8⁺ cytotoxic T cells in the tumor, and in particular in hyperplastic lesions of MMTV-PyMT⁺ transgenic animals, it also showed an increase in CD4⁺ T cells at this point in time (Figs. 15J and K). Late-stage tumors, however, did contain a larger fraction and number of CD25⁺FoxP3⁺ regulatory T cells (Figs. 15I and L, respectively), suggesting that the anti-tumor immune response eventually becomes attenuated. Closer examination of the phenotype of the CD8⁺ cytotoxic T cells in the tumor confirmed this hypothesis, as these cells showed an increased expression of activation markers CD25 and CD69 during tumor onset and progression, and a concurrent increase in the fraction of PD-1⁺ CD8⁺ cytotoxic T cells in invasive carcinomas (Figs. 15M-O), suggesting that upon initial activation of T-cell mediated immunity by early tumors, further development of the tumor may induce a functionally exhausted state of these cells.

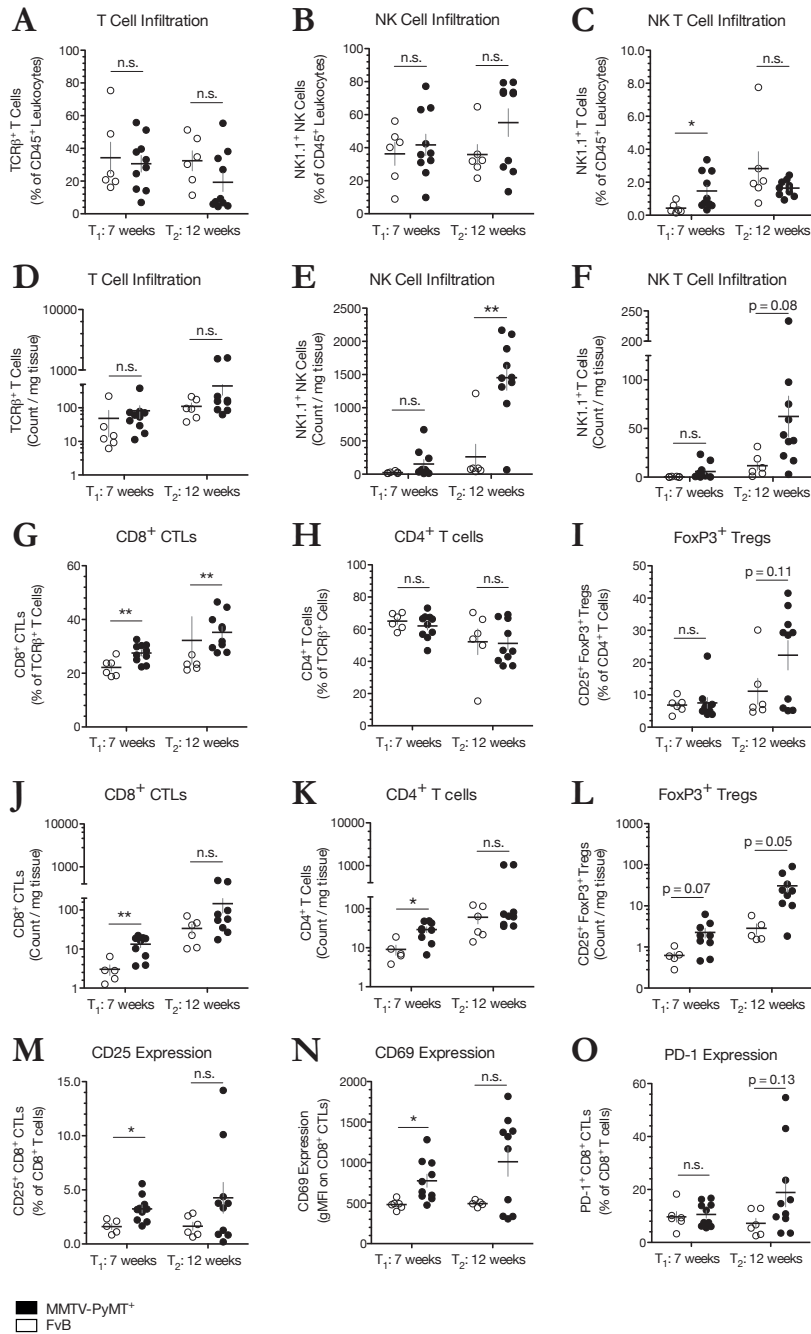


Fig. 15: Tumor growth and progression in the MMTV-PyMT model of breast cancer is characterized by early CD8⁺ T cell activation that becomes eventually becomes dampened.

A Flow cytometry analysis shows that the relative fraction of TCR-β⁺NK1.1⁺ T cells does not change during the course of tumor progression. **B** Furthermore, in the MMTV-PyMT mouse model of breast cancer, although the fraction of TCR-β⁺NK1.1⁺ NK cells of the innate immune system does also not increase over time, **C** an increase in TCR-β⁺NK1.1⁺ NK T cells can be seen in early hyperplastic lesions as compared to WT tumor-free mice. **D** Analysis of the numbers of these cells corroborates that overall T cell infiltration did not change in the inguinal mammary gland of MMTV-PyMT⁺ tumor-bearing mice as compared to WT littermate controls, but did show an increase in both **E** TCR-β⁺NK1.1⁺ NK cells as well

◀ **Fig. 15: Tumor growth and progression in the MMTV-PyMT model of breast cancer is characterized by early CD8⁺ T cell activation that becomes eventually becomes dampened, continued from p. 72.**

as **F** TCR-β⁺NK1.1⁺ NK T cells, particularly in invasive carcinomas. **G** Analysis of the different T cell subsets in the tumor revealed an increase in CD8⁺ cytotoxic T cells at onset of hyperplasia that continued until lesions progressed to invasive carcinomas, whereas **H** no particular change in the fraction of CD4⁺ T cells could be observed at either time point. **I** Among the CD4⁺ T cell subset, however, invasive carcinomas contain an increase in the percentage of CD25⁺FoxP3⁺ regulatory T cells, suggesting that the induced acquired immune response eventually becomes dampened. **J** Analysis of the number of either T cell subset showed that, although both CD8⁺ cytotoxic T cells and **L** CD25⁺FoxP3⁺ regulatory T cells indeed increased, particularly in early hyperplastic lesions, the number of CD4⁺ T cells was also increased at this point in time as compared to the inguinal mammary gland of WT tumor-free mice. **M** Analysis of the activation status of CD8⁺ cytotoxic T cells confirms this, as shown by expression levels of CD25 and **N** CD69, which increase during tumor progression, whereas **O** the fraction of PD-1⁺ CD8⁺ cytotoxic T cells also increases at this time point, suggesting that these cells may become functionally exhausted. Plotted values show mean ± SEM, each dot represents one animal. Statistical analysis performed with two-tailed Student's *t*-test. Experiment was performed once with n = 10 animals per group.

To investigate whether and how inhibition of VEGFR-3-mediated signaling affects the acquired immune response, I next evaluated the anti-tumor T cell response in MMTV-PyMT⁺ tumor-bearing mice upon administration of mF4-31C1. Akin to innate immunity, abrogated VEGFR-3 signaling did not alter the induction or quality of the adaptive immune response to the developing tumor in MMTV-PyMT⁺ transgenic mice. Indeed, upon analysis of the overall infiltration of CD3e⁺NK1.1⁻ T cells, CD3e⁻NK1.1⁺ NK innate cells of the innate immune response and NK1.1⁺CD3e⁺ NK T cells, no difference could be observed between the two conditions (Figs. 16A-C). Analysis of the number of these cells verified these findings, as neither the number of CD3e⁺NK1.1⁻ T cells, CD3e⁻NK1.1⁺ NK cells or NK1.1⁺CD3e⁺ NK T cells in the tumor changed when VEGFR-3-mediated signaling was inhibited as compared to IgG-treated control animals (Figs. 16D, E and F, respectively). Furthermore, upon closer examination of the various T cell populations in the tumor, the relative fractions or numbers of CD8⁺ cytotoxic T cells and CD4⁺ T cells, respectively, did not change in α-VEGFR-3-treated MMTV-PyMT⁺ tumor-bearing mice as compared to IgG-treated animals (Figs. 16G and H, as well as J and K). Moreover, among the latter subset, treatment with mF4-31C1 did also not alter the relative fraction or number of and CD25⁺FoxP3⁺ regulatory T cells, thus not changing the ratio of regulatory T cells to CD8⁺ cytotoxic T cells in the tumor (Figs. 16I and L, as well as O, respectively). Finally, analysis of the phenotype of the infiltrating CD8⁺ cytotoxic T cells revealed that inhibition of VEGFR-3-mediated signaling in transgenic MMTV-PyMT⁺ mice did not change the activation status of these cells, as determined by the expression levels of CD25 and CD69 on the surface, respectively (Figs. 16M and N). In conclusion, although developing neoplastic lesions in the MMTV-PyMT model of breast cancer induce a potent T-cell-mediated anti-tumor immune response, which eventually becomes exhausted as the nascent tumor progresses, these data suggest that inhibition of tumor-associated lymphangiogenesis does not alter the acquired immune response to the tumor.

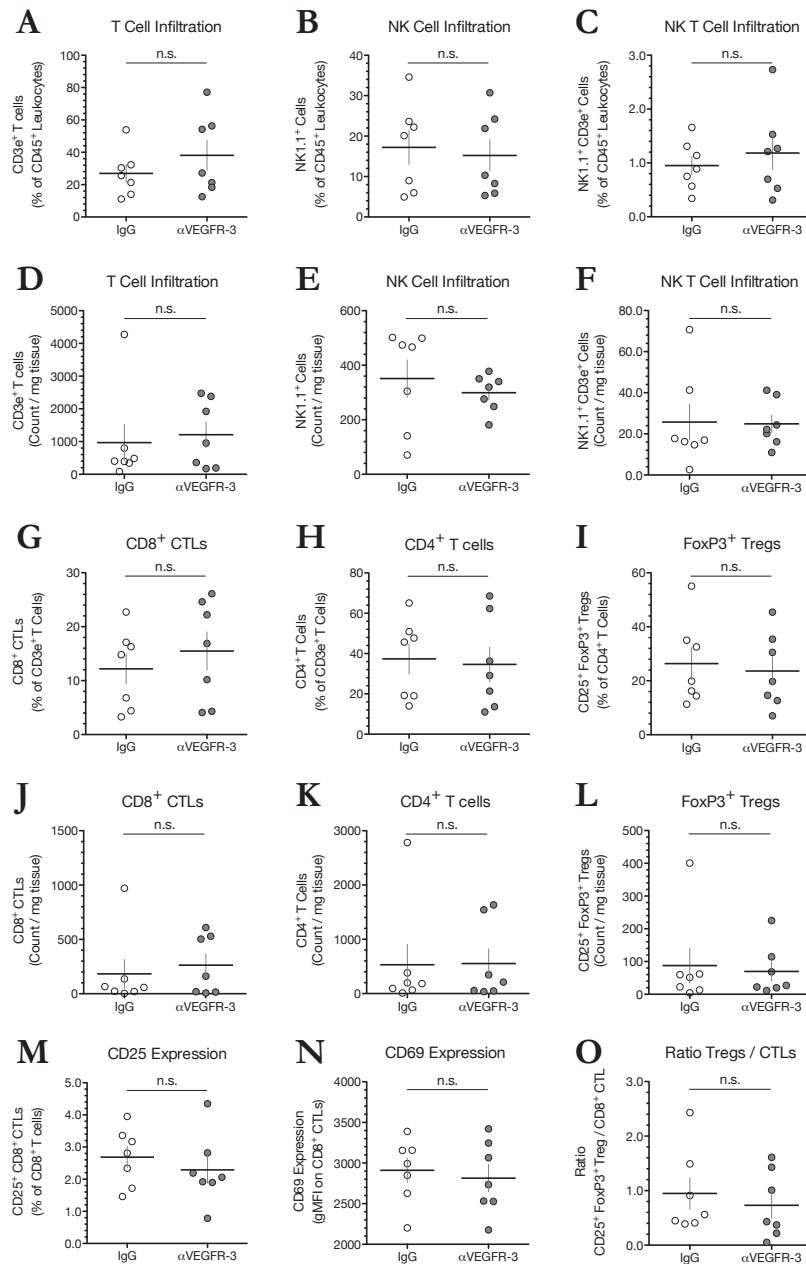


Fig. 16: Inhibition of VEGFR-3-mediated signaling does not affect the induction of an acquired T-cell-mediated immune response against the tumor.

A Flow cytometry analysis of the primary tumor shows that, whereas abrogated VEGFR-3-mediated signaling did not alter the overall infiltration of CD3e⁺NK1.1⁺ T cells into the tumor, the treatment also did not affect the relative fractions of **B** CD3e⁺NK1.1⁺ NK cells or **C** CD3e⁺NK1.1⁺ NK T cells. **D** Analysis of cell numbers verified that administration of mF4-31C1 in transgenic MMTV-PyMT⁺ tumor-bearing mice indeed did not change the density of CD3e⁺NK1.1⁺ T cells, **E** CD3e⁺NK1.1⁺ NK cells or **F**

◀ **Fig. 16: Inhibition of VEGFR-3-mediated signaling does not affect the induction of an acquired T-cell-mediated immune response against the tumor, continued from p. 70.**

CD3e⁺NK1.1⁺ NK T cells in the tumor, as compared to IgG-treated control animals. **G** Examination of the different T cell subsets revealed that inhibition VEGFR-3-mediated signaling also did not affect the relative distribution of CD8⁺ cytotoxic T lymphocytes, as well as **H** CD4⁺ T cells in the tumor. **I** Furthermore, among the CD4⁺ subset, the fraction of CD25⁺Foxp3⁺ regulatory T cells also did not change in α -VEGFR-3-treated animals as compared to IgG-treated controls. **J** Furthermore, administration of mF4-31C1 also did not affect the number of CD8⁺ cytotoxic T lymphocytes and **K** CD4⁺ T cells in the tumor, including **L** CD25⁺Foxp3⁺ regulatory T cells within invasive carcinomas. **M** In-depth analysis of the phenotype of the infiltrating CD8⁺ cytotoxic T lymphocytes also showed that mF4-31C1 did not change the activation status of these cells, as assessed by their expression of CD25 and **N** CD69 on the cell surface. **O** Whereas the infiltration of both CD8⁺ cytotoxic T lymphocytes as well as CD25⁺Foxp3⁺ regulatory T cells did not change upon termination of the treatment, as a consequence, the overall ratio of CD25⁺Foxp3⁺ regulatory T cells to CD8⁺ cytotoxic T lymphocytes in the primary was not affected upon inhibition of tumor-associated lymphangiogenesis. Plotted values show mean \pm SEM, each dot represents one animal. Statistical analysis performed with two-tailed Student's *t*-test. Experiment was performed once with n = 7 animals per treatment group.

To assess whether induction of tumor-associated lymphangiogenesis could alter the adaptive immune response to the tumor, I next turned my attention to the induction of the acquired immune response, and the induction of T-cell-mediated immunity in particular, in the orthotopic model. Enhanced VEGF-C expression did not affect the relative fraction or number of TCR β ⁺NK1.1⁻ T cells or TCR β ⁺NK1.1⁺ NK T cells into the tumor, nor the TCR β ⁺NK1.1⁺ NK cells of the innate cells of the lymphocyte lineage (Figs. 17A-F, respectively). Furthermore, analysis of the infiltrating T cells showed no difference in the relative distribution or the number of CD8⁺ cytotoxic T lymphocytes and CD4⁺ T lymphocytes in VEGF-C⁺ tumors, as compared to control tumors (Figs. 17G and H, as well as J and K, respectively). Among the CD4⁺ T cells in the tumor, increased expression of VEGF-C also did not affect the infiltration of CD25⁺FoxP3⁺ regulatory T cells, neither the relative fraction nor their density (Figs. 17I and L). Interestingly, however, induction of VEGF-C-mediated lymphangiogenesis in the primary tumor was observed to slightly alter the activation status of CD8⁺ cytotoxic T lymphocytes in the tumor. In VEGF-C⁺ tumors, although CD25 expression levels did not change, these cells displayed less CD69 on their surface (Figs. 17M and N, respectively). Moreover, a trend towards an increase in the fraction of PD-1⁺ CD8⁺ cytotoxic lymphocytes was observed (Fig. 16O), suggesting that the CD8⁺ cytotoxic T cells might have been previously primed against the tumor, but are now functionally exhausted.

Fig. 17: Enhanced expression of VEGF-C does not alter overall T cell infiltration, but affects the activation status CD8⁺ cytotoxic T cells in the tumor. ▶

A Flow cytometry analysis shows that enhanced expression of VEGF-C does not affect overall infiltration of TCR β ⁺NK1.1⁻ T cells, **B** TCR β ⁺NK1.1⁺ NK cells of the innate cells of the lymphocyte lineage or **C** TCR β ⁺NK1.1⁺ NK T cells into the tumor. **D** Furthermore, VEGF-C⁺ tumors did also not contain a different number of TCR β ⁺NK1.1⁻ T cells, **E** TCR β ⁺NK1.1⁺ NK cells or **F** TCR β ⁺NK1.1⁺ NK T cells, respectively. **G** Among the infiltrating T cells, also no difference in the fraction of CD8⁺ cytotoxic T cells,

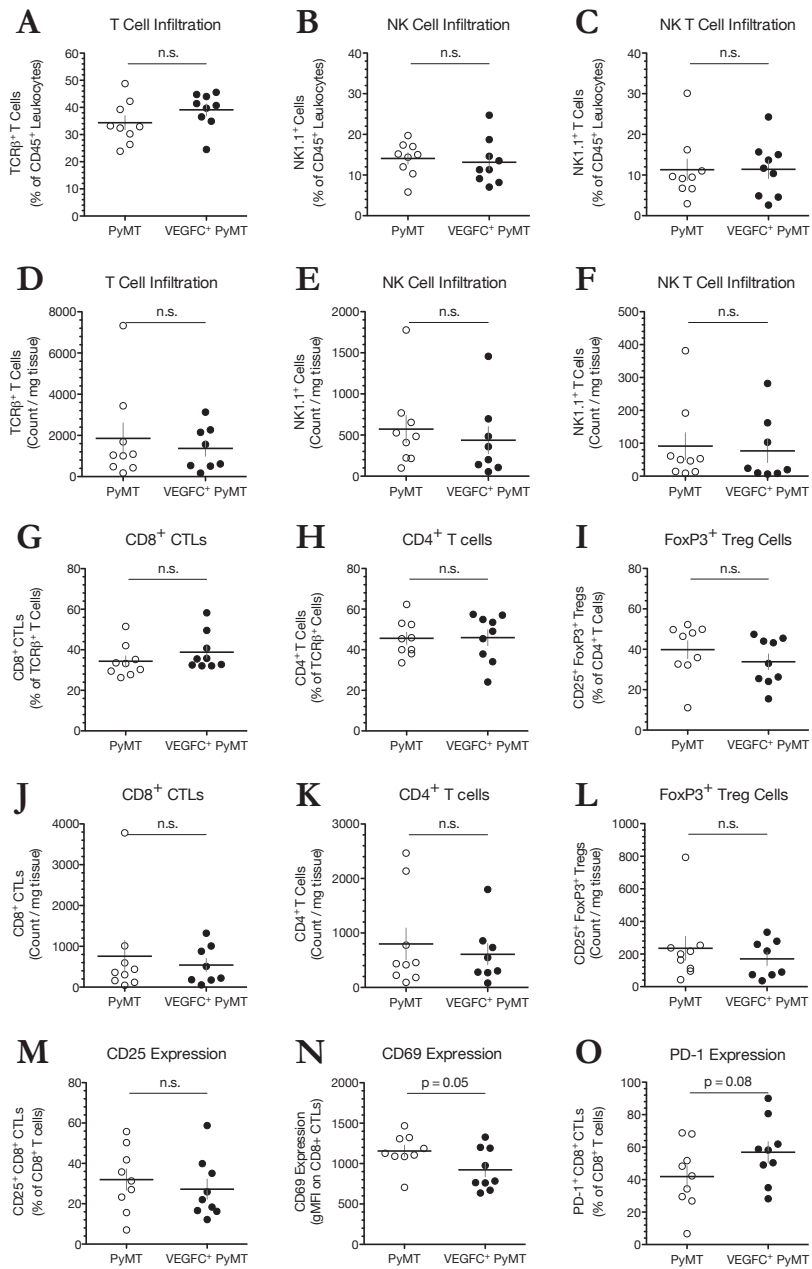


Fig. 17: Enhanced expression of VEGF-C does not alter overall T cell infiltration, but affects the activation status CD8⁺ cytotoxic T cells in the tumor, continued from p. 75.

or **H** CD4⁺ T lymphocytes could be observed. **I** CD25⁺FoxP3⁺ regulatory T cell infiltration did also not change lymphangiogenic tumors as compared to control tumors. **J** Analysis of the number of each T cell subset confirmed these findings, as no difference in either CD8⁺ cytotoxic T lymphocytes, **K** CD4⁺ T cells or **I** CD25⁺FoxP3⁺ regulatory T cells was observed between VEGF-C⁺ and control tumors. **M** Finally, VEGF-C expression did not alter the CD25 expression levels, but **N** resulted in reduced CD69 expression levels on the CD8⁺ cytotoxic T cells in the tumor. **O** Finally, a trend towards an increase in PD-1⁺ T cells could also be observed upon overexpression of VEGF-C in the primary tumor. Plotted values show mean \pm SEM, each dot represents one animal. Statistical analysis performed with two-tailed Student's *t*-test with *n* = 10 animals per group.

Interestingly, the observed effects of VEGF-C-induced lymphangiogenesis on the phenotype of CD8⁺ cytotoxic T cells in the tumor were also visible, and slightly more pronounced upon stimulation of the lymphatic network in the tumor-draining LN. Much the same to the primary tumor, VEGF-C-induced LN lymphangiogenesis did not affect the overall content in terms of relative fraction or number of TCRβ⁺NK1.1⁻ T cells, TCRβ⁺NK1.1⁺ NK T cells, or the TCRβ⁺NK1.1⁺ NK cells of the innate cells of the lymphocyte lineage in the LN (Figs. 18A-F, respectively). Moreover, within the T cell population in the draining LN, the proportions of CD8⁺ cytotoxic T cells and CD4⁺ T cells, as well as the fraction of CD25⁺FoxP3⁺ regulatory T cells among the latter, did not change upon activation of the lymphatic endothelium (Figs. 18G, H and I). Moreover, the total number of each T cell subset also did not differ between LNs draining VEGF-C⁺ or control tumors, respectively (Figs. 18J, K and L). Again, in agreement with the observed phenotype of the CD8⁺ cytotoxic T cells in the primary tumor, the CD8⁺ cytotoxic T lymphocytes in the LNs draining VEGF-C⁺ tumors showed no difference in the expression levels of CD25, but significantly reduced levels of CD69 on their surface, as compared to the CD8⁺ T cell population in the LN downstream of control tumors (Figs. 18M and N). Similarly, a trend towards an increase in the fraction of PD-1⁺ CD8⁺ cytotoxic T lymphocytes could be observed in VEGF-C⁺ tumor-draining LNs, suggesting that VEGF-C-mediated induction of LN lymphangiogenesis renders these cells functionally exhausted (Fig. 18O).

Taken together, these results suggest that, modulation of tumor-associated lymphatic vessels via the VEGF-C / VEGFR-3 signaling axis does not notably alter the different components of the tumor microenvironment evaluated in the scope of this thesis, i.e. the desmoplastic response, as well as the innate and adaptive immune responses that are induced by the developing tumor in the experimental models of breast cancer that were employed for these experiments.

Fig. 18: VEGF-C-mediated activation of the lymphatic vasculature in the tumor-draining LN changes the activation of CD8⁺ T cells in the LN. ►

A VEGF-C expression by metastatic tumor cells in the regional LN does not alter the overall distribution of TCRβ⁺NK1.1⁻ T cells, **B** TCRβ⁺NK1.1⁺ NK innate cells of the lymphocyte lineage, or **C** the TCRβ⁺NK1.1⁺ NK T cells in the LN. **D** Furthermore, the total number of TCRβ⁺NK1.1⁻ T cells, **E** TCRβ⁺NK1.1⁺ NK cells, or **F** the TCRβ⁺NK1.1⁺ NK T cells in the draining LN downstream of VEGF-C⁺ tumors did not differ from the total number of each cell population in control tumor-draining LNs, respectively. **G** VEGF-C-mediated activation of the lymphatic endothelium in the tumor-draining LN also does not alter the relative fractions of CD8⁺, **H** CD4⁺, or **I** CD25⁺FoxP3⁺ regulatory T cells among the

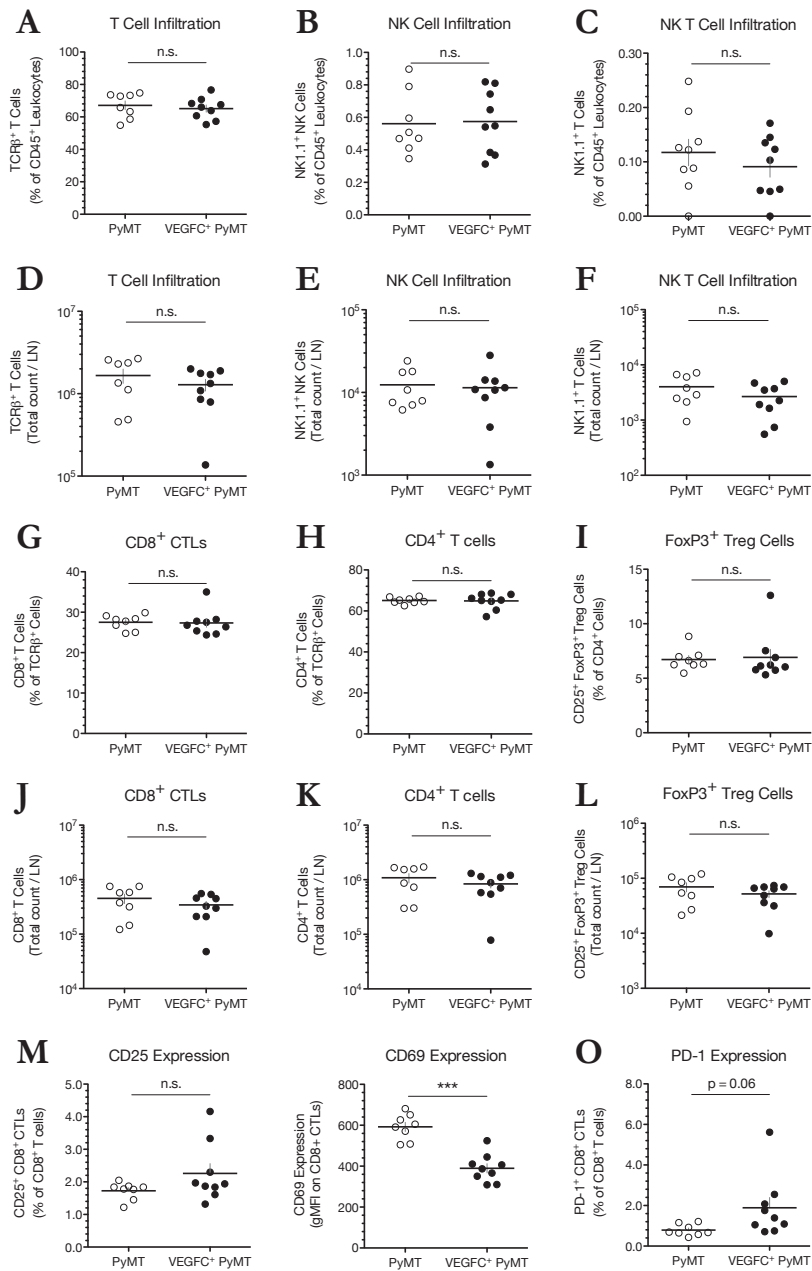


Fig. 18: VEGF-C-mediated activation of the lymphatic vasculature in the tumor-draining LN changes the activation of CD8⁺ T cells in the LN, continued from p. 77.

latter. Analysis of the total number of each T cell subset confirmed that indeed CD8⁺ cytotoxic T cells, **K** CD4⁺ T cells, or **L** CD25⁺FoxP3⁺ regulatory T cells did not change in the regional LN draining lymphangiogenic tumors. **M** Finally, the expression levels of CD25 on CD8⁺ cytotoxic T cells in the draining LN did not change, whereas **N** CD69 expression levels were significantly decreased on these cells in lymphangiogenic LNs. **O** Concurrently, a trend towards an increase in the fraction of PD-1⁺ CD8⁺ cytotoxic T lymphocytes was observed in VEGF-C⁺ tumor-draining LNs as compared to control tumor-draining LNs, suggesting that these cells are functionally exhausted. Plotted values show mean \pm SEM, each dot represents one animal. Statistical analysis performed with two-tailed Student's *t*-test with *n* = 10 animals per group.

4

Discussion and Perspectives

4.1 Experimental modulation of lymphatic vessels in the context of breast cancer

In the thesis work presented herein, I investigated whether modulation of the tumor-associated lymphatic vasculature could actively shape the tumor microenvironment to promote the regional and distant metastatic dissemination of the primary tumor in the context of breast cancer. Indeed, during the past decade, both clinical data and a multitude of experimental models have established the relevance of tumor-associated lymphatic vessels for breast cancer metastasis beyond question (Ran et al., 2010; Skobe et al., 2001a). Moreover, the presence of tumor cells in the tumor-draining LN represents an important prognostic indicator for disease outcome, and is routinely used in the clinic for staging of the disease upon its diagnosis (Tuttle, 2004). However, in recent years it has become apparent that not only thwarted neoplastic cells, but also the surrounding stromal cells, which under physiological conditions typically act to maintain tissue homeostasis, coercively contribute to tumor growth, progression and metastasis, and the concept of the tumor microenvironment is now widely accepted (Hanahan and Weinberg, 2000). In light of this novel conceptual progress, I therefore aimed to establish a link between previously unrelated components of the tumor stroma, specifically tumor-associated lymphatic vessels, tensional homeostasis and anti-tumor immunity, to elucidate their concerted role in transition to malignancy and metastatic dissemination of breast cancer (Swartz and Lund, 2012).

As activation of VEGFR-3 by its ligands VEGF-C or VEGF-D is known as the principal pathway for the induction of lymphangiogenesis during embryonic development, but also in pathological conditions in the adult, such as inflammation and cancer, experimental modulation of tumor-associated lymphangiogenesis was achieved upon alteration of different components of the VEGF-C/VEGF-D - VEGFR-3 signaling axis in various breast cancer models. In a first approach, I chose to inhibit VEGFR-3-mediated activation of the tumor-associated lymphatic vasculature in the transgenic MMTV-PyMT model of breast cancer upon administration of mF4-31C1, an antagonistic antibody that specifically binds to and ablates VEGFR-3 signaling (Pytowski et al., 2005). Conversely, a second approach, orthotopic implantation of a primary tumor cell line isolated from an invasive lesion of an MMTV-PyMT⁺ tumor-bearing transgenic mouse that was transduced to stably express increased levels of VEGF-C into the fat tissue surrounding the inguinal mammary gland, was employed to investigate whether induction of tumor-associated lymphangiogenesis yielded similar results. Although earlier experiments in similar orthotopic models have previously already firmly established a causal link between VEGF-C expression and tumor metastasis, these models depend on the use of immune deficient animals due to the human origin of the breast cancer cell lines that were employed to inoculate the tumor (Skobe et al., 2001a; Karpanen et al., 2001; Mattila et al., 2002). However, given the recently uncovered immunomodulatory roles of lymphatic vessels in cancer progression (Swartz, 2014), this model thus represents the first experimental model to investigate the interplay between the lymphatic vasculature and the anti-tumor immune response upon induction of tumor-associated lymphangiogenesis in the context of breast cancer. Hence, this work is based on two different models that allow experimental modulation of tumor-associated lymphatic vessels in order to discern their interactions with the tumor stroma.

4.2 Tumor-associated lymphangiogenesis and metastasis

In consideration of the relevance of lymphatic vessels for breast cancer metastasis, I first explored whether modulation of tumor-associated lymphangiogenesis affected regional or distant metastasis in either experimental model described above. In line with previous experiments demonstrating reduced pulmonary metastasis upon systemic administration of mF4-31C1 in an orthotopic model of breast cancer (Roberts, 2006), I found that inhibition of VEGFR-3-mediated signaling upon administration of mF4-31C1 in transgenic MMTV-PyMT⁺ tumor-bearing animals did not affect the growth of the primary tumor, but instead reduced distant metastasis of the primary tumor to the lungs. However, the second approach, i.e. induction of lymphangiogenesis upon orthotopic inoculation of VEGF-C⁺ PyMT tumor cells in the inguinal fat pad, yielded no such difference in pulmonary metastasis, as micrometastatic lesions were observed in the lungs of both VEGF-C⁻ and control-tumor-bearing animals 35 days post-tumor inoculation. These findings were somewhat unexpected, as forced expression of VEGF-C in an orthotopic model of breast cancer has previously been reported to promote metastatic dissemination of the primary tumor to the lungs (Skobe et al., 2001a). Yet, as I opted for inoculation of tumors using only a small number of tumor cells in this model, so as to foster a slower tumor growth rate to favor co-evolution of the tumor and the recruited stromal cells, the chosen time point to assess pulmonary metastasis may have well been too early, and more time may be needed to observe a significant difference in the distant metastatic dissemination of the tumor upon induction of VEGF-C expression.

Since modulation of various components of the VEGF-C/VEGF-D - VEGFR-3 signaling axis has previously also been shown to have a pronounced effect on the rate of regional metastasis to the tumor-draining LN, I also investigated whether and to which extent the tumor-draining sentinel LN was involved (Roberts, 2006; Skobe et al., 2001a). Despite this notion, however, the presence of disseminated tumor cells was practically not detected in the LN draining invasive carcinomas of the inguinal mammary gland in transgenic MMTV-PyMT⁺ tumor-bearing animals, neither upon routine histological analysis of H&E-stained tumor sections by a pathologist, nor by immunostaining with an antibody specific for the PyMT antigen expressed by the transformed mammary epithelium, except in one case, in which a large focus of tumor cells was observed by both aforementioned methods. In consideration of the reputed importance of the tumor-associated lymphatic vasculature for regional metastasis to the tumor-draining LN in human disease, however, these findings thus raise the question whether lymphogenous metastatic dissemination of the primary tumor indeed occurs in this particular transgenic tumor model. The initial description of the model solely indicates the presence of foci of disseminated mammary carcinoma cells in the lungs of MMTV-PyMT⁺ transgenic animals, whereas the presence of metastatic lesions in the inguinal LN are only described upon orthotopic inoculation of primary tumors into the fat pad of syngeneic hosts (Guy et al., 1992). Nevertheless, subsequent studies regarding metastatic dissemination in breast cancer, however, occasionally do detect similar tumor foci in the draining LN, yet the relative contributions of hematogenous and lymphatic spread in the formation of these LN metastases are unclear (Garmy-Susini et al., 2013). In fact, it has

also been postulated that disseminated tumor cells may even enter the tumor-draining LN via the high endothelial venules of the blood vasculature, rather than via tumor-associated lymphatic vessels in the MMTV-PyMT model of breast cancer (Fantozzi and Christofori, 2006). Thus, as up to present date definite proof of lymphogenous metastasis in this particular transgenic tumor model has not yet been presented, these observations therefore might point out a possible discrepancy between the metastatic processes as it presumably occurs in human disease and in the animal model, rendering the transgenic MMTV-PyMT model unsuitable to study this aspect of human breast cancer.

Consistent with the aforementioned study, however, I did observe an increase in metastasis to the inguinal LN draining VEGF-C⁺ tumors, particularly in the size of the metastatic foci, as compared to the inguinal LN downstream of control tumors, upon immunostaining for the PyMT antigen expressed by the tumor cells used to inoculate the primary tumor, confirming the notion that regional LN metastasis occurs early on in the metastatic process (Skobe et al., 2001a). Though initially an area of controversy, several reports have now indeed demonstrated a correlation between VEGF-C expression in the tumor, and increased LN metastasis, as well as reduced disease-free and overall survival (DFS and OS, respectively) in clinical specimens of breast cancer, suggesting that this particular model might better recapitulate lymphogenous metastasis as it is assumed in human disease (Mohammed et al., 2007; Nakamura et al., 2005, 2003).

4.3 The tumor microenvironment

Whereas the importance of lymphatic vessels for breast cancer metastasis has been well established, not much is known about how tumor-associated lymphatic vessels promote regional and distant metastatic dissemination of the primary tumor. Although lymphatic vessels have traditionally been considered as merely providing an escape route for invasive tumor cells, it is becoming increasingly clear that tumors actively induce remodeling of the lymphatic vasculature to facilitate metastasis to distant organs (Stacker et al., 2014). However, as previous experiments have predominantly focused on the interaction between the nascent tumor and its associated lymphatic vessels, the current thesis work thus aimed to discern whether interactions between the evolving tumor stroma and the lymphatic vasculature could promote the metastatic dissemination of invasive carcinomas of the breast. Remarkably, experimental modulation of VEGF-C / VEGFR-3-mediated activation of the lymphatic endothelium did not result in changes in the desmoplastic response, or the innate and adaptive immune responses to the tumor. Similar to human breast cancer, developing tumors in MMTV-PyMT⁺ transgenic mice are associated with the induction of a substantial desmoplastic stroma that results in altered tensional homeostasis upon co-evolution of the transformed epithelium and the fibroblasts of the connective tissue. However, inhibition of VEGFR-3-mediated signaling upon administration of mF4-31C1 did not alter the expanse or the composition of the desmoplastic ECM in MMTV-PyMT⁺ tumor-bearing mice, as compared to IgG-treated control animals. Earlier experiments from our laboratory have shown that LECs can activate fibroblasts through production of TGF- β 1 upon stimulation with VEGF-C

(manuscript in preparation). However, in this particular model, abrogated VEGFR-3 signaling in the primary tumor did not translate into an effect on the desmoplastic stroma in transgenic MMTV-PyMT⁺ tumor-bearing animals. One reason for these findings may be that, although LECs may contribute directly to stromal stiffening during tumor growth and progression in developing tumors, these effects may be more relevant in early hyperplastic lesions, where the formation of the reactive stroma is induced. Notably, upon initiation of the treatment with mF4-31C1, there is already a substantial activation of the tumor stroma ongoing in transgenic MMTV-PyMT⁺ tumor-bearing animals, and as fibroblasts constitute the principal source of TGF- β 1 in the tumor, activation of CAFs at this point in time may thus override the initial effects of TGF- β 1 that is secreted by LECs on the tumor stroma.

In light of the close association of lymphangiogenesis and inflammation, I next assessed whether modulation of tumor-associated lymphatic vessels affected the inflammatory response to the tumor in both experimental models of breast cancer. In MMTV-PyMT⁺ transgenic mice, tumor development is accompanied by a potent inflammatory response, particularly in early hyperplastic lesions, that is mediated by infiltrating TAMs. However, upon treatment with mF4-31C1, which was initiated at the onset of hyperplasia and continued until the lesions had progressed to invasive carcinomas, I observed no changes in the infiltration of F4/80⁺ TAMs or their relative phenotype, respectively. Conversely, enhanced expression of VEGF-C in the primary tumor yielded similar results, as it did not alter the infiltration of innate myeloid cells, and TAMs in particular, into the tumor, suggesting that tumor-associated lymphatic vessels do not actively promote inflammation in the nascent tumor in the breast cancer models that were employed in this thesis. Furthermore, in contrast to earlier reports, these results also indicate that the recruitment of TAMs into developing tumors in these experimental models is not mediated by VEGF-C (Schoppmann et al., 2002). Indeed, RNA sequencing of TAMs isolated from invasive carcinomas in MMTV-PyMT⁺ tumor-bearing mice demonstrated that, at least in this particular transgenic model, TAMs do not express VEGFR-3, thus providing an explanation for these observations.

Finally, modulation of tumor-associated lymphangiogenesis did not notably alter the infiltration or phenotype of the T lymphocytes in the tumor in either model, suggesting that tumor-associated lymphatic vessels do not affect T-cell-mediated immunity in the experimental breast cancer models employed in this thesis. Yet, in VEGF-C⁺ tumors, I observed a slight trend towards immune suppression, reflected in an increase in the fraction of PD-1⁺ CD8⁺ cytotoxic T cells in the tumor, and simultaneous decrease in expression levels of CD69 on their surface, respectively, as compared to control tumors. However, as orthotopic implantation of VEGF-C⁺ PyMT tumor cells in the inguinal fat pad resulted in a 44-fold increase in VEGF-C expression levels in these tumors, these observations thus raise the question how relevant these findings may be for human breast cancer.

Altogether, the obtained results demonstrate that tumor-associated lymphatic vessels do not alter the tumor stroma in various experimental models of breast cancer. These observations were unusually consistent, in that both VEGF-C-mediated induction of tumor-associated lymphangiogenesis, as well as inhibition of VEGFR-3-mediated signaling did not bring about any changes, as far as the different parameters that were

measured to assess the various components of the tumor microenvironment in these experiments is concerned. Hence, these findings suggest that VEGF-C / VEGFR-3-mediated signaling in breast cancer may thus promote metastatic dissemination of the tumor through specific interactions between the developing tumor and its associated lymphatic vasculature, and accordingly strengthen previous publications discerning mechanisms of tumor cell-lymphatic cross-talk that contribute to the preferential lymphogenous spread of invasive carcinomas of the breast (Issa et al., 2009; Shields et al., 2007).

4.4 VEGF-C / VEGFR-3 signaling and angiogenesis

All in all, the observation that inhibition of VEGFR-3-mediated signaling upon administration of mF4-31C1 in transgenic MMTV-PyMT⁺ tumor-bearing animals reduced pulmonary metastasis, while obvious lymphogenous spread of the primary tumor could not be detected in this model, is certainly interesting and prompts a more thorough investigation into the mechanism of metastatic dissemination in breast cancer. Although suppression of VEGFR-3 signaling significantly impeded the expansion of tumor-associated lymphatic vessels as compared to IgG-treated animals, it cannot be excluded that mF4-31C1 mediates the observed effect on pulmonary metastasis through an effect on the tumor-associated blood vasculature. In fact, the blood and lymphatic system are intimately linked, which is reflected in their common origin in the developing embryo, and as such modulation of VEGFs or their respective receptors might thus affect components of both vascular systems. Indeed, VEGFR-3 is initially expressed by the evolving blood vasculature before the onset of lymphatic vessel development, at which point it becomes largely restricted to the lymphatic endothelium (Kaipainen et al., 1995). Accordingly, targeted deletion of *vegfr3* in the early embryo resulted in lethality due to severe defects in the blood vasculature, demonstrating the importance of VEGFR-3 in the development of the cardiovascular system (Dumont et al., 1998). However, in the adult, weak expression of VEGFR-3 has also been found on capillaries of the blood vascular endothelium in normal breast tissue, which increases in angiogenic blood vessels in invasive tumors (Valtola et al., 1999). Likewise, administration of mF4-31C1 led to a reduction in blood vessel density in various orthotopic and subcutaneous tumor models of breast and other solid cancers, respectively, thus supporting the hypothesis that administration of an antagonistic antibody that specifically binds to and ablates VEGFR-3 signaling exerts dual effects on both the tumor-associated blood and lymphatic vasculature (Roberts, 2006; Laakkonen et al., 2007). More specifically, VEGFR-3 was recently demonstrated to be highly expressed by the leading endothelial tip cells in angiogenic sprouts, and genetic and pharmacological disruption of VEGFR-3 signaling in the context of various physiological and pathological settings significantly impaired the growth of blood vessels, demonstrating the importance of VEGFR-3-mediated sprouting in both developmental and tumor angiogenesis (Tammela et al., 2008). Nonetheless, despite these findings, I observed but a slight trend towards a reduction in the number of CD31⁺gp38⁻ BECs in the primary tumor that was not significant ($p = 0.23$). However, functional experiments to dissect the relative

contributions of VEGFR-2- and VEGFR-3-mediated signaling to angiogenesis *in vivo*, showed that, although VEGFR-3 ligands VEGF-C or VEGF-D alone failed to induce an expansion of the blood vasculature, these growth factors could sustain angiogenesis in blood vessels that were previously primed with VEGFR-2 ligands, even in the presence of VEGFR-2 inhibitors (Tammela et al., 2008). These observations thus suggest that, whereas VEGFR-2-mediated signaling represents the main pathway for the induction of angiogenic growth of blood vessels during development or in incipient tumors, VEGFR-2 ligands may additionally act to sensitize these vessels to other growth factors of the VEGF family, including those that are principally known to induce lymphangiogenesis, which may then act in concert to support further development and maintenance of the blood vasculature. In line with these findings, I observed a significant increase in the expression VEGF-A in early hyperplastic lesions in MMTV-PyMT⁺ tumor-bearing mice, but not in VEGF-C or VEGF-D, which may indeed induce the expression of VEGFR-3 on tumor-associated blood vessels. Interestingly, expression levels of VEGF-C were significantly increased in invasive carcinomas, as compared to WT tumor-free mice, suggesting that VEGF-C may, in addition to its effects on tumor-associated lymphatic vessels, additionally act to support angiogenic blood vessels at this point in time. Collectively, these considerations may thus provide an explanation for the observed reduction in pulmonary metastasis in the absence of lymphogenous spread of the primary tumor upon administration of mF4-31C1 in MMTV-PyMT⁺ transgenic mice.

Conversely, in consideration of the complex reciprocal regulation of angiogenesis and lymphangiogenesis by the various endothelial growth factors of the VEGF family and their corresponding receptor tyrosine kinases, I also considered whether enhanced expression of VEGF-C in the primary tumor could affect the tumor-associated blood vasculature. In agreement with previous findings, I observed a 10-fold increase in the number of CD31⁺gp38⁺ LECs in the primary tumor upon orthotopic implantation of VEGF-C⁺ PyMT tumor cells into the inguinal fat pad, which translated into a substantial increase in peritumoral CD31⁺lyve-1⁺ lymphatic vessels as compared to tumors that were inoculated with control-transduced PyMT tumor cells (Skobe et al., 2001a). However, initially, forced expression of VEGF-C was not reported to induce an expansion of the tumor-associated blood vasculature (Skobe et al., 2001a). Yet, more recently, expression of VEGF-C was also associated with an increase in MVD in clinical specimens of breast cancer, thus suggesting that, besides promoting tumor-associated lymphangiogenesis, VEGF-C may indeed also exert an effect on the blood vessels within the tumor (Mohammed et al., 2007). Accordingly, although the number of CD31⁺gp38⁻ BECs in the tumor was seemingly not affected by enhanced expression of VEGF-C in the primary tumor, histological analysis of CD31⁺lyve-1⁻ blood vascular endothelium, on the other hand, demonstrated an increase, albeit not significant ($p = 0.10$), in the relative area occupied by these vessels. The apparent discrepancy between these findings might arise from the different approaches that were used to quantify MVD in the tumors, as the relative blood vessel density was previously determined in so-called 'hot spots' with the highest frequency of lymphatic vessels (Skobe et al., 2001a). In addition to the fundamental bias that may result from such measurements, the occurrence of new blood vessels may also not coincide spatially with the growth of lymphatic vessels. Indeed,

although the question whether lymphangiogenesis ensues in human breast cancer has been a matter of intense debate, lymphatic hyperplasia is frequently observed at the tumor periphery, whereas blood vessels usually appear scattered throughout the developing tumor (Mohammed et al., 2009). In my experiments, I assessed blood and lymphatic density using a whole-tissue based approach, thus avoiding a possible bias that may result from a manual selection of areas with the highest quantity of vessels. Although VEGF-C may mediate an expansion of tumor-associated blood vessels upon activation of VEGFR-3 on the blood vascular endothelium, another possibility may be that secreted VEGF-C may affect other VEGF receptor tyrosine kinases. Indeed, proteolytic processing of VEGF-C in the extracellular space yields shorter forms that have an increasing affinity for VEGFR-2 (Joukov et al., 1997). Although VEGF-C expression levels in the tumor were determined by an immunoassay that specifically detects full-length VEGF-C, it cannot exclude the presence of other, shorter forms of the protein, yet this possibility was not assessed in this thesis.

In consideration of a surmised modulation of the blood vascular endothelium upon alteration of different components of the VEGF-C / VEGFR-3 signaling axis in the various breast cancer models employed in this thesis, one could accordingly anticipate possible consequences for tumor growth. Indeed, in various orthotopic models of breast and other cancers, anti-angiogenic effects mediated by mF4-31C1 translated into a reduction in the rate of tumor growth (Roberts, 2006; Laakkonen et al., 2007). However, neither administration of mF4-31C1 in MMTV-PyMT⁺ tumor-bearing mice, or enhanced expression of VEGF-C affected the size of the primary tumor. One possible explanation for these observations may be that, although VEGFR-3-mediated activation of the blood vascular endothelium may provide support to angiogenic blood vessels within the tumor, the relative contribution to the formation of new blood vessels may in fact be rather limited in comparison to VEGFR-2-mediated angiogenesis. In fact, VEGF-A is highly expressed in both the transgenic, as well as the orthotopic model, suggesting that canonical activation of VEGFR-2 by its ligand VEGF-A constitutes the main signal transduction pathway that induces blood vessel growth in these experimental models, and, activation of VEGFR-3 in angiogenic blood vascular endothelium may, as previously proposed, solely provide sustenance to the developing vasculature. Additionally, due to the heterogeneity of the transgenic MMTV-PyMT model, in which tumors often display different kinetics with regard to tumor growth and progression, a rather limited number of 7 animals per treatment group may not suffice to see an effect on tumor size upon administration of mF4-31C1. However, even upon orthotopic implantation of VEGF-C⁺ PyMT tumor cells in the inguinal fat pad, which induces tumors that grow more reproducibly, although VEGF-C⁺ tumors were consistently slightly bigger compared to control tumors, a significant effect on the rate of tumor growth could not be observed. Despite these findings, a reduction was only observed when tumors notably expanded. Hence, a possible effect on the primary tumor may not manifest itself until the tumor reaches a certain size, and due to the legal restrictions on tumor volume, a difference may thus not become apparent. Nonetheless, these results suggest that modulation of VEGF-C / VEGFR-3 signaling in experimental models of breast cancer may in part mediate metastatic dissemination via effects on the blood vasculature.

4.5 Lymphogenous or hematogenous metastasis?

The possible contribution of the blood vasculature to breast cancer metastasis renders us at the initial debate on the relative contributions of hematogenous and lymphogenous spread in the formation of regional and distant metastases. The fact that tumor cells indeed preferentially invade lymphatic vessels rather than blood vessels, establishes a connection between LVI and LN metastasis (Van den Eynden et al., 2006). Nevertheless, although the presence of tumor cells in the draining LN is a major prognostic factor in the staging of breast cancer, it is not known whether disseminated tumor cells in the regional LN actively contribute to further metastatic spread. Consequently, two different models, which are not mutually exclusive, have been proposed to explain the formation of distant metastases in patients diagnosed with breast cancer (Ran et al., 2010). The first model suggests that lymphatic-independent hematogenous metastasis is the sole route for the emergence of metastatic lesions in distant organs is through invasion of tumor-associated blood vessels, with little or no contribution of the lymphatic vasculature beyond regional dissemination to the tumor-draining LN. Indeed, metastatic tumor cells that emerge within the sentinel LN may merely reflect the aggressiveness of the primary tumor and nothing else. The fact that metastatic foci in the tumor-draining LN in themselves are not life threatening, which is reflected in the high DFS despite the spread of invasive tumor cells, supports this hypothesis. In contrast, the lymphatic-dependent sequential model of metastasis states that remodeling of the lymphatic vasculature associated with the tumor and beyond by the developing neoplastic lesion may actively promote metastatic dissemination of the primary tumor to the tumor-draining LN, and ultimately distant organs, which these cells may reach through either the blood or lymphatic vasculature upon egress from the LN. Although direct proof of the contribution of lymphatic vessels to distant metastasis is lacking, the prognostic value of LN status for disease outcome would suggest otherwise, and in view of this current debate it would thus be enticing to investigate whether and how the tumor-draining LN may promote metastasis progression (Van den Eynden et al., 2007). Interestingly, increased expression of VEGF-C in the primary tumor resulted in increased metastasis to the tumor-draining LN. However, as an inherent consequence of the model, metastatic tumor cells that arrive in the tumor-draining LN will continue to express VEGF-C, and as such stimulate the sinusoidal lymphatic endothelium in the LN. Considering the current controversy, it would thus be interesting to investigate whether different mitogenic stimuli may not only quantitatively, but also qualitatively alter the lymphatic endothelium in the LN to promote further metastatic spread of disseminated tumor cells. Moreover, in light of the different clinical manifestations of breast cancer, further efforts should also be directed towards discerning whether different tumors arising in different anatomical locations, i.e. ductal or lobular carcinomas of the breast, or different molecular subtypes within the histological subtypes may display a preference towards hematogenous or lymphatic metastasis. Regardless of the prevalence of either pathway for metastatic dissemination, the question whether and how inhibition or stimulation of VEGFR-3-mediated signaling may simultaneously affect both hematogenous and lymphatic metastatic dissemination of the primary tumor is intriguing, and opens up an avenue for combined targeting of the

blood and lymphatic vasculature, which may display increased efficacy in the clinic. In consideration of this, other therapeutic modalities targeting related vascular signaling systems, such as the Ang-TIE signaling axis, that were previously reported to reduce distant metastasis upon inhibition of tumor-associated angiogenesis may simultaneously affect the lymphatic vascular endothelium (Mazzieri et al., 2011). Therefore, these findings definitely prompt further investigation to determine the effects of modulation of the VEGF-C / VEGFR-3 signaling axis, as well as related vascular signaling systems, on both the blood and lymphatic vasculature and their relative contributions to hematogenous metastasis, as opposed to lymphogenous spread, in breast cancer.

5

Experimental Procedures

5.1 Modulation of tumor-associated lymphatic vessels in different mouse models of breast cancer

5.1.1 Inhibition of tumor-associated lymphangiogenesis during tumor progression in a transgenic mouse model of breast cancer

The MMTV-PyMT mouse model of breast cancer

Transgenic FvB/N-Tg (MMTV-PyVT)634Mul/J mice (Cat. # 002374, Jackson Laboratories), also known as the mouse mammary tumor virus (MMTV)-polyoma middle T antigen (PyMT) model of breast cancer, have been previously described (Guy et al., 1992). In MMTV-PyMT⁺ transgenic animals, expression of the PyMT oncogene, which is under the control of the MMTV promoter and thus directed to the mammary epithelium, results in its transformation throughout the ductal tree, leading to the development of hyperplastic lesions that gradually progress to form invasive carcinomas, and eventually pulmonary metastases (Lin et al., 2003). Female wild-type FvB/N mice were bred in-house with FvB/N males bearing the MMTV-PyMT mutation to yield concurrent litters of female wildtype (WT) FvB/N and MMTV-PyMT⁺ transgenic mice. Genotyping of transgenic animals was routinely performed by Transnetyx (Memphis, Tennessee). For the experimental procedures described below, animals were used between 6-7 weeks of age (onset of hyperplastic lesions) and 11-12 weeks of age (progression to invasive carcinomas), respectively. All experimental procedures were approved by the Veterinary Authorities of the Canton Vaud according to Swiss Law.

Inhibition of tumor-associated lymphangiogenesis

To examine the importance of tumor-associated lymphangiogenesis on tumor growth and progression in a relevant preclinical model of breast cancer, a function-blocking antibody against murine (m)VEGFR-3 (mF4-31C1, ImClone / Eli Lilly and Company, (Pytowski et al., 2005)), the main receptor for the lymphangiogenic growth factors VEGF-C and -D, respectively, that is expressed predominantly on the lymphatic endothelium, was administered to female MMTV-PyMT⁺ transgenic mice upon onset of hyperplasia at 7 weeks of age. Prior to the treatment, mice were randomized according to tumor burden up to the extent that palpation allowed identification of tumor onset within the inguinal fat pad. Upon start of the trial, 500 µg of αVEGFR-3 or its corresponding rat IgG isotype control (purified rat IgG, Cat. # I4131, Sigma-Aldrich) was administered 3 times per week via intraperitoneal (i.p.) injection until these lesions progressed to an invasive carcinoma at 12 weeks of age. To determine whether treatment with therapeutic antibodies provoked adverse effects in healthy animals, one group of age-matched WT littermate controls received i.p. injections with rat IgG isotype control for the duration of the experiment.

5.1.2 Development of an orthotopic tumor model to induce lymphatic vessel growth in the context of breast cancer

5.1.2.1 Generation of stable VEGF-C-overexpressing (VEGF-C⁺) tumor cell lines

Plasmid DNA for lentiviral expression vectors

pD2109 lentiviral expression vector containing the sequence for murine (m)VEGFC cDNA (GeneID 22341), in the following abbreviated as pD2109-mVEGFC, was purchased from DNA2.0 (Newark, California). The corresponding control lentiviral expression vector, designated as pD2109-control, was obtained by removing the aforementioned sequence from the original vector through restriction enzyme digest. Briefly, pD2109-mVEGFC was digested for 3 hours at 37°C with PstI and XbaI (Cat. # R3140 and R0145, New England Biolabs). Following separation of the plasmid fragments by gel electrophoresis, the linearized plasmid backbone was isolated using the High Pure PCR Product Purification Kit according to the manufacturers instructions (Cat. # 11 732 676 001, Roche). The circular plasmid was then obtained by blunting the 5' and 3' overhangs generated upon enzymatic restriction digestion for 2 hours at room temperature with the Quick Blunting Kit (Cat. # E1201, New England Biolabs) and subsequent ligation for 20 minutes at room temperature with the Quick Ligase Kit (Cat. # M2200, New England Biolabs) following a plasmid purification step as described above.

Amplification and purification of plasmid DNA

For amplification of the pD2109-mVEGFC and pD2109-control plasmids, competent *E. coli* (One-Shot TOP10 Competent Cells, Cat. # C4040, Invitrogen) were transformed for 45 seconds at 42°C and plated on LB-agar plates containing 50 µg/ml kanamycin (CAS # 59-01-8, SV-IN, EPFL) to obtain single colonies. Following over night incubation at 37°C, 5-6 antibiotic-resistant colonies were picked and amplified in 3 ml of LB-kanamycin for 16-20 hours. To select the bacterial colonies that contain the correct pD2109-mVEGFC or pD2109-control plasmids, respectively, a diagnostic restriction digest was performed with XmaI and PvuII (Cat. # R0180 and R3151, New England Biolabs) upon purification of plasmid DNA from 2 ml of each bacterial culture using the Zippy Plasmid Miniprep Kit (Cat. # D4019, Zymo Research). For further amplification of the correct transfer plasmids, the remaining 1 ml of one bacterial culture previously transformed with pD2109-mVEGFC or pD2109-control, respectively, was then inoculated in 500 ml of LB-kanamycin and incubated at 37°C and 225 rpm during 16 hours. The corresponding plasmids were subsequently isolated using the NucleoBond Xtra Plasmid Maxiprep Kit (Cat. # 740414, Machery-Nagel) and the presence, or absence of the VEGF-C insert was confirmed by DNA sequencing prior to production of pseudo-lentiviral particles (Microsynth, Switzerland).

Production and titration of lentiviral vectors

Lentiviral vectors for the generation of stable VEGF-C-overexpressing or control murine breast cancer cell lines were kindly provided by M. Squadrito. To this end, human embryonic kidney (HEK)293T cells (CRL-3216, ATCC) were co-transfected in the presence of 125 mM calcium chloride (CaCl₂, CAS # 10043-52-4) with 32 µg of either transfer plasmid pD2109-mVEGFC or pD2109-control, respectively, as well as 12.5 µg and 6.25 µg packaging plasmids pMDL9/pRRE and pRSV-Rev (gifts of D. Trono, Addgene plasmids #12251 and #12253), and 9 µg envelope plasmid pMD2 (gift of D. Trono, Addgene plasmid #12259) to yield third-generation pseudo-lentiviral particles. To increase the efficiency of lentiviral vector production, 15 µg of pAdvantage vector (Cat. #1711, Promega) was added during the procedure. Total vector concentration and biological titer of each vector stock were determined by anti-p24 immunoassay (Cat. # 0801111, ZeptoMetrix) and TaqMan qPCR assay for HIV-1-specific *gag* with *albumin* as a reference gene as previously described (Table 1, Appendix A1.1, Barde et al., 2010). The packaging efficiency of the pseudo-lentiviral particles was then calculated for each vector stock by dividing the biological titer by the physical titer.

Transduction of murine breast cancer cell lines

An invasive primary tumor cell line isolated from the spontaneous MMTV-PyMT mouse model of breast cancer, in the following abbreviated as PyMT tumor cells, was kindly provided by I. Keklikoglou. PyMT tumor cells were routinely maintained in IMDM with GlutaMax (Cat. # 31980, Gibco), supplemented with 10% heat-inactivated FBS (Cat. # 10-082, Gibco) and passaged 1:10 every 4-5 days, whereas medium was changed every 2-3 days during subculture. P. Corthésy regularly tested cells for the absence of mycoplasma. To generate stable VEGF-C-overexpressing (VEGF-C⁺) or control murine breast cancer cell lines, PyMT tumor cells were transduced with unconcentrated pD2109-mVEGFC or pD2109-control vector. Briefly, 1.0·10⁵ PyMT tumor cells were seeded per well in a 6-well-plate (CellStar, Cat. # 657160, Greiner) in full medium on the evening prior to infection. The following afternoon, the cells were transduced during 12-16 hours with a multiplicity of infection (MOI) of ca. 10³ transducing units (TU) of either pD2109-mVEGFC or pD2109-control lentiviral vector, respectively. To avoid lentivirus-mediated toxicity, PyMT tumor cells were transduced with three doses of each vector, i.e. by addition of a 1:1, 1:5 or a 1:20 dilution of each lentiviral vector stock in full medium. The next morning, the cells were washed twice with 1x PBS (Cat. # 10010, Gibco), and fresh medium was added to allow the cells to recover for 48-72 hours prior to antibiotic selection of successfully transduced tumor cells.

Selection of stable VEGF-C⁺ and control breast cancer cell lines

To select only those tumor cells that integrated the proviral DNA into their genome, the cells were cultured in the presence of 2 µg/ml puromycin (CAS # 58-58-2, Cat. # 54041,

Calbiochem) in full medium for 4-5 days upon their recovery after infection. The sensitivity of the parental PyMT tumor cell line to puromycin was determined previously by treating the cells with different doses of the antibiotic in full medium, at 1, 2 or 5 µg/ml for up to 72 hours. Cell viability was then assessed by flow cytometry after 24, 48 and 72 hours upon addition of propidium iodide to a final concentration of 1 µg/ml (PI, CAS # 25535-16-4, Cat. # P4864, Sigma-Aldrich). Untreated cells were used to determine baseline viability at each time point. To confirm that no replication-competent recombinant viral particles emerged, the resulting polyclonal batch culture was subsequently tested for residual HIV-1-specific p24 antigen by immunoassay according to the manufacturers instructions (Cat. # 0801111, ZeptoMetrix) before further analysis.

5.1.2.2 Characterization of stable VEGF-C⁺ and control breast cell lines *in vitro*

Calculation of lentiviral DNA copy number

As transduction with different doses of lentiviral vectors yielded three VEGF-C-overexpressing, i.e. VEGF-C⁺, and three control tumor cell lines, respectively, each cell line was characterized extensively prior to further functional experiments. First, as a measure of transduction efficiency, the number of proviral DNA copies that integrated into the genome was determined for each VEGF-C⁺ and control-transduced cell line by TaqMan qPCR assay for HIV-1-specific *gag* using *titin* as a reference gene as previously described (Table 1, Appendix A1.1, Barde et al., 2010). Briefly, 2.5·10⁵ tumor cells were seeded per well in a 12-well plate (CellStar, Cat. # 665180, Greiner) in full medium in triplicate on the evening prior to the experiment. Untransfected PyMT cells were used as a negative control. The ensuing morning, genomic DNA was extracted using the High Pure PCR Template Preparation Kit (Cat. # 11 796 828 001, Roche) and the concentration of each sample was measured with Nanodrop. Samples were stored at -20°C until needed. The proviral DNA copy number within the genome of each cell line was then calculated as follows:

$$\text{Genomic copy number of proviral DNA} = \frac{\text{Mean Cq (gag)}}{\text{Mean Cq (titin)}} \cdot 2$$

Determination of cell division rate

Next, as integration of the proviral DNA can occur randomly within the genome and may cause disruptions within functional genes, the proliferation rate was assessed for each cell line as compared to the parental PyMT cell line. To this end, 1.0·10⁴ tumor cells were seeded per well in a 24-well plate (CellStar, Cat. # 662160, Greiner) in full medium, and the number of cells was then determined in 24-hour intervals for 5 consecutive days using a Neubauer chamber and 0.4% Trypan Blue solution (Cat. # 15-250-061, Gibco) to exclude dead cells. To determine the growth rate, total cell number was plotted on a logarithmic scale against the time of counting, and the generation time and division rate

of each cell line during the exponential growth phase were then calculated from the slope of each growth function using the following formulas:

$$\text{Generation time (hours)} = \frac{\ln 2}{k},$$

where k represents the specific growth rate in hours, and

$$\text{Division rate (hours)} = \frac{24 \text{ hours}}{\text{Generation time (hours)}}$$

Analysis of VEGF-C expression levels *in vitro*

Finally, the functionality of the transgene was assessed by analysis of VEGF-C expression levels by qRT-PCR and immunoassay, respectively. In short, $2.5 \cdot 10^5$ tumor cells were seeded per well in a 12-well plate in full medium in triplicate on the evening prior to the experiment. For cell counts, one extra well was prepared per cell line. The next morning, the cells were washed twice with 1x PBS and IMDM medium containing 2% FBS was added to the cells. After 24 hours, the supernatant was harvested, as well as total RNA of each corresponding sample extracted using the RNeasy Plus Micro Kit (Cat. # 74034, Qiagen) and samples were stored at -20°C until needed. VEGF-C mRNA expression levels were determined by two-step reverse transcription (RT)-qPCR. Briefly, 1 μg of total RNA was reverse transcribed using the iScript cDNA Synthesis Kit (Cat. # 1708890, BioRad) to yield cDNA. Following determination of the Cq values for *vegfc* and *β -actin* as a reference gene with Sybr Green I dye (Lightcycler 480 Sybr Green I Master Mix, Cat. # 04707516001, Roche) on a Lightcycler 480 qPCR instrument (Roche), VEGF-C mRNA expression levels were subsequently calculated using the $2^{-\Delta\Delta\text{Cq}}$ method. Levels of secreted VEGF-C in the supernatant were determined by VEGF-C immunoassay (Quantikine Human VEGF-C ELISA kit, Cat. # DVEEC00, R&D).

5.1.2.3 Induction of tumor-associated lymphangiogenesis upon orthotopic injection of VEGF-C⁺ breast cancer cell lines *in vivo*

Orthotopic inoculation of tumor cells

Female FvB/N mice were purchased from Charles Rivers Laboratory (France) and used between 8-10 weeks of age. All procedures were performed according to protocols approved by the Veterinary Authorities of the Canton Vaud according to Swiss law. For orthotopic inoculation of PyMT tumors, either $2.5 \cdot 10^5$ VEGF-C⁺ or control-transduced tumor cells were injected into the inguinal mammary gland as previously described (Fridman et al., 2012). To this end, mice were anesthetized by i.p. administration of 200 μl of a mixture consisting of 1 mg/kg medetomidine (Dorbene®, Graeb) and 80 mg/kg ketamine (Ketasol 100®, Graeb), and their left flank was shaved before making

a small incision located above the inguinal mammary gland. Once exposed, $2.5 \cdot 10^5$ tumor cells were injected directly into the fat tissue surrounding the glands in a volume of 20 μ l of growth factor (GF)-reduced Matrigel™ (Cat. # 356231, BD Biosciences) at a final concentration of 7 mg/ml per gland using a 30G needle (U-100 insulin syringes, 0.3 ml capacity, Cat. #324826, BD Medical). For the duration of the surgical procedure, anesthetized animals were placed on a heating pad, and a layer of Viscotears® (Alcon) was applied on the eyes to protect the corneas. Upon its completion, the wounds were then closed using 7.5 mm wound clips (Cat. # BN507R, Aesculap, B. Braun), and the previously induced anesthesia was antagonized at least 30 minutes post-induction with by i.p. injection of 1 mg/kg of atipamezole (Alzane®, Graeub). Finally, to minimize pain, the animals received 0.1 mg/kg buprenorphine (Temgesic®, Reckitt Benckiser), administered s.c. in the scruff of the neck directly after the procedure, as well as paracetamol (Dafalgan®, Bristol-Meyers Squibb), 1 sachet of 250 mg administered in the drinking water (250 ml) during the next 3-4 days as analgesic. The surgical staples used to close the wound were removed one week post-surgery, and tumor growth was monitored twice per week by palpation and caliper measurement for the duration of each experiment. Tumor volumes were calculated assuming an ellipsoid shape of the tumor, using the following formula where r_1 and r_2 represent the long and short radius of the ellipsoid in mm, respectively:

$$Tumor\ volume\ (mm^3) = \frac{4}{3} \cdot \pi \cdot r_1 \cdot r_2^2$$

5.2 Deconvolution of the tumor microenvironment during tumor growth and progression in transgenic and orthotopic mouse models of breast cancer

5.2.1 Enzyme-Linked ImmunoSorbent Assay

Analysis of cytokine content was performed by immunoassay on whole-tissue protein extracts for the following secreted factors: VEGF-A (Mouse VEGF Quantikine ELISA kit, Cat. # MMV00, R&D), VEGF-C (Human VEGF-C Quantikine ELISA kit, Cat. # DVEC00, R&D), VEGF-D (Mouse DuoSet VEGF-D ELISA kit, Cat. # Dy469, R&D), and TGF- β 1 (Mouse TGF- β 1 DuoSet ELISA kit, Cat. # Dy1679, R&D) according to the manufacturers instructions. Briefly, mice were sacrificed by CO₂ asphyxiation and tumors and their draining LNs harvested. The obtained tissues were then weighed and transferred to 2 ml-capacity tubes containing ceramic beads for sample lysis (Lysing Matrix D, Cat. # 116913, MP Biomedicals). Total protein was extracted in tissue protein extraction (T-PER) buffer (Cat. # 78510, Thermo Scientific), supplemented with one tablet of protease inhibitor (Complete EDTA-free, Cat. # 11873580001, Roche) per 20 ml of buffer, upon disruption of the tissue using a rotary tissue homogenizer set to three cycles of 4.0 m/s (FastPrep®-24, MP Biomedicals). Protein lysates were cleared by two rounds of centrifugation at full speed and at 4°C in a table top centrifuge and stored at -80°C until needed. Prior to each immunoassay, total protein content was determined using the Pierce BCA Protein Assay Kit (Cat. # 23227, Thermo Scientific).

5.2.2 Flow cytometry

Preparation of single cell suspensions

Stromal and immune cell populations in the tumor and tumor-draining LN were analyzed by flow cytometry. To this end, mice were sacrificed by CO₂ asphyxiation and tumors and their draining LNs harvested, and processed to yield single-cell suspensions as previously described (Broggi et al., 2014). Briefly, upon coarse mechanical disruption with scissors, tumors were subsequently digested with 3.3 mg/ml Collagenase D (Cat. # 11088866001, Roche) and 40 µg/ml DNase I (Cat. # 11284932001, Roche) in digestion medium consisting of DMEM, high glucose (Cat. # 41965, Gibco) supplemented with 2% heat-inactivated FBS and 1.2 mM calcium chloride (CaCl₂, CAS # 10043-52-4) for 1 hour at 37°C under agitation. In addition, tumors were further disrupted by pipetting up and down 100 times with an automated pipette every 20 minutes during the digestion, before addition of EDTA (prepared in-house by P. Corthésy) to a final concentration of 5 mM and filtration through a 70 µm cell strainer (Cat. # 352350, Falcon, Corning Inc.) to obtain a single-cell suspension. To process the draining LNs, the capsule of each LN was gently opened using a 26G needle prior to digestion. In contrast to tumors, tumor-draining LNs were subjected to a two-step protocol, consisting of a first digestion in digestion medium containing 1 mg/ml Collagenase IV (Cat. # LS004188, Worthington) and 40 µg/ml DNase I for 30 minutes at 37°C under agitation, followed by a second treatment in digestion medium containing 3.3 mg/ml Collagenase D and 40 µg/ml DNase I. LNs were further disassembled upon one round of disruption with an automated pipette prior to addition of 5 mM EDTA and filtration through a 70 µm cell strainer as described above. Single cell suspensions of tumors and LNs were then washed once with 1x PBS, and prepared for flow cytometric analysis as described below.

Staining procedure for flow cytometry

Upon preparation of a single cell suspension, cells were first incubated with Live/Dead fixable Dead Cell Stain Kit (Blue, 1:1'000 final dilution in PBS, Cat. # 23105, Thermo Fischer Scientific) for 30 minutes on ice for cell viability. Subsequently, cells were washed once with 3 ml of FACS buffer consisting of 1x PBS supplemented with 2% heat-inactivated FBS. Prior to cell surface staining, cells were incubated with purified rat anti-mouse CD16/CD32 (1 : 200, Cat. # 553141, BD Pharmingen) for 10 minutes on ice to block Fc receptors. Cell surface staining was then performed without an intermediate wash for 20 minutes on ice. If required, subsequent staining for intracellular antigens was then performed over night at 4°C using the FoxP3/Transcription Factor Staining Buffer Set (Cat. # 005523, eBioscience) according to the manufacturers instructions. All antibodies used for cell surface and intracellular staining are listed in Table 3 (Appendix A1.2). Unless stated otherwise, both stromal and myeloid cell populations were analyzed directly without fixation on a BD LSR-II cytometer, whereas lymphocytes were then analyzed during the following day.

5.2.3 Histological analysis

Preparation of tissue sections

For histological analysis of the tumor or its draining LN, as well as pulmonary metastasis, the inguinal fat pads containing both the tumor and its draining LN, as well as the lungs were harvested from MMTV-PyMT⁺ transgenic animals, or from mice bearing orthotopically inoculated VEGF-C⁺ or control tumors, respectively, following CO₂ asphyxiation and post-mortem cardiac perfusion with HBSS (Cat. # 14175, Gibco) supplemented with 5 ml of heparin (25'000 I.E./5 ml, B. Braun). The obtained tissue specimens were directly fixed over night in 20 volumes of 4% paraformaldehyde (PFA, prepared in-house by P. Corthésy), unless stated otherwise. The following day, tissue samples were washed three times with 20 volumes of 1x PBS under gentle agitation for ca. 2-3 hours per wash, prior to over night dehydration in a Leica ASP200 tissue processor and subsequent paraffin embedding. Using a Microm HM325 microtome, 4- μ m sections were prepared and captured on Superfrost Plus microscope slides (Cat. # J1800AMNZ, Thermo Scientific). Tissue sections were allowed to dry over night in an oven at 30°C prior to the staining procedures listed below.

Histological evaluation of tumor progression and metastasis

For a delineation of tumor growth and progression in our MMTV-PyMT⁺ transgenic mice bred in-house, as well as the extent of regional and distant metastasis to the inguinal LN and lungs in MMTV-PyMT⁺ tumor-bearing mice and their age-matched WT littermates, respectively, previously prepared 4- μ m sections of tumors and lungs were stained in hematoxylin and eosin (H&E) for 30 minutes using an automated slide stainer (Sakura). Histological classification of tumor stage and evaluation of metastasis was kindly performed by Nadine Stokar (Pathology, HCF, EPFL). To ensure a thorough analysis of the extent of pulmonary metastasis in either breast cancer model, lungs were sectioned completely, and one section with 3 tissue specimens at every ca. 50 μ m was evaluated for the presence of metastatic lesions. Images of micrometastatic lesions were recorded at 40x magnification in brightfield illumination using an Olympus Slide Scanner VSL120-L100. The presence of metastatic tumor cells in the regional tumor-draining LN was confirmed by immunofluorescence with an antibody specific for the PyMT antigen (Tables 4 and 5, Appendix A1.4, staining procedure described below).

Immunofluorescence staining procedure

Immunostaining of paraffin-embedded tissue specimens was performed as follows. Briefly, sections were rehydrated, and, if required, submitted to heat-mediated antigen retrieval in citrate buffer pH6.0 for 20 minutes at 95°C (PT module, Thermo Scientific), or epitope unmasking with proteinase K treatment (Cat. # 03115879001, Roche) in 1x tris-buffered saline (TBS, SV-IN, EPFL) for 10 minutes (Table 4, Appendix A1.4).

Subsequently, tissue specimens were washed three times for 5 minutes in TBS before drawing an outline of each sample with a water-repellent pen (ImmEdge, Cat. # H-4000, Vector Laboratories), blocked in 0.5% casein (Cat. # 218682, CAS 9000-71-9, Calbiochem) dissolved in TBS for 1 hour at room temperature, and directly incubated with the appropriate primary antibodies in 0.5% casein-TBS containing 0.01% Triton-X100 (CAS 9002-93-1, Applichem) over night at 4°C in a humidified staining chamber (Table 4, Appendix A1.4). The next morning, slides were washed twice with 0.1% Triton-X100 in TBS, and once in TBS for 5 minutes per wash, and incubated with the corresponding secondary antibodies in 0.5% casein-TBS containing 0.01% Triton-X100 for 1 hour at room temperature (Table 5, Appendix A1.4). Lastly, slides were washed once more as described above, and incubated with DAPI (Cat. # 1306, Thermo Scientific) diluted 1 : 5'000 in TBS for 20 minutes at room temperature. Slides were washed once more, this time in TBS only, and mounted using ProLong Gold anti-fade mountant (Cat. # 36930, Molecular Probes), coverslipped (Menzel-Gläser #1, 24x60 mm) and sealed with nail polish. All antibodies used for immunofluorescence staining are listed in Tables 4 and 5 in Appendix A1.4. Unless otherwise specified, sections were imaged at 20x magnification, using an Olympus Slide Scanner VSL120-L100.

Immunohistochemistry and picrosirius red double chromogenic staining

Total collagen content and collagen-crosslinking enzyme LOX in the tumor were visualized using double chromogenic staining of picrosirius red in combination with 3, 3-diaminobenzidine (DAB) chromogen. To this end, sections were rehydrated and washed three times for 5 minutes in TBS before drawing an outline of each sample with a water-repellent pen as described above in the staining procedure for immunofluorescence. Next, endogenous peroxidases were quenched using 3% H₂O₂ (Cat. # 107209, Merck Millipore) in 1x TBS for 10 minutes, after which sections were washed 3 times in TBS for 5 minutes per wash, blocked in 0.5% casein-TBS for 30 minutes at room temperature, and directly incubated with the appropriate primary antibody diluted in 0.01% Triton-X100 in 0.5% casein-TBS over night at 4°C in a humidified staining chamber (Table 4, Appendix A1.4). The ensuing morning, sections were washed 3 times in TBS for 5 minutes per wash, and incubated with a secondary HRP-conjugated antibody diluted in 0.01% Triton-X100 in 0.5% casein-TBS at room temperature for 45 minutes. Finally, sections were washed 3 times TBS for 5 minutes per wash once more before developing the sections with DAB substrate (SigmaFAST DAB tablets, Cat. # D4293, Sigma-Aldrich). Upon reaching the desired intensity, while background staining is still low, the reaction is quenched by dipping the slides in 1 x in Tris-HCl pH 7.6, washed 3 times and directly stained with picrosirius red using an automated slide stainer (Sakura). To enhance the contrast between picrosirius red and the DAB chromogen, the DAB substrate solution was supplemented with 10% nickel (CAS # 7440-02-0, Cat. # 09885, Sigma). Pictures were taken at 20x magnification under brightfield and polarized illumination using an Olympus AX70 microscope.

Quantification of blood and lymphatic vessel area

Lymphatic and blood vessel area were determined upon immunofluorescence for the tumor-associated vasculature with antibodies against pan-endothelial CD31, gp38, and lymphatic-specific lyve-1 and VEGFR-3, respectively (Tables 4 and 5, Appendix A1.4). To determine the area fraction covered by blood or lymphatic vessels in whole-tissue sections, respectively, a semi-automated approach was applied using a macro written by O. Burri (BIOP, EPFL, see Appendix A1.5). Briefly, to determine the percentage of area that is covered by lymphatic vessels, the tumor or draining LN was outlined manually on the DAPI channel as the region of interest (ROI), in which the lymphatic or blood vessel area was then quantified upon selection of the appropriate threshold. The area fraction of lymphatic vessels for each imaging plane was then obtained using the following formula:

$$\text{Lymphatic vessel density (\%)} = \frac{\text{Area (LYVE1}^+)}{\text{Area (DAPI}^+)} \cdot 100\%$$

Unless stated otherwise, plotted values represent the average of the lymphatic and blood vessel density as quantified in three separate imaging planes. Initially, quantification of the area covered by lymphatic vessels in the inguinal LN of MMTV-PyMT⁺ tumor-bearing animals or age-matched FvB/N WT tumor-free mice was determined upon quantification of the lyve-1⁺ area. However, to distinguish between blood and lymphatic vessels, later on, an added image parser function in version 7 allowed quantification of both the CD31⁺lyve-1⁻ blood vessel and CD31⁺lyve-1⁺ lymphatic vessel area in the tumor and draining LN of VEGF-C⁻ or control tumor-bearing mice, respectively.

Quantification of ECM deposition

To evaluate the desmoplastic response during tumor growth and progression, and upon VEGFR-3-mediated inhibition of tumor-associated lymphangiogenesis in MMTV-PyMT⁺ transgenic animals, various ECM components, i. e. total collagen content, as well as collagen-III, fibronectin and tenascin-C, respectively, were analyzed using a combination of immunohistochemistry and immunofluorescence on zinc-fixed tissue sections (see previous sections on staining procedures, and Tables 4 and 5 in Appendix A1.4). Analogous to quantification of blood and lymphatic vessel area, ECM deposition in the tumor was determined in a similar manner by a semi-automated approach using the same macro for area measurements described in the previous section (see Appendix A1.5). Contrary the abovementioned approach, however, the density of the various ECM components was then determined in 3 ROIs each extracted from the core of the primary tumor, or the invasive edge at scaling 1, with the invasive edge of the primary tumor focus determined by staining of the basement membrane with collagen-IV, which is disrupted upon tumor progression from hyperplastic to invasive lesions. Calculation of the percentage of area coverage of each ECM component was then done using the same formula for lymphatic vessel density listed above.

Statistical analysis

The statistical analysis of each experiment is described in the respective figure legends. Unless stated otherwise, the plotted values represent the standard error of the mean (SEM). The following symbols: *, **, and ***, indicate a statistical significance of $p < 0.05$, $p < 0.01$ and $p < 0.001$, respectively. For the most part, statistical analysis on the data was performed by unpaired student's *t*-test, with the exception of characterization of the murine breast cancer cell lines *in vitro*, which was analyzed by 2-way ANOVA. For assessment of lymphangiogenesis and angiogenesis, as well as deconvolution of the tumor immune microenvironment during tumor growth and progression in the MMTV-PyMT model of breast cancer, statistical analysis was performed by unpaired student's *t*-test, as only comparisons between transgenic MMTV-PyMT⁺ tumor-bearing mice and tumor-free WT littermate control of the same age were made.

Appendices

Appendix 1: Supplementary Experimental Procedures

A1.1: Primer sequences and qPCR conditions

Table 1 - Primer sequences and qPCR conditions for TaqMan qPCR

Gene name	Sequence	
<i>Albumin</i>	Forward	5'-GCTGTCATCTCTTGTGGGCTGT
	Reverse	5'-ACTCATGGGAGCTGCTGGTTC
	Probe	5'-CCTGTCATGCCACACAAATCTCTCC
<i>Gag</i>	Forward	5'-GGAGCTAGAACGATTTCGAGTTA
	Reverse	5'-GGTGTAGCTGTCCCAGTATTTGTC
	Probe	5'-ACAGCCTTCTGATGTTTCTAACAGGCCAGG
<i>Titin</i>	Forward	5'-AAAACGAGCAGTGACGTGAGC
	Reverse	5'-TTCAGTCATGCTGCTAGCGC
	Probe	5'-TGCACGGAAGCGTCTCGTCTCAGTC

Table 1: Primer and probe sequences for TaqMan qPCR

Conditions: 10 minutes at 95°C followed by 50 cycles of:

- 95°C: 15 seconds
- 60°C: 60 seconds

Table 2 - Primer sequences and qPCR conditions for SYBR Green qPCR

Gene name	Sequence	
<i>Vegfc</i>	Forward	5'-CAGCCCACCCTCAATACCAG
	Reverse	5'-GACGGACACACATGGAGGTT

Table 2: Primer and probe sequences for SYBR Green qPCR

Conditions: 10 minutes at 95°C followed by 40 cycles of:

- 95°C: 15 seconds
- 60°C: 60 seconds

A1.2: Flow cytometry: antibodies and reagents

Table 3 - Antibodies used for flow cytometry

Antigen	Clone	Isotype	Conjugate	Conc.	Dilution	Cat. #	Manufacturer
CD3e	145-2C11	Hamster	APC	0.2 mg/ml	1 : 800	100312	Biologend
CD4	RM4-5	Rat IgG2a, κ	BV711	0.5 mg/ml	1 : 100	100549	Biologend
CD4	RM4-5	Rat IgG2b, κ	Pacific Blue	0.5 mg/ml	1 : 800	100531	Biologend
CD8	53-6.7	Rat IgG2a	BV650	0.2 mg/ml	1 : 100	100741	Biologend
CD8	53-6.7	Rat IgG2a, κ	APC/eF1780	0.2 mg/ml	1 : 800	47-0081-82	eBioscience
CD11b	M1/70	Rat IgG2b, κ	BV711	0.2 mg/ml	1 : 300	101241	Biologend
CD11c	N418	Hamster	PE	0.2 mg/ml	1 : 200	117308	Biologend
CD25	3C7	Rat IgG2b, κ	FITC	0.5 mg/ml	1 : 200	101908	Biologend
CD25	PC61	Rat IgG1, δ	PE-Texas-Red	0.2 mg/ml	1 : 200	562694	BD
CD31	390	Rat IgG2a, κ	eF1450	0.2 mg/ml	1 : 200	48-0311-82	eBioscience
CD44	IM7	Rat IgG2a	PerCP-Cy5.5	0.2 mg/ml	1 : 800	45-0441-82	eBioscience
CD45	30-F11	Rat IgG2b, κ	APC/Cy7	0.2 mg/ml	1 : 300	47-0451-82	eBioscience
CD45	30-F11	Rat IgG2b, κ	BV786	0.2 mg/ml	1 : 200	564225	BD
CD62L	MEL-14	Rat IgG2a, κ	APC/eF1780	0.2 mg/ml	1 : 200	47-0621-82	eBioscience
CD69	H1.2F3	Hamster	PE/Cy7	0.2 mg/ml	1 : 200	104512	Biologend
CD69	H1.2F3	Hamster	APC	0.5 mg/ml	1 : 300	104518	Biologend
CD206	C068C2	Rat	APC	0.5 mg/ml	1 : 400	141712	Biologend
EpCAM	G8.8	Rat IgG2a, κ	PE/Cy7	0.2 mg/ml	1 : 300	25-5791-80	eBioscience
F4/80	BM8	Rat IgG2a, κ	FITC	0.5 mg/ml	1 : 200	123120	Biologend
F4/80	BM8	Rat IgG2a, κ	PerCP-Cy5.5	0.5 mg/ml	1 : 200	123128	Biologend
FoxP3	FJK-16s	Rat IgG2a, κ	FITC	0.5 mg/ml	1 : 200	11-5773-82	eBioscience
gp38	8.1.1	Hamster	APC	0.5 mg/ml	1 : 200	127410	Biologend
Gr-1	RB6-8C5	Rat IgG2b, κ	Biotin*	0.5 mg/ml	1 : 200	13-5931-82	eBioscience
Ly6C	HK1.4	Rat IgG2c, κ	PE/Cy7	0.2 mg/ml	1 : 500	128017	Biologend
Ly6G	1A8	Rat	Pacific Blue	0.5 mg/ml	1 : 300	127612	Biologend
LYVE-1	Polyclonal	Rabbit	AF488**	0.2 mg/ml	1 : 200	103-PA50	Reliatech
MHC-II (IA-IE)	M5/114.15.2	Rat IgG2b, κ	PerCP-Cy5.5	0.2 mg/ml	1 : 400	107626	Biologend
NK1.1	PK136	Rat IgG2b, κ	PE	0.2 mg/ml	1 : 200	107608	Biologend
PD-1	RMP1-30	Rat IgG2b, κ	PE/Cy7	0.2 mg/ml	1 : 200	109109	Biologend
TCR-β	H57-597	Hamster	eF1450	0.2 mg/ml	1 : 400	48-5961-82	eBioscience
TGF-β (LAP)	TW7-20B9	Mouse IgG1, κ	PE	0.2 mg/ml	1 : 200	141306	Biologend

Table 3: Antibodies used for flow cytometry

Application notes:

* Use secondary streptavidin-pacific orange conjugate at 1 : 200

** Use secondary anti-rabbit AF488 conjugate at 1 : 400

A1.3: Flow cytometry: phenotype of cells in the tumor microenvironment

The cell populations in the tumor microenvironment, comprising the tumor and its draining LN, were analyzed by flow cytometry according to the phenotypes listed below:

Stromal cells in the tumor and draining LN:

- **LECs:** CD45⁻EpCAM⁻CD31⁺gp38⁺ and Lyve-1⁺ or lyve-1⁻
- **BECs:** CD45⁻EpCAM⁻CD31⁺gp38⁻
- **FRCs:** CD45⁻EpCAM⁻CD31⁻gp38⁺

Stromal cell populations were analyzed as previously described in (Link et al., 2007).

Myeloid cells in the tumor:

- **Myeloid cells:** CD45⁺CD11b^{hi}
- **MDSCs:** CD45⁺CD11b^{hi}Gr-1⁺
- **Neutrophils:** CD45⁺CD11b^{hi}Ly6G⁺Ly6C⁻F4/80⁻
- **Monocytes:** CD45⁺CD11b^{hi}Ly6G⁻Ly6C⁺F4/80⁻
- **TAMs:** CD45⁺CD11b^{hi}Ly6G⁻Ly6C⁻F4/80⁺
- **M1-like TAMs:** CD11c⁺CD206⁻ TAMs
- **M2-like TAMs:** CD11c⁻CD206⁺ TAMs

The distinction between CD11c⁺ M1-like and CD206⁺ M2-like TAMs was made based on a previous description in (Squadrito and De Palma, 2011).

T lymphocytes in the tumor and draining LN

- **T cells:** CD45⁺TCR-β⁺NK1.1⁻ or CD45⁺CD3e⁺NK1.1⁻
- **NK cells:** CD45⁺TCR-β⁻NK1.1⁺ or CD45⁺CD3e⁻NK1.1⁺
- **NK T cells:** CD45⁺TCR-β⁺NK1.1⁺ or CD45⁺CD3e⁺NK1.1⁺
- **CD4⁺ T cells:** CD45⁺TCR-β⁺NK1.1⁻CD4⁺CD8⁻
- **CD8⁺ CTLs:** CD45⁺TCR-β⁺NK1.1⁻CD4⁻CD8⁺
- **FoxP3⁺ T_{reg} cells:** CD45⁺TCR-β⁺NK1.1⁻CD4⁺CD8⁻FoxP3⁺
- **Activated CTLs:** CD45⁺TCR-β⁺NK1.1⁻CD4⁻CD8⁺ and CD25⁺ or CD69⁺
- **Suppressive CTLs:** CD45⁺TCR-β⁺NK1.1⁻CD4⁻CD8⁺ and PD-1⁺

Note: alternative to TCR-β, CD3e has also been used as a marker to identify the T lymphocytes in the tumor and LN, in which case all subsequent subsets are described by expression of CD3e instead of TCR-β.

A1.4: Histology: antibodies and reagents

Table 4 - Primary antibodies used for histological analysis

Antigen	Clone	Species	Antigen Retrieval	Conc.	Dilution	Cat. #	Manufacturer
CD31	SZ31	Rat	Citrate pH6.0	0.2 mg/ml	1 : 50	DIA-310	Dianova
Collagen-III	Polyclonal	Rabbit	N/D	1.0 mg/ml	1 : 200	Ab7778	Abcam
Collagen-IV	Polyclonal	Rabbit	N/D	1.0 mg/ml	1 : 500	Ab6581	Abcam
Fibronectin	Polyclonal	Rabbit	N/D	1.0 mg/ml	1 : 100	Ab23750	Abcam
gp38	Polyclonal	Goat	Not necessary	0.1 mg/ml	1 : 200	AF3244	R&D Systems
LOX	Polyclonal	Rabbit	Citrate pH6.0	1.0 mg/ml	1 : 200	Ab31238	Abcam
LYVE-1	Polyclonal	Rabbit	Citrate pH6.0, PK	0.2 mg/ml	1 : 200	103-PA50	Reliatech
PyMT	Monoclonal	Rat	Citrate pH6.0	-	1 : 50	MAB7374	Abnova
Tenascin-C	Polyclonal	Goat	PK	0.2 mg/ml	1 : 200	AF3358	R&D Systems
VEGFR-3	Polyclonal	Goat	Citrate pH6.0, PK	0.2 mg/ml	1 : 50*	AF743	R&D Systems

Table 4: Antibodies used for histology

Application notes:

* Use intermediate anti-goat biotin conjugate at 1 : 200 to amplify signal

N/D Not determined, used on zinc-fixed tissue specimens

Table 5 - Secondary antibodies used for histological analysis

Fluorophore	Host	Species	Antigen Retrieval	Conc.	Dilution	Cat. #	Manufacturer
AF488	Donkey	Goat	N/A	2.0 mg/ml	1 : 200	A-11055	Invitrogen
	Donkey	Rabbit	N/A	2.0 mg/ml	1 : 200	A-21206	Invitrogen
	Donkey	Rat	N/A	2.0 mg/ml	1 : 200	A-21208	Invitrogen
AF546	Goat	Rabbit	N/A	2.0 mg/ml	1 : 200	A-11010	Invitrogen
	Goat	Rat	N/A	2.0 mg/ml	1 : 200	A-11081	Invitrogen
AF647	Donkey	Rabbit	N/A	2.0 mg/ml	1 : 200	A-31573	Invitrogen
	Chicken	Rat	N/A	2.0 mg/ml	1 : 200	A-21472	Invitrogen
Biotin	Donkey	Goat	N/A	N/A	1 : 200	N/A	HCF, EPFL
AF488-SA	N/A	N/A	N/A	5 mM	1 : 200	S11223	Invitrogen
AF647-SA	N/A	N/A	N/A	5 mM	1 : 200	S21374	Invitrogen

Table 5: Antibodies used for histology

A1.5: Macro for area measurements

```
// Action Bar for Area quantifications
// By Olivier Burri
// EPFL BIOP 2014

// Install the BIOP Library
call("BIOP_LibInstaller.installLibrary", "BIOP"+File.separator+"BIOPLib.ijm");

// Name ActionBar
bar_name = "BIOP Ingrid version7";

bar_file = replace(bar_name, " ", "_").ijm";
bar_jar = replace(bar_name, " ", "_").jar";

runFrom = "jar:file:BIOP/"+bar_jar+"/"+bar_file;
////////////////////////////////////
// The line below is for debugging. Place this VSI file in the ActionBar folder within Plugins
////////////////////////////////////
runFrom = "/plugins/ActionBar/"+bar_file;

if(isOpen(bar_name) {
    run("Close AB", bar_name);
}

run("Action Bar",runFrom);
exit();

<codeLibrary>

function toolName() {
    return "Area Measurements Ingrid";
}

function countRoisOfCategory(category) {
    nRois = roiManager("count");
    roiNum = 0;
    for (i=0; i<nRois; i++) {
        name = call("ij.plugin.frame.RoiManager.getName", i);
        expr = roiNameExp(category);
        if (matches(name, expr)) {
            roiNum++;
        }
    }
    print("There are "+roiNum+" ROIs of category '"+category+"'");
    return roiNum;
}

function roiName(category, index) {
    return category+" #"+index;
}

function roiNameExp(category) {
    return category+" #\\d+";
}

function renameLastRoi(category, index) {
    nRois = roiManager("Count");
    roiManager("Select", nRois-1);
    name = roiName(category, index);
    roiManager("Rename", name);
    roiManager("Sort");
    return name;
}

function DrawRois(category) {
    if (getVersion>="1.37r")
        setOption("DisablePopupMenu", true);

    // Setup some variables. Basically these numbers
    // Represent an action that has taken place (it's the action's ID)
    shift=1;
    ctrl=2;
```

```

rightButton=4;
alt=8;
leftButton=16;
insideROI = 32; // requires 1.42i or later

// Now we initialize the ROI counts and check if there are already ROIs with this name.

roiNum = countRoisOfCategory(category);

// done boolean to stop the loop that checks the mouse's location
done=false;

// rightClicked to make sure the function saves the ROI ONCE and not
// continuously while "right click" is pressed
rightClicked = false;
print("Started mouse tracking for "+category+", press 'ALT' to stop");
while(!done) {
    // getCursorLoc gives the x,y,z position of the mouse and the flags associated
    // to see if a particular action has happened, say a left click while shift is
    // pressed, you do it like this:
    // if (flags&leftButton!=0 && flags&shift!=0) { blah blah... }

    getCursorLoc(x,y,z,flags);
    // print(x,y,z,flags);
    // If a freehand selection exists and the right button was clicked AND that right click was not pressed before
already
    if (flags&rightButton!=0 && selectionType!=-1 && !rightClicked) {
        // set rightClicked to true to stop this condition from writing several times the same ROI
        rightClicked = true;

        // Add the ROI to the manager
        roiManager("Add");

        renameLastRoi(category, roiNum+1);
        roiNum++;
        print(roiNum+" saved.");
    }

    // Once we stopped pressing the right mouse button, we can then click it again and add a new ROI
    if (flags&rightButton==0) {
        rightClicked = false;
    }

    // We stop the loop when the user presses ALT
    if(isKeyDown("alt")) {
        done=true;
        print("ALT Pressed: Done");
        setKeyDown("none");
    }
}

}

function addRoi(name) {
    roiManager("Add");
    roiManager("Select", roiManager("Count")-1);
    roiManager("Rename", name);
}

function drawRoi() {
    isLymph = getDataD("Draw Lymph Node", 1);
    isTumorCore = getDataD("Draw Tumor Core", 1);
    isInvasiveEdge = getDataD("Draw Invasive Edge", 1);
    isNonInvasiveTumor = getDataD("Draw Non-Invasive Tumor", 1);

    roiManager("Reset");

    waitForUser("Draw a ROI for the background, then press OK");
    addRoi("BG");

    if (isLymph) {
        waitForUser("Draw a ROI around the Lymph Node, then press OK");
        addRoi("Lymph Node");
    }

    if (isTumorCore) {
        waitForUser("Draw a ROI around the Tumor Core, then press OK");
        addRoi("Tumor Core");
    }
}

```

```

    }

    if (isInvasiveEdge) {
        waitForUser("Draw a ROI around the Invasive Edge, then press OK");
        addRoi("Invasive Edge");
    }

    if (isNonInvasiveTumor) {
        waitForUser("Draw a ROI around the Non-Invasive Tumor, then press OK");
        addRoi("Non-Invasive Tumor");
    }

    saveRois("Open");
}

function selectRoi(name) {
    n = roiManager("Count");
    //print("looking for"+name);
    for (i=0; i<n; i++) {
        rName = call("ij.plugin.frame.RoiManager.getName", i);
        if (rName == name) {
            roiManager("Select", i);
            return i;
        }
    }
    return -1;
}

function buildSettings() {
    // Get the number of categories and Their Names
    dapi = getDataD("DAPI Channel", 1);
    dapiTh = getDataD("DAPI threshold", "Huang");
    channels = getDataD("Channels Of Interest", "2,3,4");
    channelNames = getDataD("Channel Names", "GP38,Lyve1,CD31");
    channelThr = getDataD("Threshold Methods", "Moments,Triangle,Triangle");
    chClear = getDataD("Channels With Bright Artifacts","");
    isArea = parseInt(getDataD("Perform Area Logic", 1));
    areas = getDataD("Area Logic Measurements","A&&B&&C,A&&B,A&&B&&C,A&&C,A&&C");

    minSize = getDataD("Min Particle Size", 30);
    isDebug = parseInt(getDataD("Debug", 0));

    isLymph = getDataD("Draw Lymph Node", 1);
    isTumorCore = getDataD("Draw Tumor Core", 1);
    isInvasiveEdge = getDataD("Draw Invasive Edge", 1);
    isNonInvasiveTumor = getDataD("Draw Non-Invasive Tumor", 1);

    methods = getList("threshold.methods");
    if (isDebug == 1) {
        isDebug = true;
    } else {
        isDebug = false;
    }
    Dialog.create("Detection Settings");
    Dialog.addNumber("DAPI Channel", dapi);
    Dialog.addString("DAPI threshold", dapiTh);
    Dialog.addString("Channels Of Interest", channels);
    Dialog.addString("Channel Names", channelNames);
    Dialog.addString("Threshold Methods", channelThr);
    Dialog.addString("Channels With Bright Artifacts", chClear);
    Dialog.addCheckbox("Perform Area Logic", isArea);

    Dialog.addString("Channel Logic For Area Measurement", areas);

    Dialog.addNumber("Minimum Particle Size", minSize);
    Dialog.addCheckbox("Debug Mode", isDebug);
    Dialog.addCheckbox("Draw Lymph Node", isLymph);
    Dialog.addCheckbox("Draw Tumor Core", isTumorCore);
    Dialog.addCheckbox("Draw Invasive Edge", isInvasiveEdge);
    Dialog.addCheckbox("Draw Non-Invasive Tumor", isNonInvasiveTumor);
    Dialog.show();

    dapi = Dialog.getNumber();
    dapiTh = Dialog.getString();
    channels = Dialog.getString();
    channelNames = Dialog.getString();
}

```

```

channelThr = Dialog.getString();
chClear = Dialog.getString();
isArea = Dialog.getCheckbox();
areas = Dialog.getString();
minSize = Dialog.getNumber();
isDebug = Dialog.getCheckbox();
isLymph = Dialog.getCheckbox();
isTumorCore = Dialog.getCheckbox();
isInvasiveEdge = Dialog.getCheckbox();
isNonInvasiveTumor = Dialog.getCheckbox();

setData("DAPI Channel", dapi);
setData("DAPI threshold", dapiTh);
setData("Channels Of Interest", channels);
setData("Channel Names", channelNames);
setData("Threshold Methods", channelThr);
setData("Channels With Bright Artifacts", chClear);

setData("Perform Area Logic", isArea);
setData("Area Logic Measurements", areas);
setData("Min Particle Size", minSize);
setData("Debug", isDebug);

setData("Draw Lymph Node", isLymph);
setData("Draw Tumor Core", isTumorCore);
setData("Draw Invasive Edge", isInvasiveEdge);
setData("Draw Non-Invasive Tumor", isNonInvasiveTumor);
}
function cleanup() {
name = getTitle();
getDimensions(x,y,c,z,t);
run("Select None");
newName = name+" - BG Corrected";
run("Duplicate...", "title=["+newName+"] duplicate");
bg = newArray(c);
for (i=0; i<c; i++) {
selectRoi("BG");
Stack.setChannel(i+1);
run("Measure");
bg[i] = getResult("Mean", nResults-1);
run("Select None");
run("Subtract...", "value="+bg[i]+" slice");
}
IJ.deleteRows(nResults-c, nResults-1);
return newName;
}
function detectTissue() {
name = getTitle();
dapi = parseInt(getData("DAPI Channel"));
dapiTh = getData("DAPI threshold");
setSlice(dapi);
dapiFull = name+" - DAPI full";
run("Duplicate...", "title=["+dapiFull+" tmp]");
run("Gaussian Blur...", "sigma=10");
setAutoThreshold(dapiTh+" dark");
run("Analyze Particles...", "size=1000-Infinity pixel show=Masks");
rename(dapiFull);
close(dapiFull+" tmp");
selectImage(dapiFull);
run("Clear Results");

setThreshold(128,255);
// Measure DAPI areas in all ROIs
nR = roiManager("Count");
lab = newArray(0);
ar = newArray(0);
for (r=1; r<nR; r++) {
roiManager("Select", r);
rName = Roi.getName();
run("Measure");

lastLab = "DAPI"+ " - "+rName;
lastAr = getResult("Area", nResults-1);
lab = Array.concat(lab,lastLab);
ar = Array.concat(ar,lastAr);
}
}

```

```

    }
    // Add measurements to final table;
    prepareTable("Area Measurements");

    n = nResults;
    setResult("Label", n, name);
    for (r=0; r<lab.length; r++) {
        setResult(lab[r], n, ar[r]);
    }
    closeTable("Area Measurements");
    return dapiFull;
}

function detectChannels(dapi) {
    name = getTitle();
    minSize = getData("Min Particle Size");
    ch = split(getData("Channels Of Interest"), ",");
    chNames = split(getData("Channel Names"), ",");
    chThr = split(getData("Threshold Methods"), ",");
    chClear = split(getData("Channels With Bright Artifacts"), ",");
    nR = roiManager("Count");
    nchNames = newArray(chNames.length);

    ar = newArray(0);
    lab = newArray(0);
    imageNames = newArray(ch.length*2);
    nR = roiManager("Count");

    for (i=0; i<ch.length;i++) {
        selectImage(name);
        nchNames[i] = name + " - " + chNames[i];
        // Extract the channel
        run("Duplicate...", "title=[" + nchNames[i] + " tmp] duplicate channels=" + ch[i]);
        // Blur it slightly
        run("Smooth");
        // Apply thr
        if (hasMatch(ch[i], chClear)) {
            clearArtifacts();
        }
        setAutoThreshold(chThr[i] + " dark");
        run("Analyze Particles...", "size=" + minSize + "-Infinity pixel show=Masks");
        rename(nchNames[i]);
        imageNames[2*i] = nchNames[i];
        selectImage(nchNames[i] + " tmp");
        close();
        // AND with DAPIs
        imageCalculator("AND create", dapi, nchNames[i]);
        rename(nchNames[i] + " - DAPI");
        imageNames[2*i+1] = nchNames[i] + " - DAPI";
        setThreshold(128,255);

        for (r=1; r<nR; r++) {
            selectImage(nchNames[i] + " - DAPI");
            roiManager("Select", r);
            rName = Roi.getName();
            run("Measure");

            lastLab = chNames[i] + " - " + rName;
            lastAr = getResult("Area", nResults-1);
            lab = Array.concat(lab, lastLab);
            ar = Array.concat(ar, lastAr);
        }
    }
    selectWindow("Results");
    prepareTable("Area Measurements");
    n = nResults;
    for (i=0; i<lab.length; i++) {
        print(lab[i]);
        setResult(lab[i], n-1, ar[i]);
    }
    closeTable("Area Measurements");
    updateResults();
    isDebug = getData("Debug");
    if (isDebug == "1") {
        waitForUser("Check resulting masks");
    }
}

```

```

    }

    return imageNames;
}

function clearArtifacts() {
    //Image is already duplicated, need to set bright things to NaN
    run("32-bit");
    setAutoThreshold("MaxEntropy");
    run("NaN Background");
}

function hasMatch(txt, array) {
    for (i=0; i< array.length; i++) {
        if (txt == array[i]) {
            return true;
        }
    }
    return false;
}

function measureCurrentImage() {
    bgImage = cleanup();
    dapi = detectTissue();
    selectImage(bgImage);
    detectChannels(dapi);

    isArea = parseInt(getDataD("Perform Area Logic", 1));

    if(isArea == 1) {
        channelLogic();
    }

    function channelLogic() {
        // Do some image logic
        logic = split(getData("Area Logic Measurements"), ",");
        names = split(getData("Channel Names"), ",");

        // Get image names that are matching and build expression
        str = "";
        letters = newArray("a","b","c","d","e","f","g","h");
        l=0;
        nR = roiManager("Count");
        lab = newArray(0);
        ar = newArray(0);

        for(k=0; k<names.length; k++) {
            for(i=0; i< nImages; i++) {
                selectImage(i+1);
                name = getTitle();
                print(name);
                if(matches(name,"*-"+names[k]+"- DAPI")) {
                    print("Match between "+name+" and "+names[k]);
                    getVoxelSize(vx,vy,vz,vU);
                    str+=" "+letters[l]+"=["+name+"]";
                    l++;
                    i=nImages;
                }
            }
        }
        print(str);
        for (i=0; i<logic.length;i++){
            expression = logic[i];
            run("Image Expression Parser (Macro)", "expression="+expression+str);
            setVoxelSize(vx,vy,vz,vU);
            currentImage = getTitle();

            setThreshold(1,255);
            // Measure All ROIs

```

```

        for (r=1; r<nR; r++) {
            selectImage(currentImage);
            roiManager("Select", r);
            rName = Roi.getName();
            run("Measure");

            lastLab = currentImage+ " - "+rName;
            lastAr = getResult("Area", nResults-1);
            lab = Array.concat(lab,lastLab);
            ar = Array.concat(ar,lastAr);
        }
        run("Select None");
    }
    prepareTable("Area Measurements");
    n = nResults;
    for (i=0; i<lab.length; i++) {
        print(lab[i]);
        setResult(lab[i], n-1, ar[i]);
    }
    closeTable("Area Measurements");
    updateResults();

    // Everyone in same stack
    run("Images to Stack", "name=Stack title=Parsed use");
}
</codeLibrary>

<line>
<button>
label=Select Image
icon=noicon
arg=<macro>

selectImageDialog();
</macro>
</line>

<line>
<button>
label=Save image (+ ROI)
icon=noicon
arg=<macro>

saveCurrentImage();
//Saves the ROI Set with the name of the current image
saveRois("Open");
</macro>
</line>

<line>
<button>
label=Settings
icon=noicon
arg=<macro>
buildSettings();
</macro>
</line>

<line>
<button>
label=Save Settings
icon=noicon
arg=<macro>
saveParameters();
</macro>

<button>
label=Load Settings
icon=noicon
arg=<macro>
loadParameters();
</macro>
</line>

```

```

<line>
<button>
label=Draw ROI
icon=noicon
arg=<macro>
// Make user draw tissue ROI
drawRoi();
</macro>

<button>
label=Batch Draw ROI
icon=noicon
arg=<macro>
nI = getNumberImages();

for (i=0; i<nI; i++) {

    openImage(i);
    drawRoi();
    close();
}
</macro>
</line>

<line>
<button>
label=Measure Current Image
icon=noicon
arg=<macro>

measureCurrentImage();

</macro>
</line>
<line>
<button>
label=Batch Measure
icon=noicon
arg=<macro>

run("Clear Results");

nI = getNumberImages();
print(nI);
for (i=0; i<nI; i++) {
    roiManager("reset");
    openImage(i);
    measureCurrentImage();
    saveCurrentImage();
    //Close the image before going to the next one
    close();
}
</macro>
</line>

<line>
<button>
label=Close Others
icon=noicon
arg=<macro>
close("\Others");
</macro>
</line>

<line>
<button>
label=Area Logic
icon=noicon
arg=<macro>
channellLogic();
</macro>
</line>

```

Bibliography

- Achen, M.G., Jeltsch, M., Kukk, E., Mäkinen, T., Vitali, A., Wilks, A.F., Alitalo, K., and Stacker, S.A. (1998). Vascular endothelial growth factor D (VEGF-D) is a ligand for the tyrosine kinases VEGF receptor 2 (Flk1) and VEGF receptor 3 (Flt4). *Proc. Natl. Acad. Sci.* *95*, 548–553.
- Alitalo, K., Tammela, T., and Petrova, T.V. (2005). Lymphangiogenesis in development and human disease. *Nature* *438*, 946–953.
- Augustin, H.G., Young Koh, G., Thurston, G., and Alitalo, K. (2009). Control of vascular morphogenesis and homeostasis through the angiopoietin–Tie system. *Nat. Rev. Mol. Cell Biol.* *10*, 165–177.
- Baldwin, M.E., Halford, M.M., Roufail, S., Williams, R.A., Hibbs, M.L., Grail, D., Kubo, H., Stacker, S.A., and Achen, M.G. (2005). Vascular Endothelial Growth Factor D Is Dispensable for Development of the Lymphatic System. *Mol. Cell. Biol.* *25*, 2441–2449.
- Balkwill, F., Charles, K.A., and Mantovani, A. (2005). Smoldering and polarized inflammation in the initiation and promotion of malignant disease. *Cancer Cell* *7*, 211–217.
- Baluk, P., Fuxe, J., Hashizume, H., Romano, T., Lashnits, E., Butz, S., Vestweber, D., Corada, M., Molendini, C., Dejana, E., et al. (2007). Functionally specialized junctions between endothelial cells of lymphatic vessels. *J. Exp. Med.* *204*, 2349–2362.
- Barde, I., Salmon, P., and Trono, D. (2010). Production and Titration of Lentiviral Vectors. In *Current Protocols in Neuroscience*, J.N. Crawley, C.R. Gerfen, M.A. Rogawski, D.R. Sibley, P. Skolnick, and S. Wray, eds. (Hoboken, NJ, USA: John Wiley & Sons, Inc.), p.
- Bergers, G., Brekken, R., McMahon, G., Vu, T.H., Itoh, T., Tamaki, K., Tanzawa, K., Thorpe, P., Itohara, S., Werb, Z., et al. (2000). Matrix metalloproteinase-9 triggers the angiogenic switch during carcinogenesis. *Nat. Cell Biol.* *2*, 737–744.
- Betterman, K.L., Paquet-Fifield, S., Asselin-Labat, M.-L., Visvader, J.E., Butler, L.M., Stacker, S.A., Achen, M.G., and Harvey, N.L. (2012). Remodeling of the Lymphatic Vasculature during Mouse Mammary Gland Morphogenesis Is Mediated via Epithelial-Derived Lymphangiogenic Stimuli. *Am. J. Pathol.* *181*, 2225–2238.
- Bhowmick, N.A., Neilson, E.G., and Moses, H.L. (2004). Stromal fibroblasts in cancer initiation and progression. *Nature* *432*, 332–337.
- Bingle, L., Brown, N.J., and Lewis, C.E. (2002). The role of tumour-associated macrophages in tumour progression: implications for new anticancer therapies. *J. Pathol.* *196*, 254–265.
- Biswas, S.K., and Mantovani, A. (2010). Macrophage plasticity and interaction with lymphocyte subsets: cancer as a paradigm. *Nat. Immunol.* *11*, 889–896.
- Boardman, K.C. (2003). Interstitial Flow as a Guide for Lymphangiogenesis. *Circ. Res.* *92*, 801–808.
- Bono, P., Wasenius, V.-M., Heikkilä, P., Lundin, J., Jackson, D.G., and Joensuu, H. (2004). High LYVE-1-positive lymphatic vessel numbers are associated with poor outcome in breast cancer. *Clin. Cancer Res.* *10*, 7144–7149.
- Broggi, M.A.S., Schmalzer, M., Lagarde, N., and Rossi, S.W. (2014). Isolation of Murine Lymph Node Stromal Cells. *J. Vis. Exp.*

Bron, S., Henry, L., Faes-van't Hull, E., Turrini, R., Vanhecke, D., Guex, N., Ifticene-Treboux, A., Marina Iancu, E., Semilietof, A., Rufer, N., et al. (2016). TIE-2-expressing monocytes are lymphangiogenic and associate specifically with lymphatics of human breast cancer. *OncoImmunology* 5, e1073882.

Butcher, D.T., Alliston, T., and Weaver, V.M. (2009). A tense situation: forcing tumour progression. *Nat. Rev. Cancer* 9, 108–122.

Cao, R., Björndahl, M.A., Religa, P., Clasper, S., Garvin, S., Galter, D., Meister, B., Ikomi, F., Tritsarlis, K., Dissing, S., et al. (2004). PDGF-BB induces intratumoral lymphangiogenesis and promotes lymphatic metastasis. *Cancer Cell* 6, 333–345.

Caunt, M., Mak, J., Liang, W.-C., Stawicki, S., Pan, Q., Tong, R.K., Kowalski, J., Ho, C., Reslan, H.B., Ross, J., et al. (2008). Blocking neuropilin-2 function inhibits tumor cell metastasis. *Cancer Cell* 13, 331–342.

Chang, H.Y., Chi, J.-T., Dudoit, S., Bondre, C., van de Rijn, M., Botstein, D., and Brown, P.O. (2002). Diversity, topographic differentiation, and positional memory in human fibroblasts. *Proc. Natl. Acad. Sci.* 99, 12877–12882.

Chang, H.Y., Sneddon, J.B., Alizadeh, A.A., Sood, R., West, R.B., Montgomery, K., Chi, J.-T., Rijn, M. van de, Botstein, D., and Brown, P.O. (2004). Gene Expression Signature of Fibroblast Serum Response Predicts Human Cancer Progression: Similarities between Tumors and Wounds. *PLoS Biol.* 2, e7.

Ciriello, G., Gatza, M.L., Beck, A.H., Wilkerson, M.D., Rhie, S.K., Pastore, A., Zhang, H., McLellan, M., Yau, C., Kandoth, C., et al. (2015). Comprehensive Molecular Portraits of Invasive Lobular Breast Cancer. *Cell* 163, 506–519.

Condeelis, J., and Pollard, J.W. (2006). Macrophages: Obligate Partners for Tumor Cell Migration, Invasion, and Metastasis. *Cell* 124, 263–266.

Coso, S., Bovay, E., and Petrova, T.V. (2014). Pressing the right buttons: signaling in lymphangiogenesis. *Blood* 123, 2614–2624.

Coussens, L.M., and Werb, Z. (2002). Inflammation and cancer. *Nature* 420, 860–867.

Cursiefen, C., Chen, L., Borges, L.P., Jackson, D., Cao, J., Radziejewski, C., D'Amore, P.A., Dana, M.R., Wiegand, S.J., and Streilein, J.W. (2004). VEGF-A stimulates lymphangiogenesis and hemangiogenesis in inflammatory neovascularization via macrophage recruitment. *J. Clin. Invest.* 113, 1040–1050.

Das, S., Sarrou, E., Podgrabinska, S., Cassella, M., Mungamuri, S.K., Feirt, N., Gordon, R., Nagi, C.S., Wang, Y., Entenberg, D., et al. (2013). Tumor cell entry into the lymph node is controlled by CCL1 chemokine expressed by lymph node lymphatic sinuses. *J. Exp. Med.* 210, 1509–1528.

De Palma, M., Venneri, M.A., Galli, R., Sergi, L.S., Politi, L.S., Sampaolesi, M., and Naldini, L. (2005). Tie2 identifies a hematopoietic lineage of proangiogenic monocytes required for tumor vessel formation and a mesenchymal population of pericyte progenitors. *Cancer Cell* 8, 211–226.

DeNardo, D.G., Barreto, J.B., Andreu, P., Vasquez, L., Tawfik, D., Kolhatkar, N., and Coussens, L.M. (2009). CD4⁺ T Cells Regulate Pulmonary Metastasis of Mammary Carcinomas by Enhancing Protumor Properties of Macrophages. *Cancer Cell* 16, 91–102.

Deng, Y., Zhang, X., and Simons, M. (2015). Molecular controls of lymphatic VEGFR3 signaling. *Arterioscler. Thromb. Vasc. Biol.* 35, 421–429.

-
- Desmoulière, A., Geinoz, A., Gabbiani, F., and Gabbiani, G. (1993). Transforming growth factor-beta 1 induces alpha-smooth muscle actin expression in granulation tissue myofibroblasts and in quiescent and growing cultured fibroblasts. *J. Cell Biol.* *122*, 103–111.
- Dumont, D.J., Jussila, L., Taipale, J., Lymboussaki, A., Mustonen, T., Pajusola, K., Breitman, M., and Alitalo, K. (1998). Cardiovascular failure in mouse embryos deficient in VEGF receptor-3. *Science* *282*, 946–949.
- Dunn, G.P., Old, L.J., and Schreiber, R.D. (2004). The immunobiology of cancer immunosurveillance and immunoediting. *Immunity* *21*, 137–148.
- Dvorak, H.F. (1986). Tumors: wounds that do not heal. Similarities between tumor stroma generation and wound healing. *N. Engl. J. Med.* *315*, 1650–1659.
- Erez, N., Truitt, M., Olson, P., and Hanahan, D. (2010). Cancer-Associated Fibroblasts Are Activated in Incipient Neoplasia to Orchestrate Tumor-Promoting Inflammation in an NF- κ B-Dependent Manner. *Cancer Cell* *17*, 135–147.
- Fantozzi, A., and Christofori, G. (2006). Mouse models of breast cancer metastasis. *Breast Cancer Res.* *8*, 1.
- Fidler, I.J. (2003). The pathogenesis of cancer metastasis: the 'seed and soil' hypothesis revisited. *Nat. Rev. Cancer* *3*, 453–458.
- Fridman, R., Benton, G., Aranoutova, I., Kleinman, H.K., and Bonfil, R.D. (2012). Increased initiation and growth of tumor cell lines, cancer stem cells and biopsy material in mice using basement membrane matrix protein (Cultrex or Matrigel) co-injection. *Nat. Protoc.* *7*, 1138–1144.
- Gale, N.W., Thurston, G., Hackett, S.F., Renard, R., Wang, Q., McClain, J., Martin, C., Witte, C., Witte, M.H., Jackson, D., et al. (2002). Angiopoietin-2 is required for postnatal angiogenesis and lymphatic patterning, and only the latter role is rescued by Angiopoietin-1. *Dev. Cell* *3*, 411–423.
- Garmy-Susini, B., Avraamides, C.J., Desgrosellier, J.S., Schmid, M.C., Foubert, P., Ellies, L.G., Lowy, A.M., Blair, S.L., Vandenberg, S.R., Datnow, B., et al. (2013). PI3K activates integrin 4 1 to establish a metastatic niche in lymph nodes. *Proc. Natl. Acad. Sci.* *110*, 9042–9047.
- Germano, G., Allavena, P., and Mantovani, A. (2008). Cytokines as a key component of cancer-related inflammation. *Cytokine* *43*, 374–379.
- Gogineni, A., Caunt, M., Crow, A., Lee, C.V., Fuh, G., van Bruggen, N., Ye, W., and Weimer, R.M. (2013). Inhibition of VEGF-C Modulates Distal Lymphatic Remodeling and Secondary Metastasis. *PLoS ONE* *8*, e68755.
- Gordon, S., and Martinez, F.O. (2010). Alternative Activation of Macrophages: Mechanism and Functions. *Immunity* *32*, 593–604.
- Gordon, E.J., Rao, S., Pollard, J.W., Nutt, S.L., Lang, R.A., and Harvey, N.L. (2010). Macrophages define dermal lymphatic vessel calibre during development by regulating lymphatic endothelial cell proliferation. *Dev. Camb. Engl.* *137*, 3899–3910.
- Gorsch, S.M., Memoli, V.A., Stukel, T.A., Gold, L.I., and Arrick, B.A. (1992). Immunohistochemical staining for transforming growth factor beta 1 associates with disease progression in human breast cancer. *Cancer Res.* *52*, 6949–6952.
-

-
- Guy, C.T., Cardiff, R.D., and Muller, W.J. (1992). Induction of mammary tumors by expression of polyomavirus middle T oncogene: a transgenic mouse model for metastatic disease. *Mol. Cell Biol.* *12*, 954–961.
- Halin, C., Tobler, N.E., Vigl, B., Brown, L.F., and Detmar, M. (2007). VEGF-A produced by chronically inflamed tissue induces lymphangiogenesis in draining lymph nodes. *Blood* *110*, 3158–3167.
- Hanahan, D., and Coussens, L.M. (2012). Accessories to the Crime: Functions of Cells Recruited to the Tumor Microenvironment. *Cancer Cell* *21*, 309–322.
- Hanahan, D., and Weinberg, R.A. (2000). The hallmarks of cancer. *Cell* *100*, 57–70.
- Hanahan, D., and Weinberg, R.A. (2011). Hallmarks of cancer: the next generation. *Cell* *144*, 646–674.
- Harvey, N.L., and Gordon, E.J. (2012). Deciphering the roles of macrophages in developmental and inflammation stimulated lymphangiogenesis. *Vasc. Cell* *4*, 1.
- He, Y., Rajantie, I., Pajusola, K., Jeltsch, M., Holopainen, T., Yla-Herttuala, S., Harding, T., Jooss, K., Takahashi, T., and Alitalo, K. (2005). Vascular endothelial cell growth factor receptor 3-mediated activation of lymphatic endothelium is crucial for tumor cell entry and spread via lymphatic vessels. *Cancer Res.* *65*, 4739–4746.
- Helm, C.-L.E., Fleury, M.E., Zisch, A.H., Boschetti, F., and Swartz, M.A. (2005). Synergy between interstitial flow and VEGF directs capillary morphogenesis in vitro through a gradient amplification mechanism. *Proc. Natl. Acad. Sci. U. S. A.* *102*, 15779–15784.
- Hirakawa, S. (2009). From tumor lymphangiogenesis to lymphovascular niche. *Cancer Sci.* *100*, 983–989.
- Hirakawa, S., Kodama, S., Kunstfeld, R., Kajiya, K., Brown, L.F., and Detmar, M. (2005). VEGF-A induces tumor and sentinel lymph node lymphangiogenesis and promotes lymphatic metastasis. *J. Exp. Med.* *201*, 1089–1099.
- Hirakawa, S., Brown, L.F., Kodama, S., Paavonen, K., Alitalo, K., and Detmar, M. (2006). VEGF-C-induced lymphangiogenesis in sentinel lymph nodes promotes tumor metastasis to distant sites. *Blood* *109*, 1010–1017.
- Hoshida, T. (2006). Imaging Steps of Lymphatic Metastasis Reveals That Vascular Endothelial Growth Factor-C Increases Metastasis by Increasing Delivery of Cancer Cells to Lymph Nodes: Therapeutic Implications. *Cancer Res.* *66*, 8065–8075.
- Issa, A., Le, T.X., Shoushtari, A.N., Shields, J.D., and Swartz, M.A. (2009). Vascular Endothelial Growth Factor-C and C-C Chemokine Receptor 7 in Tumor Cell-Lymphatic Cross-talk Promote Invasive Phenotype. *Cancer Res.* *69*, 349–357.
- Jeltsch, M. (1997). Hyperplasia of Lymphatic Vessels in VEGF-C Transgenic Mice. *Science* *276*, 1423–1425.
- Joukov, V., Pajusola, K., Kaipainen, A., Chilov, D., Lahtinen, I., Kukk, E., Saksela, O., Kalkkinen, N., and Alitalo, K. (1996). A novel vascular endothelial growth factor, VEGF-C, is a ligand for the Flt4 (VEGFR-3) and KDR (VEGFR-2) receptor tyrosine kinases. *EMBO J.* *15*, 290.
-

Joukov, V., Sorsa, T., Kumar, V., Jeltsch, M., Claesson-Welsh, L., Cao, Y., Saksela, O., Kalkkinen, N., and Alitalo, K. (1997). Proteolytic processing regulates receptor specificity and activity of VEGF-C. *EMBO J.* *16*, 3898–3911.

Kaipainen, A., Korhonen, J., Mustonen, T., Van Hinsbergh, V.W., Fang, G.-H., Dumont, D., Breitman, M., and Alitalo, K. (1995). Expression of the *fms*-like tyrosine kinase 4 gene becomes restricted to lymphatic endothelium during development. *Proc. Natl. Acad. Sci.* *92*, 3566–3570.

Kalluri, R., and Zeisberg, M. (2006). Fibroblasts in cancer. *Nat. Rev. Cancer* *6*, 392–401.

Karkkainen, M.J., Haiko, P., Sainio, K., Partanen, J., Taipale, J., Petrova, T.V., Jeltsch, M., Jackson, D.G., Talikka, M., Rauvala, H., et al. (2004). Vascular endothelial growth factor C is required for sprouting of the first lymphatic vessels from embryonic veins. *Nat. Immunol.* *5*, 74–80.

Karpanen, T., Egeblad, M., Karkkainen, M.J., Kubo, H., Ylä-Herttuala, S., Jäättelä, M., and Alitalo, K. (2001). Vascular endothelial growth factor C promotes tumor lymphangiogenesis and intralymphatic tumor growth. *Cancer Res.* *61*, 1786–1790.

Koboldt, D.C., Fulton, R.S., McLellan, M.D., Schmidt, H., Kalicki-Veizer, J., McMichael, J.F., Fulton, L.L., Dooling, D.J., Ding, L., Mardis, E.R., et al. (2012). Comprehensive molecular portraits of human breast tumours. *Nature* *490*, 61–70.

Kuperwasser, C., Chavarria, T., Wu, M., Magrane, G., Gray, J.W., Carey, L., Richardson, A., and Weinberg, R.A. (2004). Reconstruction of functionally normal and malignant human breast tissues in mice. *Proc. Natl. Acad. Sci. U. S. A.* *101*, 4966–4971.

Laakkonen, P., Waltari, M., Holopainen, T., Takahashi, T., Pytowski, B., Steiner, P., Hicklin, D., Persaud, K., Tonra, J.R., Witte, L., et al. (2007). Vascular Endothelial Growth Factor Receptor 3 Is Involved in Tumor Angiogenesis and Growth. *Cancer Res.* *67*, 593–599.

Levental, K.R., Yu, H., Kass, L., Lakins, J.N., Egeblad, M., Erler, J.T., Fong, S.F.T., Csiszar, K., Giaccia, A., Weninger, W., et al. (2009). Matrix Crosslinking Forces Tumor Progression by Enhancing Integrin Signaling. *Cell* *139*, 891–906.

Lin, E.Y., Nguyen, A.V., Russell, R.G., and Pollard, J.W. (2001). Colony-stimulating factor 1 promotes progression of mammary tumors to malignancy. *J. Exp. Med.* *193*, 727–740.

Lin, E.Y., Jones, J.G., Li, P., Zhu, L., Whitney, K.D., Muller, W.J., and Pollard, J.W. (2003). Animal Model. Progress. Malig. Polyoma Middle T Oncoprotein Mouse Breast Cancer Model Provid. Reliab. Model Hum. Dis. *Am. J. Pathol.* *163*, 14.

Link, A., Vogt, T.K., Favre, S., Britschgi, M.R., Acha-Orbea, H., Hinz, B., Cyster, J.G., and Luther, S.A. (2007). Fibroblastic reticular cells in lymph nodes regulate the homeostasis of naive T cells. *Nat. Immunol.* *8*, 1255–1265.

Louveau, A., Smirnov, I., Keyes, T.J., Eccles, J.D., Rouhani, S.J., Peske, J.D., Derecki, N.C., Castle, D., Mandell, J.W., Lee, K.S., et al. (2015). Structural and functional features of central nervous system lymphatic vessels. *Nature* *523*, 337–341.

Lund, A.W., Duraes, F.V., Hirosue, S., Raghavan, V.R., Nembrini, C., Thomas, S.N., Issa, A., Hugues, S., and Swartz, M.A. (2012). VEGF-C Promotes Immune Tolerance in B16 Melanomas and Cross-Presentation of Tumor Antigen by Lymph Node Lymphatics. *Cell Rep.* *1*, 191–199.

Mäkinen, T., Veikkola, T., Mustjoki, S., Karpanen, T., Catimel, B., Nice, E.C., Wise, L., Mercer, A., Kowalski, H., Kerjaschki, D., et al. (2001). Isolated lymphatic endothelial cells transduce

growth, survival and migratory signals via the VEGF-C/D receptor VEGFR-3. *EMBO J.* *20*, 4762–4773.

Mäkinen, T., Adams, R.H., Bailey, J., Lu, Q., Ziemiecki, A., Alitalo, K., Klein, R., and Wilkinson, G.A. (2005). PDZ interaction site in ephrinB2 is required for the remodeling of lymphatic vasculature. *Genes Dev.* *19*, 397–410.

Mantovani, A., Allavena, P., Sica, A., and Balkwill, F. (2008). Cancer-related inflammation. *Nature* *454*, 436–444.

Maruyama, K., Ii, M., Cursiefen, C., Jackson, D.G., Keino, H., Tomita, M., Van Rooijen, N., Takenaka, H., D'Amore, P.A., Stein-Streilein, J., et al. (2005). Inflammation-induced lymphangiogenesis in the cornea arises from CD11b-positive macrophages. *J. Clin. Invest.* *115*, 2363–2372.

Mattila, M.M.-T., Ruohola, J.K., Karpanen, T., Jackson, D.G., Alitalo, K., and Härkönen, P.L. (2002). VEGF-C induced lymphangiogenesis is associated with lymph node metastasis in orthotopic MCF-7 tumors: VEGF-C Induced Lymph Node Metastasis. *Int. J. Cancer* *98*, 946–951.

Mazzieri, R., Pucci, F., Moi, D., Zonari, E., Ranghetti, A., Berti, A., Politi, L.S., Gentner, B., Brown, J.L., Naldini, L., et al. (2011). Targeting the ANG2/TIE2 Axis Inhibits Tumor Growth and Metastasis by Impairing Angiogenesis and Disabling Rebounds of Proangiogenic Myeloid Cells. *Cancer Cell* *19*, 512–526.

Mohammed, R.A.A., Green, A., El-Shikh, S., Paish, E.C., Ellis, I.O., and Martin, S.G. (2007). Prognostic significance of vascular endothelial cell growth factors -A, -C and -D in breast cancer and their relationship with angio- and lymphangiogenesis. *Br. J. Cancer* *96*, 1092–1100.

Mohammed, R.A.A., Ellis, I.O., Elsheikh, S., Paish, E.C., and Martin, S.G. (2009). Lymphatic and angiogenic characteristics in breast cancer: morphometric analysis and prognostic implications. *Breast Cancer Res. Treat.* *113*, 261–273.

Murray, P.J., and Wynn, T.A. (2011). Protective and pathogenic functions of macrophage subsets. *Nat. Rev. Immunol.* *11*, 723–737.

Nagy, J.A., Vasile, E., Feng, D., Sundberg, C., Brown, L.F., Detmar, M.J., Lawitts, J.A., Benjamin, L., Tan, X., Manseau, E.J., et al. (2002). Vascular permeability factor/vascular endothelial growth factor induces lymphangiogenesis as well as angiogenesis. *J. Exp. Med.* *196*, 1497–1506.

Nakamura, Y., Yasuoka, H., Tsujimoto, M., Yang, Q., Tsukiyama, A., Imabun, S., Nakahara, M., Nakao, K., Nakamura, M., Mori, I., et al. (2003). Clinicopathological Significance of Vascular Endothelial Growth Factor-C in Breast Carcinoma with Long-Term Follow-Up. *Mod. Pathol.* *16*, 309–314.

Nakamura, Y., Yasuoka, H., Tsujimoto, M., Imabun, S., Nakahara, M., Nakao, K., Nakamura, M., Mori, I., and Kakudo, K. (2005). Lymph vessel density correlates with nodal status, VEGF-C expression, and prognosis in breast cancer. *Breast Cancer Res. Treat.* *91*, 125–132.

Ng, C.P. (2005). Interstitial fluid flow induces myofibroblast differentiation and collagen alignment in vitro. *J. Cell Sci.* *118*, 4731–4739.

Noy, R., and Pollard, J.W. (2014). Tumor-Associated Macrophages: From Mechanisms to Therapy. *Immunity* *41*, 49–61.

Oka, M., Iwata, C., Suzuki, H.I., Kiyono, K., Morishita, Y., Watabe, T., Komuro, A., Kano, M.R., and Miyazono, K. (2008). Inhibition of endogenous TGF-beta signaling enhances lymphangiogenesis. *Blood* *111*, 4571–4579.

Padera, T.P. (2002). Lymphatic Metastasis in the Absence of Functional Intratumor Lymphatics. *Science* *296*, 1883–1886.

Padera, T.P., Meijer, E.F.J., and Munn, L.L. (2016). The Lymphatic System in Disease Processes and Cancer Progression. *Annu. Rev. Biomed. Eng.* *18*, 125–158.

Paszek, M.J., Zahir, N., Johnson, K.R., Lakins, J.N., Rozenberg, G.I., Gefen, A., Reinhart-King, C.A., Margulies, S.S., Dembo, M., Boettiger, D., et al. (2005). Tensional homeostasis and the malignant phenotype. *Cancer Cell* *8*, 241–254.

Pathak, A.P. (2006). Lymph Node Metastasis in Breast Cancer Xenografts Is Associated with Increased Regions of Extravascular Drain, Lymphatic Vessel Area, and Invasive Phenotype. *Cancer Res.* *66*, 5151–5158.

Polyak, K., Haviv, I., and Campbell, I.G. (2009). Co-evolution of tumor cells and their microenvironment. *Trends Genet.* *25*, 30–38.

Pucci, F., Venneri, M.A., Biziato, D., Nonis, A., Moi, D., Sica, A., Di Serio, C., Naldini, L., and De Palma, M. (2009). A distinguishing gene signature shared by tumor-infiltrating Tie2-expressing monocytes, blood “resident” monocytes, and embryonic macrophages suggests common functions and developmental relationships. *Blood* *114*, 901–914.

Pytowski, B., Goldman, J., Persaud, K., Wu, Y., Witte, L., Hicklin, D.J., Skobe, M., Boardman, K.C., and Swartz, M.A. (2005). Complete and Specific Inhibition of Adult Lymphatic Regeneration by a Novel VEGFR-3 Neutralizing Antibody. *JNCI J. Natl. Cancer Inst.* *97*, 14–21.

Qian, B.-Z., and Pollard, J.W. (2010). Macrophage Diversity Enhances Tumor Progression and Metastasis. *Cell* *141*, 39–51.

Qian, C.-N., Berghuis, B., Tsarfaty, G., Bruch, M., Kort, E.J., Ditlev, J., Tsarfaty, I., Hudson, E., Jackson, D.G., Petillo, D., et al. (2006). Preparing the “Soil”: The Primary Tumor Induces Vasculature Reorganization in the Sentinel Lymph Node before the Arrival of Metastatic Cancer Cells. *Cancer Res.* *66*, 10365–10376.

Ran, S., Volk, L., Hall, K., and Flister, M.J. (2010). Lymphangiogenesis and lymphatic metastasis in breast cancer. *Pathophysiology* *17*, 229–251.

Reed, A.E.M., Kutasovic, J.R., Lakhani, S.R., and Simpson, P.T. (2015). Invasive lobular carcinoma of the breast: morphology, biomarkers and ‘omics. *Breast Cancer Res.* *17*, 12.

Ristimaki, A. (1998). Proinflammatory Cytokines Regulate Expression of the Lymphatic Endothelial Mitogen Vascular Endothelial Growth Factor-C. *J. Biol. Chem.* *273*, 8413–8418.

Roberts, N. (2006). Inhibition of VEGFR-3 Activation with the Antagonistic Antibody More Potently Suppresses Lymph Node and Distant Metastases than Inactivation of VEGFR-2. *Cancer Res.* *66*, 2650–2657.

Rønnov-Jessen, L., Petersen, O.W., and Bissell, M.J. (1996). Cellular changes involved in conversion of normal to malignant breast: importance of the stromal reaction. *Physiol. Rev.* *76*, 69–125.

Ruddell, A., Harrell, M.I., Minoshima, S., Maravilla, K.R., Iritani, B.M., White, S.W., and Partridge, S.C. (2008). Dynamic Contrast-Enhanced Magnetic Resonance Imaging of Tumor-Induced Lymph Flow. *Neoplasia* 10, 706–IN4.

Ruffell, B., Affara, N.I., and Coussens, L.M. (2012). Differential macrophage programming in the tumor microenvironment. *Trends Immunol.* 33, 119–126.

Schäfer, M., and Werner, S. (2008). Cancer as an overhealing wound: an old hypothesis revisited. *Nat. Rev. Mol. Cell Biol.* 9, 628–638.

Schledzewski, K., Falkowski, M., Moldenhauer, G., Metharom, P., Kzhyskowska, J., Ganss, R., Demory, A., Falkowska-Hansen, B., Kurzen, H., Ugurel, S., et al. (2006). Lymphatic endothelium-specific hyaluronan receptor LYVE-1 is expressed by stabilin-1+, F4/80+, CD11b+ macrophages in malignant tumours and wound healing tissue in vivo and in bone marrow cultures in vitro: implications for the assessment of lymphangiogenesis. *J. Pathol.* 209, 67–77.

Schoppmann, S., Fenzl, A., Nagy, K., Unger, S., Bayer, G., Geleff, S., Gnant, M., Horvat, R., Jakesz, R., and Birner, P. (2006). VEGF-C expressing tumor-associated macrophages in lymph node positive breast cancer: impact on lymphangiogenesis and survival. *Surgery* 139, 839–846.

Schoppmann, S.F., Birner, P., Stöckl, J., Kalt, R., Ullrich, R., Caucig, C., Kriehuber, E., Nagy, K., Alitalo, K., and Kerjaschki, D. (2002). Tumor-associated macrophages express lymphatic endothelial growth factors and are related to peritumoral lymphangiogenesis. *Am. J. Pathol.* 161, 947–956.

Schoppmann, S.F., Bayer, G., Aumayr, K., Taucher, S., Geleff, S., Rudas, M., Kubista, E., Hausmaninger, H., Samonigg, H., Gnant, M., et al. (2004). Prognostic Value of Lymphangiogenesis and Lymphovascular Invasion in Invasive Breast Cancer. *Ann. Surg.* 240, 306–312.

Shieh, A.C., Rozansky, H.A., Hinz, B., and Swartz, M.A. (2011). Tumor Cell Invasion Is Promoted by Interstitial Flow-Induced Matrix Priming by Stromal Fibroblasts. *Cancer Res.* 71, 790–800.

Shields, J.D., Fleury, M.E., Yong, C., Tomei, A.A., Randolph, G.J., and Swartz, M.A. (2007). Autologous chemotaxis as a mechanism of tumor cell homing to lymphatics via interstitial flow and autocrine CCR7 signaling. *Cancer Cell* 11, 526–538.

Sica, A., and Mantovani, A. (2012). Macrophage plasticity and polarization: in vivo veritas. *J. Clin. Invest.* 122, 787–795.

Simons, M., Gordon, E., and Claesson-Welsh, L. (2016). Mechanisms and regulation of endothelial VEGF receptor signalling. *Nat. Rev. Mol. Cell Biol.* 17, 611–625.

Skalli, O., Ropraz, P., Trzeciak, A., Benzouana, G., Gillesen, D., and Gabbiani, G. (1986). A monoclonal antibody against alpha-smooth muscle actin: a new probe for smooth muscle differentiation. *J. Cell Biol.* 103, 2787–2796.

Skobe, M., Hawighorst, T., Jackson, D.G., Prevo, R., Janes, L., Velasco, P., Riccardi, L., Alitalo, K., Claffey, K., and Detmar, M. (2001a). Induction of tumor lymphangiogenesis by VEGF-C promotes breast cancer metastasis. *Nat. Med.* 7, 192–198.

Skobe, M., Hamberg, L.M., Hawighorst, T., Schirner, M., Wolf, G.L., Alitalo, K., and Detmar, M. (2001b). Concurrent induction of lymphangiogenesis, angiogenesis, and macrophage recruitment by vascular endothelial growth factor-C in melanoma. *Am. J. Pathol.* 159, 893–903.

-
- Sørlie, T., Perou, C.M., Tibshirani, R., Aas, T., Geisler, S., Johnsen, H., Hastie, T., Eisen, M.B., Van De Rijn, M., Jeffrey, S.S., et al. (2001). Gene expression patterns of breast carcinomas distinguish tumor subclasses with clinical implications. *Proc. Natl. Acad. Sci.* *98*, 10869–10874.
- Squadrito, M.L., and De Palma, M. (2011). Macrophage regulation of tumor angiogenesis: Implications for cancer therapy. *Mol. Aspects Med.* *32*, 123–145.
- Stacker, S.A., Stenvers, K., Caesar, C., Vitali, A., Domagala, T., Nice, E., Roufail, S., Simpson, R.J., Moritz, R., Karpanen, T., et al. (1999). Biosynthesis of vascular endothelial growth factor-D involves proteolytic processing which generates non-covalent homodimers. *J. Biol. Chem.* *274*, 32127–32136.
- Stacker, S.A., Caesar, C., Baldwin, M.E., Thornton, G.E., Williams, R.A., Prevo, R., Jackson, D.G., Nishikawa, S., Kubo, H., and Achen, M.G. (2001). VEGF-D promotes the metastatic spread of tumor cells via the lymphatics. *Nat. Med.* *7*, 186–191.
- Stacker, S.A., Williams, S.P., Karnezis, T., Shayan, R., Fox, S.B., and Achen, M.G. (2014). Lymphangiogenesis and lymphatic vessel remodelling in cancer. *Nat. Rev. Cancer* *14*, 159–172.
- Stein, M., Keshav, S., Harris, N., and Gordon, S. (1992). Interleukin 4 potently enhances murine macrophage mannose receptor activity: a marker of alternative immunologic macrophage activation. *J. Exp. Med.* *176*, 287–292.
- Strutz, F., Okada, H., Lo, C.W., Danoff, T., Carone, R.L., Tomaszewski, J.E., and Neilson, E.G. (1995). Identification and characterization of a fibroblast marker: FSP1. *J. Cell Biol.* *130*, 393–405.
- Swartz, M.A. (2014). Immunomodulatory Roles of Lymphatic Vessels in Cancer Progression. *Cancer Immunol. Res.* *2*, 701–707.
- Swartz, M.A., and Lund, A.W. (2012). Lymphatic and interstitial flow in the tumour microenvironment: linking mechanobiology with immunity. *Nat. Rev. Cancer* *12*, 210–219.
- Swartz, M.A., and Skobe, M. (2001). Lymphatic function, lymphangiogenesis, and cancer metastasis. *Microsc. Res. Tech.* *55*, 92–99.
- Tammela, T. (2005). Angiopoietin-1 promotes lymphatic sprouting and hyperplasia. *Blood* *105*, 4642–4648.
- Tammela, T., and Alitalo, K. (2010). Lymphangiogenesis: Molecular mechanisms and future promise. *Cell* *140*, 460–476.
- Tammela, T., Zarkada, G., Wallgard, E., Murtomäki, A., Suchting, S., Wirzenius, M., Waltari, M., Hellström, M., Schomber, T., Peltonen, R., et al. (2008). Blocking VEGFR-3 suppresses angiogenic sprouting and vascular network formation. *Nature* *454*, 656–660.
- Tomasek, J.J., Gabbiani, G., Hinz, B., Chaponnier, C., and Brown, R.A. (2002). Myofibroblasts and mechano-regulation of connective tissue remodelling. *Nat. Rev. Mol. Cell Biol.* *3*, 349–363.
- Tuttle, T.M. (2004). Technical advances in sentinel lymph node biopsy for breast cancer. *Am. Surg.* *70*, 407–413.
- Valtola, R., Salven, P., Heikkilä, P., Taipale, J., Joensuu, H., Rehn, M., Pihlajaniemi, T., Weich, H., Alitalo, K., and others (1999). VEGFR-3 and its ligand VEGF-C are associated with angiogenesis in breast cancer. *Am. J. Pathol.* *154*, 1381–1390.
-

Van den Eynden, G.G., Van der Auwera, I., Van Laere, S.J., Colpaert, C.G., van Dam, P., Dirix, L.Y., Vermeulen, P.B., and Van Marck, E.A. (2006). Distinguishing blood and lymph vessel invasion in breast cancer: a prospective immunohistochemical study. *Br. J. Cancer*.

Van den Eynden, G.G., Vandenberghe, M.K., van Dam, P.-J.H., Colpaert, C.G., van Dam, P., Dirix, L.Y., Vermeulen, P.B., and Van Marck, E.A. (2007). Increased Sentinel Lymph Node Lymphangiogenesis is Associated with Nonsentinel Axillary Lymph Node Involvement in Breast Cancer Patients with a Positive Sentinel Node. *Clin. Cancer Res.* *13*, 5391–5397.

Vaughan, M.B., Howard, E.W., and Tomasek, J.J. (2000). Transforming Growth Factor- β 1 Promotes the Morphological and Functional Differentiation of the Myofibroblast. *Exp. Cell Res.* *257*, 180–189.

de Visser, K.E., Eichten, A., and Coussens, L.M. (2006). Paradoxical roles of the immune system during cancer development. *Nat. Rev. Cancer* *6*, 24–37.

Watarai, K., Nakao, S., Fotovati, A., Basaki, Y., Hosoi, F., Bereczky, B., Higuchi, R., Miyamoto, T., Kuwano, M., and Ono, M. (2008). Role of macrophages in inflammatory lymphangiogenesis: Enhanced production of vascular endothelial growth factor C and D through NF-kappaB activation. *Biochem. Biophys. Res. Commun.* *377*, 826–831.

Williams, C.S., Leek, R.D., Robson, A.M., Banerji, S., Prevo, R., Harris, A.L., and Jackson, D.G. (2003). Absence of lymphangiogenesis and intratumoural lymph vessels in human metastatic breast cancer. *J. Pathol.* *200*, 195–206.

Wipff, P.-J., Rifkin, D.B., Meister, J.-J., and Hinz, B. (2007). Myofibroblast contraction activates latent TGF- β 1 from the extracellular matrix. *J. Cell Biol.* *179*, 1311–1323.

Wirzenius, M., Tammela, T., Uutela, M., He, Y., Odorisio, T., Zambruno, G., Nagy, J.A., Dvorak, H.F., Ylä-Herttuala, S., Shibuya, M., et al. (2007). Distinct vascular endothelial growth factor signals for lymphatic vessel enlargement and sprouting. *J. Exp. Med.* *204*, 1431–1440.

Wiseman, B.S. (2002). Stromal Effects on Mammary Gland Development and Breast Cancer. *Science* *296*, 1046–1049.

Zitvogel, L., Tesniere, A., and Kroemer, G. (2006). Cancer despite immunosurveillance: immunoselection and immunosubversion. *Nat. Rev. Immunol.* *6*, 715–727.

Zumsteg, A., Baeriswyl, V., Imaizumi, N., Schwendener, R., Rüegg, C., and Christofori, G. (2009). Myeloid Cells Contribute to Tumor Lymphangiogenesis. *PLoS ONE* *4*, e7067.

Curriculum Vitae

Ingrid Maria van Mier

Born on November 1st 1985 in Boulder, CO, USA

Nationality: Dutch

Current address

Chemin des Fleurettes 41

1007 Lausanne

Switzerland

+41-(0)79-621 69 35

ingrid.vanmier@gmail.com

Education

06/12 - 01/17 **Admitted to the Biotechnology and Bioengineering Graduate Program of the Doctoral School of EPFL Lausanne**

PhD research “*Elucidating the role of lymphatic vessels within the tumor microenvironment of breast cancer*” under the supervision of Prof. Dr. M. Swartz and Prof. Dr. M. De Palma at EPFL, Lausanne, Switzerland.

09/10 – 11/11 **Admitted to the Microbiology and Immunology Graduate Program of the Life Science Zürich Graduate School of ETH Zürich**

PhD research “*Elucidating the mechanism of antibody-mediated inhibition of cross-presentation*” under the supervision of Dr. M. Bachmann, Dr. A. Jegerlehner and Prof. Dr. A. Oxenius at Cytos Biotechnology AG, Zürich-Schlieren, Switzerland.

Preliminary termination of PhD thesis due to financial difficulties of the company.

02/08 – 08/09 **Master of Science in Medicinal and Industrial Pharmaceutical Sciences, ETH Zürich, Switzerland.**

Winner of the Willi-Studer-prize 2009 for graduating with the best average grade.

02/08 – 08/08 Master thesis “*Characterization of conditionally immortalized, murine lymphatic endothelial cells and investigating the role of ICAM-1 and CEACAM-1 in dendritic cell trafficking into lymphatic vessels*” under the supervision of Prof. C. Halin-Winter and Prof. M. Detmar, Drug Discovery Technologies Group and Pharmacogenomics Group, Institute of Pharmaceutical Sciences, ETH Zürich, Switzerland.

10/04 – 02/08 **Bachelor of Science in Pharmaceutical Sciences, ETH Zürich, Switzerland.**

Professional experience

- 01/10 – 03/10 **Practicum at the Institute of Medical Virology, Medical Faculty, University of Zürich, Group of Prof. Dr A. Trkola, Switzerland.**
Activities include managing databases and preparing samples for PhD students.
- 10/09 – 12/09 **Practicum in the Pharmaceutical Analytical Department at Novartis AG, Basel, Switzerland under the supervision of Dr. E. John.**
Investigation of powder properties regarding the ability to process them into tablets.
- 10/08 – 11/08 **Position as research assistant of Ms. A. Hafner in the Drug Formulation and Delivery Group at the Institute of Pharmaceutical Sciences, ETH Zürich, Switzerland.**
Activities included performing autonomously experiments for a PhD student, as well as correcting reports of science projects written by students.

Conferences

- 09/16 ISREC-SCCL Symposium: Horizons of Cancer Biology and Therapy, Lausanne, Switzerland. Poster presentation.
- 01/16 AACR Symposium: The Function of Tumor Microenvironment in Cancer Progression, San Diego, CA, USA. Poster presentation.
- 11/15 ISREC Faculty and Staff Retreat, Lausanne, Switzerland. Poster presentation.
- 08/14 Selected by Roche for participation in Roche Continents to explore common grounds on creativity and innovation in arts and sciences, in Salzburg, Austria.
- 06/11 8th International Symposium on the Biology of Endothelial Cells (EC8), Zürich, Switzerland.
- 01/11 Introductory Course in Laboratory Animal Science (mice, rats and rabbits), including the 4 days of continued education in laboratory animal science required by Swiss law. Accredited as FELASA Category B course 027/08.
- 08/09 Selected by Novartis for participation in the Novartis Biotechnology and Leadership Camp (BioCamp) 2009 at the Novartis campus, Basel, Switzerland.
- 03/09 Achievement of Yellow Belt Rank in Process and Project Management.

Languages

- Dutch: mother tongue
 - English: fluent
 - German: fluent
 - Swiss German: fluent
 - French: very good
-

